LOAN DOCUMENT

PHOTOGRAPH THIS SHEET

DTIC ACCESSION NUMBER

LEVEL

INVENTORY 0

AFRL-ML-TY-TR-1999-4552

DOCUMENT IDENTIFICATION

2 NOV 1998

DISTRIBUTION STATEMENT A
Approved for Public Release
Distribution Unlimited

DISTRIBUTION STATEMENT

ACCESSION FOR
NTIS GRA&I
DTIC TRAC
UNANNOUNCED
JUSTIFICATION

BY

DISTRIBUTION/

AVAILABILITY CODES

DISTRIBUTION	AVAILABILITY AND/OR SPECIAL
A-1	

DISTRIBUTION STAMP

DATE ACCESSIONED

DATE RETURNED

20000211 037

DATE RECEIVED IN DTIC

REGISTERED OR CERTIFIED NUMBER

PHOTOGRAPH THIS SHEET AND RETURN TO DTIC-FDAC

DTIC FORM 70A JUN 90

DOCUMENT PROCESSING SHEET

PREVIOUS EDITIONS MAY BE USED UNTIL STOCK IS EXHAUSTED.

LOAN DOCUMENT

DTIC QUALITY INSPECTED 1

HANDLE WITH CARE

AFRL-ML-TY-TR-1999-4552



THE EFFECTS OF CARBON PARTICLES ON AQUEOUS PHASE PULSED STREAMER CORONA

DAVID R. GRYMONPRÉ

FLORIDA STATE UNIVERSITY &
FAMU-FSU COLLEGE OF ENGINEERING
DEPARTMENT OF ENGINEERING
2525 POTTSDAMER STREET
TALLAHASSEE FL 32310-6046

Approved for Public Release: Distribution Unlimited

AIR FORCE RESEARCH LABORATORY
MATERIALS & MANUFACTURING DIRECTORATE
AIRBASE & ENVIRONMENTAL TECHNOLOGY DIVISION
TYNDALL AFB FL 32403-5323

NOTICES

USING GOVERNMENT DRAWINGS, SPECIFICATIONS, OR OTHER DATA INCLUDED IN THIS DOCUMENT FOR ANY PURPOSE OTHER THAN GOVERNMENT PROCUREMENT DOES NOT IN ANY WAY OBLIGATE THE US GOVERNMENT. THE FACT THAT THE GOVERNMENT FORMULATED OR SUPPLIED THE DRAWINGS, SPECIFICATIONS, OR OTHER DATA DOES NOT LICENSE THE HOLDER OR ANY OTHER PERSON OR CORPORATION; OR CONVEY ANY RIGHTS OR PERMISSION TO MANUFACTURE, USE, OR SELL ANY PATENTED INVENTION THAT MAY RELATE TO THEM.

THIS REPORT IS RELEASABLE TO THE NATIONAL TECHNICAL INFORMATION SERVICE (NTIS). AT NTIS, IT WILL BE AVAILABLE TO THE GENERAL PUBLIC, INCLUDING FOREIGN NATIONS.

THIS TECHNICAL REPORT HAS BEEN REVIEWED AND IS APPROVED FOR PUBLICATION.

JOSEPH D. WANDER, PhD
Program Manager

CHRISTINE WAGENER-HULME, Lt Col, USAF, BSC
Chief, Environmental Technology Development Branch

RANDY L. GROSS, Col, USAF, BSC
Chief, Airbase & Environmental Technology Division

REPORT DOCUMENTATION PAGE

Form Approved
OMB No. 0704-0188

Public reporting burden for this collection of information is estimated to average 1 hour per response, including the time for reviewing instructions, searching existing data sources, gathering and maintaining the data needed, and completing and reviewing the collection of information. Send comments regarding this burden estimate or any other aspect of this collection of information, including suggestions for reducing this burden, to Washington Headquarters Services, Directorate for Information Operations and Reports, 1215 Jefferson Davis Highway, Suite 1204, Arlington, VA 22202-4302, and to the Office of Management and Budget, Paperwork Reduction Project (0704-0188), Washington, DC 20503.

1. AGENCY USE ONLY *(Leave blank)*	2. REPORT DATE	3. REPORT TYPE AND DATES COVERED
	2 Nov 1998	Master's Thesis: January 1996 - January 1998

4. TITLE AND SUBTITLE
The Effects of Carbon Particles on Aqueous Phase Pulsed Streamer Corona

5. FUNDING NUMBERS
F08635-93-C-0020
PE: 6022F
Project Number: 1900-A35B

6. AUTHOR(S)
Grymonpré, David R.

7. PERFORMING ORGANIZATION NAME(S) AND ADDRESS(ES)
Department of Chemical Engineering
Florida State University & FAMU-FSU College of Engineering
2525 Pottsdamer Street
Tallahassee FL 32310-6046

8. PERFORMING ORGANIZATION REPORT NUMBER

9. SPONSORING/MONITORING AGENCY NAME(S) AND ADDRESS(ES)
AFRL/MLQE (Dr. Joe Wander)
139 Barnes Drive, Suite 2
Tyndall AFB, FL 32403-5323

10. SPONSORING/MONITORING AGENCY REPORT NUMBER
AFRL-ML-TY-TR-1999-4552

11. SUPPLEMENTARY NOTES
POC: Joseph D. Wander, Ph.D, AFRL/MLQE, (850) 283-6240

12a. DISTRIBUTION AVAILABILITY STATEMENT
Approved for Public Release: Distribution Unlimited

12b. DISTRIBUTION CODE
A

13. ABSTRACT *(Maximum 200 words)*

Pulsed streamer corona technology utilizes a non-thermal plasma high voltage discharge to break down various airborne and aqueous phase organic pollutants. Pulsed streamer corona discharge in a reactor using a point-to-plane electrode geometry has been studied with well-mixed aqueous solutions containing various salts (sodium chloride, potassium chloride, and calcium chloride) and particles in suspension (powdered activated carbon, porous silica gel, non-porous glass spheres, and elemental copper). The result that solution conductivity governs the electrode breakdown voltage is independent of both the salt composition and the particle properties (i.e., total surface area, particle size, conductivity, and dielectric constant). Powdered activated carbon in aqueous suspension also dramatically reduces the reactor electric power as a function of applied voltage. Elemental analysis using PIXE (proton-induced x-ray emission) of the activated carbon and the water leachate from washed activated carbon, coupled with pulsed corona treatment experiments using washed activated carbon, show that interactions of activated carbon with potassium salts are responsible for the lower reactor power. With the lower power consumption, greater amounts of contaminants can be removed at a lower power usage. The combination of pulsed corona and activated carbon enhances phenol removal through bulk reactions, adsorption, and corona-induced surface reactions. Primary oxidation products of phenol were also measured. A reaction and diffusion model was derived to analyze the phenol decomposition with combined bulk liquide and particle surface reactions.

14. SUBJECT TERMS	15. NUMBER OF PAGES
Pulsed streamer, corona, plasma, carbon particles, aqueous	186
	16. PRICE CODE

17. SECURITY CLASSIFICATION OF REPORT	18. SECURITY CLASSIFICATION OF THIS PAGE	19. SECURITY CLASSIFICATION OF ABSTRACT	20. LIMITATION OF ABSTRACT
UNCL	UNCL	UNCL	UL

Standard Form 298 (Rev. 2-89) (EG)
Prescribed by ANSI Std. 239.18
Designed using Perform Pro, WHS/DIOR, Oct 94

CLASSIFIED BY:

DECLASSIFY ON:

Preface

This thesis was prepared by Florida State University (FSU), Department of Chemical Engineering, under a subcontract with Applied Research Associates (contract No. F08635-93-C-0020), for the Air Force Research Laboratory (AFRL), Airbase and Environmental Technology Division, Tyndall AFB, FL 32403. The work was performed from January 1996 to January 1998. The AFRL project officer was Joseph D. Wander, Ph.D.

This thesis is submitted to the Defense Technical Information Center for publication exactly as it was submitted to Florida State University. This format does not conform to the usual style standards for AFRL reports but is acceptable.

The members of the Committee approve the thesis of David Grymonpré defended on February 11, 1998.

Bruce R. Locke
Professor Directing Thesis

Ronald J. Clark
Committee Member

Eric Kalu
Committee Member

Approved:

Michael H. Peters
Chair, Department of Chemical Engineering

To

Annette

ACKNOWLEDGEMENTS

I thank my thesis advisor, Dr. Bruce R. Locke, for his help and guidance for the past several years. I also thank Dr. Ronald J. Clark, and Dr. Eric Kalu for serving on my thesis committee. A special thanks goes to Wright C. Finney for being a thesis committee member as well as for all of the laboratory help over the years.

Financial support and equipment was given by the United Stated Air Force, Tyndall A.F.B., and Applied Research Associates, Panama City, FL.

I acknowledge the continuing support of this project by the Department of Chemical Engineering, FAMU-FSU College of Engineering. Additionally, I would like to thank the Department of Nuclear Services and the Department of Physics at Florida State University for providing experimental equipment and facilities to conduct some of our experimental corona runs. The help of Lori McFadden on the Scanning Electron Microscope in the Florida State University Department of Biology was greatly appreciated.

The Graduate students Swaminathan Kalyana, Giridhar Sathiamoorthy, and Craig Galban, as well as the undergraduate students Stephen White, Howell Hanson, Shawn Goldstein, and Jason Maxwell provided assistance in the laboratory.

TABLE OF CONTENTS

List of Tables..... vii
List of Figures..... xi
Abstract..... xv

Chapter **Page**

1 INTRODUCTION..... 1

1.1 Research Objectives..... 2

2 LITERATURE REVIEW..... 4

2.1 Corona Discarges..... 4

2.2 Types of Corona Discharges..... 5

2.3 Applications of Electrical Discharges..... 5

2.4 Electric Breakdown Theory for Liquids..... 9

2.5 The Oxidation of Phenol..... 17

2.6 Activated Carbon..... 18

3 EXPERIMENTAL METHODS..... 23

3.1 Pulsed Power Supply..... 23

3.2 Pulsed Corona Reactor..... 24

3.3 Experimental Procedure for Physical Effects Experiments..... 26

3.4 Analytical Instrumentation..... 28

3.5 Experimental Procedure for Chemical Effects Experiments..... 29

3.6 Experimental Procedure for Adsorption Experiments..... 32

4 MODEL FORMULATION AND SOLUTIONS..... 33

4.1 Problem Definition..... 34

4.2 Case I – Reaction in Closure, No Mass Transfer..... 36

4.3 Case II – No Reaction in Closure,

No Mass Transfer (Rectangular Geometry)..... 43

4.4 Case II – No Reaction in Closure,

No Mass Transfer (Spherical Geometry)..... 47

4.5 Case III – No Reaction in Closure, Mass Transfer..... 52

5 EXPERIMENTAL RESULTS & DISCUSSION..... 58

5.1 Particle Effects on Breakdown Voltage..... 58

5.2 Scanning Electron Microscopy Results..... 61

5.3 PIXE Analysis..... 63

5.4 Particle Effects on Reactor Power Consumption..... 64

5.5 Phenol Removal..... 69

5.6 Comparison of Experimental and Theoretical Results..... 75

6 CONCLUSIONS..... 79

7 DIRECTIONS FOR FURTHER STUDY..... 83

APPENDIX..... 136

REFERENCES..... 164

BIOGRAPHICAL SKETCH..... 169

LIST OF TABLES

Table		Page
1.	Comparison of the Constants for the 3 Model Cases.....	87
2.	Summary of Experimental Results (Physical Effects).....	88
3.	Elemental Analysis (PIXE) of Activated Carbon and Glass Spheres.	89
4.	Summary of Experimental Results (Chemical Effects).....	90
A1.	Power Consumption for 1 g/L Unwashed Carbon in DI Water.....	137
A2.	Power Consumption for 2 g/L Unwashed Carbon in DI Water.....	138
A3.	Power Consumption for No Particles and 140 μS/cm NaCl Solution	138
A4.	Power Consumption for 1 g/L Washed Carbon and 14 μS/cm NaCl Solution.....	139
A5.	Power Consumption for 2 g/L Washed Carbon and 14 μS/cm NaCl Solution.....	139
A6.	Power Consumption for 1 g/L Washed Carbon and 140 μS/cm NaCl Solution.....	140
A7.	Power Consumption for 2 g/L Washed Carbon and 140 μS/cm NaCl Solution.....	140
A8.	Power Consumption for 1 g/L Washed Glass Spheres and 14 μS/cm NaCl Solution.....	141
A9.	Power Consumption for 1 g/L Washed Glass Spheres and 140 μS/cm NaCl Solution.....	141

A10. Power Consumption for No Particles and 140 μS/cm $CaCl_2$ Solution..... 142

A11. Power Consumption for 1 g/L Washed Carbon and 14 μS/cm $CaCl_2$ Solution..... 142

A.12 Power Consumption for 2 g/L Washed Carbon and 14 μS/cm $CaCl_2$ Solution..... 143

A13. Power Consumption for 1 g/L Washed Carbon and 140 μS/cm $CaCl_2$ Solution..... 143

A14. Power Consumption for 2 g/L Washed Carbon and 140 μS/cm $CaCl_2$ Solution..... 144

A15. Power Consumption for 1 g/L Washed Glass Spheres and 14 μS/cm $CaCl_2$ Solution..... 144

A16. Power Consumption for 1 g/L Washed Glass Spheres and 140 μS/cm $CaCl_2$ Solution..... 145

A17. Power Consumption for No Particles and 140 μS/cm KCl Solution..... 145

A18. Power Consumption for 1 g/L Washed Carbon and 14 μS/cm KCl Solution..... 146

A.19 Power Consumption for 2 g/L Washed Carbon and 14 μS/cm KCl Solution..... 146

A20. Power Consumption for 1 g/L Washed Carbon and 140 μS/cm KCl Solution..... 147

A21. Power Consumption for 2 g/L Washed Carbon and 140 μS/cm KCl Solution..... 147

A22. Power Consumption for 1 g/L Washed Glass Spheres and 14 μS/cm KCl Solution..... 148

A23. Power Consumption for 1 g/L Washed Glass Spheres and 140 μS/cm KCl Solution..... 148

A24. 46 kV Corona Treatment with No Washed Carbon Phenol Removal..... 149

A25. 46 kV Corona Treatment with No Washed Carbon Catechol Formation..... 149

A26. 46 kV Corona Treatment with No Washed Carbon Hydroquinone Formation..... 150

A27. 46 kV Corona Treatment with No Washed Carbon Resorcinol Formation..... 150

A28. 57 kV Corona Treatment with No Washed Carbon Phenol Removal..... 151

A29. 57 kV Corona Treatment with No Washed Carbon Catechol Formation..... 151

A30. 57 kV Corona Treatment with No Washed Carbon Hydroquinone Formation..... 152

A31. 57 kV Corona Treatment with No Washed Carbon Resorcinol Formation..... 152

A32. 46 kV Corona Treatment with 1 g/L Washed Carbon Phenol Removal..... 153

A33. 46 kV Corona Treatment with 1 g/L Washed Carbon Catechol Formation 153

A34. 46 kV Corona Treatment with 1 g/L Washed Carbon Hydroquinone Formation 154

A35. 46 kV Corona Treatment with 1 g/L Washed Carbon Resorcinol Formation 154

A36. 57 kV Corona Treatment with 1 g/L Washed Carbon Phenol Removal..... 155

A37. 57 kV Corona Treatment with 1 g/L Washed Carbon Catechol Formation 154

A38. 57 kV Corona Treatment with 1 g/L Washed Carbon Hydroquinone Formation 156

A39. 57 kV Corona Treatment with 1 g/L Washed Carbon Resorcinol Formation 156

LIST OF FIGURES

Figure		Page
1.	Pulsed Power Supply Circuit Diagram.....	91
2.	Pulsed Power Supply, Voltage vs. Time Waveforms.....	92
3.	Liquid Phase Reactor I (Without Jacket).....	93
4.	Liquid Phase Reactor II (Jacketed Reactor).....	94
5.	The Effects of Surface Reactions on the Closure Problem ($k_p=10^{-5}s^{-1}$).....	95
6.	The Effects of Surface Reactions on the Closure Problem ($k_p=10^{-3}s^{-1}$).....	96
7.	The Effects of Surface Reactions on the Closure Problem ($k_p=10^{-1}s^{-1}$).....	97
8.	Rectangular vs. Spherical Geometry in Model Formulation.....	98
9.	The Effect of Mass Transfer Resistance on the Theoretical Model (K_{mt}= 1 m/s).....	99
10.	The Effect of Mass Transfer Resistance on the Theoretical Model (K_{mt}= 10^{-3} m/s).....	100
11.	The Effect of Mass Transfer Resistance on the Theoretical Model (K_{mt}=10^{-6} m/s).....	101
12.	The Effect of the Surface Reaction Rate on the Bulk Solution Concentration.....	102

13. Voltage Waveforms for Various Solutions..... 103

14. Current Waveforms for Deionized Water..... 104

15. The Effect of Particle Concentration on Breakdown Voltage..... 105

16. SEM Photograph of Unwashed Activated Carbon..... 106

17. SEM Photograph of Washed Activated Carbon..... 106

18. SEM Photograph of Unwashed Corona Treated Activated Carbon... 107

19. SEM Photograph of Washed Corona Treated Activated Carbon..... 107

20. The Effect of Washed Activated Carbon in a $CaCl_2$ Solution on the Reactor Power Consumption..... 108

21. The Effect of Washed Activated Carbon in a NaCl Solution on the Reactor Power Consumption..... 109

22. The Effect of Washed Activated Carbon in a KCl Solution on the Reactor Power Consumption..... 110

23. The Effect of Different Salt Solutions on the Reactor Power Consumption..... 111

24. The Effect of Different Salt Solutions and 1 g/L Washed Activated Carbon on the Reactor Power Consumption..... 112

25. The Effect of Different Salt Solutions and 2 g/L Washed Activated Carbon on the Reactor Power Consumption..... 113

26. The Effect of Different Salt Solutions and 1 g/L Washed Activated Carbon on the Reactor Power Consumption..... 114

27. The Effect of Different Salt Solutions and 2 g/L Washed Activated Carbon on the Reactor Power Consumption..... 115

28. The Comparison of Unwashed Activated Carbon and Washed Activated Carbon in a KCl Solution on the Reactor Power Consumption..... 116

29. The Effect of Different Salt Solutions and 1 g/L Washed Glass Spheres on the Reactor Power Consumption..... 117

30. The Rate of Phenol Adsorption onto 1 g/L Washed Activated Carbon..... 118

31. The Degradation of Phenol at 46 kV..... 119

32. The Degradation of Phenol at 57 kV..... 120

33. Phenol Removal at 46 kV with and without 1 g/L Washed Activated Carbon..... 121

34. The Degradation of Phenol at 46 kV and 1 g/L Washed Activated Carbon..... 122

35. Phenol Removal at 57 kV with and without 1 g/L Washed Activated Carbon..... 123

36. The Degradation of Phenol at 57 kV and 1 g/L Washed Activated Carbon..... 124

37. Catechol Formation at Various Conditions..... 125

38. Resorcinol Formation at Various Conditions..... 126

39. Hydroquinone Formation at Various Conditions..... 127

40. Byproduct Formation at 57 kV and 1 g/L Washed Activated Carbon..... 128

41. Phenol Adsorption Equilibrium onto 1 g/L Washed Activated Carbon..... 129

42. Rate Determination for Phenol Decomposition at 46 kV..... 130

43. Rate Determination for Phenol Decomposition at 57 kV..... 131

44. The Comparison of Experimental and Theoretical Results at 46 kV..... 132

45. The Comparison of Experimental and Theoretical Results at 57 kV..... 133

46. The Comparison of Experimental and Theoretical Results at 46 kV and 1 g/L Washed Activated Carbon (k_p= 0.00045 s^{-1})..... 134

47. The Comparison of Experimental and Theoretical Results at 57 kV and 1 g/L Washed Activated Carbon (k_p= 0.00175 s^{-1})..... 135

A1. HPLC Calibration for Phenol..... 160

A2. HPLC Calibration for Catechol..... 161

A3. HPLC Calibration for Hydroquinone..... 162

A4. HPLC Calibration for Resorcinol..... 163

ABSTRACT

Pulsed streamer corona technology utilizes a non-thermal plasma high voltage discharge to break down various airborne and aqueous phase organic pollutants. Pulsed streamer corona discharge in a reactor using a point-to-plane electrode geometry has been studied with well-mixed aqueous solutions containing various salts (sodium chloride, potassium chloride, and calcium chloride) and particles in suspension (powdered activated carbon, porous silica gel, non-porous glass spheres, and elemental copper). The result that solution conductivity governs the electrode breakdown voltage is independent of both the salt composition and the particle properties (i.e., total surface area, particle size, conductivity, and dielectric constant). Powdered activated carbon in aqueous suspension also dramatically reduces the reactor electric power as a function of applied voltage. Elemental analysis using PIXE (proton-induced x-ray emission) of the activated carbon and the water leachate from washed activated carbon, coupled with pulsed corona treatment experiments using washed activated carbon, show that interactions of activated carbon with potassium salts are responsible for the lower reactor power. With the lower power consumption, greater amounts of contaminants can be removed at a lower power usage. The combination of pulsed corona and activated carbon enhances phenol removal through bulk reactions, adsorption, and corona-induced surface reactions.

Primary oxidation products of phenol were also measured. A reaction and diffusion model was derived to analyze the phenol decomposition with combined bulk liquid and particle surface reactions.

CHAPTER 1

INTRODUCTION

Recently, there has been an increased interest in the efficient and cost effective removal of organic contaminants from groundwater and wastewater. Hazardous organic contaminants such as phenol, benzene, and PCBs are found in surface and subsoil water sources and also in treated sewage effluent. Several sources contribute to this problem including leaking petroleum tanks, landfill and cropland runoff, and illegal industrial waste dumping. Federal and state laws now mandate that these contaminants be removed and that clean water be returned to the environment.

Investigations in the field of removing organic contaminants from aqueous solutions have included using advanced oxidation technologies such as direct ozonation (Eisenhauer, 1968, Neigowski, 1953), supercritical oxidation (Krajnc, et al., 1996, Thornton, et al., 1992, Thornton et al., 1991), UV photolysis (Sun, et al., 1993), and ultrasonification (Pétrier, et al., 1994). Over the past decade, another technology involving the use of a pulsed streamer corona discharge in the liquid phase (Clements et al., 1985; Sharma et al., 1993; Joshi et al., 1995; Goheen et al., 1992) has been found to be an effective way to remove organic contaminants from aqueous solutions. This technique utilizes chemical radicals and highly reactive

molecules (e^-, •OH, H•, H_2O_2, O_3) produced from a pulsed streamer corona discharge that is sustained in an aqueous phase medium. Preliminary studies at the FAMU-FSU College of Engineering have demonstrated the complete degradation of phenol in solution (Sharma, 1993), and the determination of the rates of formation of hydrogen peroxide, hydroxyl radicals, and aqueous electrons (Joshi, 1994). Elsewhere, activated carbon has been used previously to adsorb organic compounds from both gas-phase and liquid-phase waste streams (Bansal, et al., 1988, Brandt, et al., 1988).

1.1 Research Objectives

The principal objective of the present work is to investigate the effects of the addition of several different types of particles to the aqueous phase pulsed streamer corona reactor, concentrating on both the physical and chemical characteristics of the discharge. It has been observed in our laboratory that the addition of particles to a test solution affects the physical characteristics (i.e., streamer length, intensity, number of streamers, and breakdown voltage) of the streamer corona discharge. The particles used for this investigation included activated carbon, solid glass spheres, porous silica gel, and elemental copper dust. The activated carbon and the glass spheres were also suspended in various salt solutions. The different salt solutions used were potassium chloride, calcium chloride, and sodium chloride.

To investigate the chemical effects of the added carbon particles, experiments were conducted to measure the degradation of phenol in the corona reactor. These phenol experiments were conducted at several applied voltages as well as by varying the amount of the washed activated carbon suspended in the reactor. Theoretical models for the bulk and particle phase reaction and diffusion in the particle were

derived, solved using averaging methods, and the solutions were compared to the experimental results.

In this thesis, a literature review in Chapter II will give the background of the pulsed corona process. The experimental equipment, methods, and procedures will be discussed in Chapter III. In Chapter IV, a model of the bulk and surface reactions and diffusion in the particle will be given. The results of a number of experiments will be presented and discussed in Chapter V. Chapter VI will give the conclusions and Chapter VII will discuss future experimental and theoretical work.

CHAPTER 2

LITERATURE REVIEW

2.1 Corona Discharge

A corona is a type of electrical discharge. It is formed when an electric potential is applied between two non-uniform electrodes where a dielectric medium is placed between the electrodes. The electrical discharge occurs in the dielectric medium between the electrodes. Corona onset begins when the discharge initiates in the dielectric medium. The corona onset voltage depends on the type of electrodes used as well as on the physical properties of the dielectric material between the two electrodes. At voltages greater than the onset voltage, a corona is formed. As the applied voltage increases, the corona discharge grows in size. At dielectric breakdown, the applied voltage is high enough to produce a direct current channel (spark) that bridges the two electrodes. At the breakdown voltage, the system essentially short-circuits. The breakdown voltage is also dependent upon the geometry of the electrodes as well as on the physical properties of the dielectric medium.

2.2 Types of Corona Discharge

There are several different types of corona discharges (summarized by Sharma, 1993, Creyghton, 1994, Kalyana, 1997). These corona discharges can be either negative or positive polarity, and have one of several electrode geometries, point to plane and wire to cylinder being the most prominent. These corona discharges can be produced in any insulating medium such as air, water, transformer oils, and liquid hydrocarbons. For most electrode configurations with a positive polarity electrical field, the corona discharge starts as a burst pulsed corona. As the electrical field increases, the discharge becomes a streamer corona and finally a single spark bridges the gap between the two electrodes (Chang et al., 1991). If the electric field has negative polarity for a point to plane electrode geometry, the corona discharge starts as a Trichel pulse corona and proceeds to a glow corona, pulseless corona, and then a spark discharge where dielectric breakdown occurs at a high enough applied electric field. The Trichel pulse corona initiates with a pulse repetition of 2 kHz when the negative polarity electrical field is high enough to produce ionization. This type of corona is very uniform in its discharge repetition rate as well as the size and magnitude of the corona discharge.

2.3 Applications of Pulsed Electrical Discharges

Pulsed corona discharges are under extensive investigation and development in the field of air and water pollution remediation. Gas-phase pulsed corona discharges have been shown to remove NO_x and SO_x from industrial waste streams (Kalyana, 1996, Clements et al, 1989). In the liquid-phase, pulsed corona discharges have been shown to remove several organic species such as phenol, methylene blue,

toluene, and benzene from wastewater streams (Sharma, et al., 1993, Goheen et al., 1992, Lubicki et al., 1996b). In the aqueous phase, it is assumed that the pulsed corona discharge injects electrons into the solution. The injected electrons then collide with the water molecules. If the energy of the electrons is high enough, the water molecule is broken apart forming a hydrogen atom and a hydroxyl radical. The hydroxyl radicals are highly oxidizing; however, they also quickly combine to form hydrogen peroxide.

Pulsed corona discharges have been shown to be useful in the degradation of organic dyes (Goheen et al., 1992). A reduction in the color of methylene blue, malachite green and new coccine was observed after pulsed corona treatment. This reactor had a point-to-plane geometry where the point electrode was in the gas phase directly above the liquid and the liquid surface served as the ground electrode. The applied voltage, the discharge current, the electrode spacing, and the oxygen composition in the gas phase affected the removal of the dyes. Increasing the applied voltage and shortening the electrode gap distance increases the electric field. The increased applied voltage led to more electrons that were injected into the gas phase, resulting in more formation of reactive species. At high oxygen composition in the gas phase, significant quantities of ozone were produced. This ozone then diffused into the liquid phase and reacted either directly with the organic or producing a hydroxyl radical. The hydroxyl radical then attacked the organic dyes.

This work was continued by Sharma et al., (1997) where the group investigated the formation of ozone in the gas phase and measured the nitric acid formed in the aqueous phase. The ozone is produced in the gas phase and then

dissolved into the aqueous phase. Ozone was concluded to be the major oxidant in the solution phase. The group also optimized the point-to-plane gap distance to be 1.5 cm and gave results for the oxidation of methylene blue and carbon tetrachloride.

Similar to the works by Goheen et al., (1992) and Sharma et al., (1997), Hoeben et al., (1997) used a pulsed electric discharge where the discharge electrode was located above the surface of the aqueous solution. This group used 31 point electrodes instead of a single discharge electrode. Hoeben et al., looked at the removal of phenol and atrazine in aqueous solutions using this electrode configuration. At an applied voltage pulse of 30 kV and a pulse frequency of 50 Hz, 90% of the phenol was converted to oxidation products in 100 minutes and 50% of the atrazine was removed in 300 minutes. The proposed reaction pathways were hydroxyl radials attacks, but the results from Sharma et al., (1997) indicate that dissolved ozone might be the primary oxidant in this case.

Creyghton (1997a) conducted experiments using electrode configurations where the discharge electrode was submerged in the aqueous solution and also where the discharge was located in air above the liquid. For both discharge electrode positions, the opposite electrode was separated from the water using a glass insulator. When the discharge electrode was immersed in the liquid, oxygen was bubbled in through a hollow discharge needle. This led to the production of hydroxyl radicals in the aqueous phase as well as ozone produced in the gas bubbles that absorb into the aqueous phase. When the discharge electrode was oriented in the gas phase, surface streamers were observed.

The destruction of different particles has been investigated using a pulsed corona (Mikula, et al., 1997). This group investigated the effects of a pulsed electrical discharge on the shattering of titanium dioxide particles and different wood particles such as pine needles and sawdust. The electric discharge occurred between point electrodes (with an electrode radius of 2.5 mm) and a gap distance of 7 mm. The pulsed discharge increased the number of titanium dioxide particles and reduced the size of these particles. Also, the wood products were broken down. In the sawdust, acid hydrolysis increased with an increase in the number of pulses applied, indicating that there was a larger surface area resulting more micropores were available for the acid to attack. The destruction was attributed to the discharge creating shock waves and sound waves.

A pulsed streamer corona has also been investigated for the inactivation of microorganisms (Sato et al., 1996). The reactor used had a point-to-plane electrode geometry with a 5 cm electrode gap distance, with both electrodes in the aqueous phase. Sato investigated the lethal effects of the pulsed corona for yeast cells at an applied voltage of 19 kV and a pulse frequency of 50 Hz. He showed that as time was increased, the survival of the yeast cells decreases. Sato concluded that the destruction of the yeast cells was due to reactions of the hydrogen peroxide with the cell membrane.

One of the factors affecting the effectiveness of these processes is the voltage at which the electrode system reaches electrical breakdown. This phenomenon occurs when the voltage applied to the system is large enough to bridge the two electrodes and cause the system to break down. For more conducting liquids such as water, the

breakdown strength of the liquid (the lowest applied electric field that would cause complete breakdown) is lower than that of more insulating liquids such as transformer oil.

At applied fields of less than the breakdown strength of the liquid, prebreakdown phenomena are observed. This manifests itself as a partial discharge, or streamer, that does not completely bridge the two electrodes. This prebreakdown phenomenon is also observed before the electrical breakdown occurs. Electrical breakdown can be affected by the temperature and pressure of the system, the conductivity of the solution, the particles found in the solution, and the electric field applied to the solution.

Lubicki, et al. (1996a,b) investigated the feasibility of using a pulsed electric discharge in water as a sterilization process. In this investigation, they looked at the effect of solution conductivity on the breakdown voltage of the solution. The conclusion from this work is that the breakdown voltage decreased for increasing conductivity. The salt used was copper sulfate.

Another group investigating water sterilization was Mizuno et al. (1990). This group investigated the inactivation of viruses using pulsed high electric fields. Virus inactivation was observed at applied electric fields of 30 kV/cm applied between 60-120 pulses. Using an electron microscope, the core of the virus containing RNA and DNA was damaged by the electrical discharges.

2.4 Electrical Breakdown Theories for Liquids

Creyghton (1994) summarized many different models on how streamers are formed in the gas phase. Streamers are a single discharge channel

emanating from the high voltage electrode. Creyghton also discusses the maximum stable electrical field in gas phase discharge. When the electric field applied to a system is higher than the maximum stable field, the primary streamer reaches the anode and a secondary streamer is formed. He refers to this secondary streamer as an arc, which is considered to be the electrical breakdown or breakdown. The conditions that govern the maximum stabile field are the charge density of the medium, the electric field, and the propagation velocity of the streamer. It is possible that additional parameters as well as those proposed for the gas phase discharges also govern the breakdown in the liquid phase.

There are several theories on the electrical breakdown of liquids. First, there is the hypothesis of a thermal breakdown that is usually associated with pulsed electric fields of a microsecond or longer. The electric breakdown theory is associated with pulsed input of less than one microsecond pulse width for liquids with high electron mobility such as the liquid noble gasses. Both have been proposed as mechanisms for electrical breakdown but neither has been proven exclusively (Sharbaugh, et al., 1978). Techniques such as oscilloscope traces, shadowgraph photography, and ultrafast photography have been employed to further investigate both of these phenomena (Klimkin, 1981, Klimkin, 1990, Klimkin, 1992, Klimkin, et al., 1979, Kuskova, 1983, Wong et al., 1977). In the following paragraphs, a summary will be given for each of these breakdown mechanisms and will also discuss some of the physical principles involved.

In the thermal breakdown mechanism theory, the electric pulse heats the liquid to form bubbles and then a Townsend electron avalanche causes the discharge

in the gas (bubble) phase (Devins, et al., 1981). Several experimental results would tend to favor this theory. It has been shown experimentally that the breakdown strength of liquids decreases with increased temperature (Kok, 1961). Bubbles will form in the liquid if the local temperature of the liquid causes the liquid to boil and thus form the micro-bubbles where the gas phase discharge would take place.

Sharbough (1978) first estimated the heat input, W (units of energy per unit volume per unit time), to 1 cm^3 of hexane liquid per microsecond of applied voltage (Devins, et al., 1981). For hexane the breakdown field is about 1.6 $MVcm^{-1}$. The current density, j, in the liquid has been measured to be on the order of 1 to 10 Acm^{-2}. Then,

$$W = E_{local}\, j_{local} \qquad (2.1)$$

and

$$W = 20 \text{ cal } cm^{-3}\, \mu s^{-1} = 40 \text{ cal } g^{-1}\, \mu s^{-1} \qquad (2.2)$$

The amount of heat required to increase the temperature of m grams of liquid from the ambient temperature T_a to the boiling point T_b and then to vaporize it is

$$\Delta H = m[c_p\,(T_b - T_a) + L_b] = 100 \text{ cal } g^{-1} \qquad (2.3)$$

where c_p is the average specific heat and L_b is the latent heat of vaporization. This equation has been calculated for hexane. Thus, for hexane, if the voltage pulse duration is more then 2.5 μs, there is enough energy for the formation of a vapor bubble.

For water, the breakdown voltage is 300 kV/cm (Jones and Kunhardt, 1995a) and the average power density applied to an electrical discharge is on the order of 10^8 Wcm^{-3} of 24 cal $g^{-1}\mu s^{-1}$. The energy required for vapor bubble formation is

619 cal g^{-1}, which would indicate that the pulse would need to be 26 μs long to form a vapor bubble. When the applied voltage is introduced to a liquid at a higher temperature, the heat necessary to form a vapor phase is less due to a decreasing difference between ambient and boiling temperature. Thus, the bubble forms sooner and the electron avalanche forms much quicker, leading to lower breakdown strength as the temperature rises.

It has been shown experimentally that the breakdown strength of liquids increases as the ambient pressure increases (Jones and Kunhardt, 1995b). From the argument used in the previous paragraph, the breakdown strength decreased due to the temperature of the liquid increasing. If the liquid was kept at a constant temperature and the pressure was increased, the boiling point would then rise with the pressure. This increased boiling temperature would then increase the difference between the boiling point and the ambient temperature. With this increase in boiling point, it would require more energy to heat and vaporize the liquid, requiring the electric discharge to have a longer pulse width. This effect of increasing pressure would then cause the breakdown strength of the liquid to increase.

Other evidence supporting the role of bubble formation involves ultra fast photography and shadowgraph techniques (Klimkin, 1981, Klimkin, 1990, Klimkin, 1992, Klimkin, et al., 1979). In some studies, shock waves were observed using a Schlieren system, possibly indicating the formation of a gaseous cavity (Klimkin, 1992). Sonic, current, and light signals occur simultaneous with the onset of breakdown (Klimkin, 1990). It is believed that the sonic signal comes from the gas phase and the light signals are then produced by electrical discharges in the gas phase.

Prebreakdown streamers were observed to scatter light and to decay into large bubbles as time went on. For viscous liquids, the electrical discharge was observed microscopically and the formation and growth of a gas bubble was observed.

There are discrepancies in the thermal bubble mechanism. In the observations of the scattered light, the time at which the light occurred was 5 μs after the applied discharge. This mechanism says nothing about how the bubbles precede or follow local breakdown. It is still not clear whether the bubbles lead to breakdown or if the breakdown leads to bubbles. The Townsend electron avalanche theory developed for gas phase discharge predicts that the discharge initiates from the cathode, whereas the discharge in the liquid phase initiates from the anode. Further, the temperature dependence of the intensity of the light pulses is opposite to that expected for a change in surface (expansion of a bubble).

As stated above, the theory of thermal bubble formation does not explain dielectric breakdown in liquids where the applied voltage is sustained for less than a microsecond. The other common theory is more of an electric method (Wong, et al., 1977). This theory assumes that the current is initiated from the field emission and then current grows by electron multiplication, similar to that of the Townsend breakdown in gases, but occurring in the liquid. The resulting positive ions enhance the cathodic field and lead to extremely high currents. Once the electrons are injected into the liquid, they gain strength from the applied electric field. It is assumed that the field is high enough that the electrons will gain more energy from the field than they will lose in non-ionizing molecular collisions with the liquid. These electrons then gain enough energy to start to ionize the liquid molecules and then form the

electron avalanche. The energy of the electron is highly dependent on the mean free path of the electron. When this number is low, there will be higher energy losses from non-ionizing collisions. Likewise, the higher the mean free path, the longer the applied field has to energize the electron before it ionizes a molecule.

Again, there has been experimental data in support of the electric breakdown theory. There has been experimental evidence of electrons having energies higher than 2.5 eV from the emission of light under high electrical stress (Kok, 1961). This electron energy is high enough to cause the liquid molecules to ionize. This is evidence for the production of highly energetic electrons, but it does not differentiate between electrons produced in a gas or a liquid.

Furthermore, there is experimental evidence that when the phase is changed from a liquid to a gas at the critical temperature in SF_6, CO_2, and hexane, there is continuity in the breakdown strength (Sharbaugh et al., 1978). The breakdown strength is a measure of the liquid breakdown voltage. The higher the breakdown strength for a given liquid medium, the higher the applied voltage is necessary to cause breakdown. This indicates that the mechanism for the breakdown is the same for both phases, and gives some credence to the electric effect because in both the gas phase and the liquid phase both have collisional ionization mechanisms (electron avalanches). This collisional ionization has also been observed in monatomic molecules such as Xenon and liquid Argon. It is thought that polyatomic molecules such as hydrocarbons would cause higher electron energy losses and might allow the creation of high-energy electrons necessary for the electron avalanche.

Experimental evidence that does not support the electric theory of breakdown has also been shown. The theory does not deal with the pressure dependence consistently. Even with high-pressure changes in the liquid, the mean free path should not change very much for a nearly incompressible fluid and thus the electric strength of the liquid should not change very much. For a change of 25 atm, the breakdown strength increases about 50% for hydrocarbons.

Another theory of the liquid breakdown is the suspended particle theory (Kok, 1961, Zhekul, 1983). Many liquids such as transformer oil contain high levels of particles on the order of 1 μm and smaller. They are present in virtually all liquids at some size and concentration. This theory bases the liquid breakdown process on particle interactions with the electrical field. The suspended particles are assumed to have a dielectric constant that is larger than that of the liquid. As a result of an applied electrical field, the electrical forces in the direction of the electrical stresses move the particles. Eventually, the particles will form a "string" that will connect the anode and the cathode and a discharge will take place along this path. This theory is dependent upon the size and concentration of the particles, the viscosity of the liquid, and the duration of the electric pulse. The size of the particles as well as the viscosity of the liquid determines the friction losses of the particle motion through the liquid. The duration of the electric pulse affects the time allowed for the electrophoretic motion of the particle. This process has been shown experimentally in some systems of transformer oil with added metallic particles. Although there is electrophoretic motion of particles in virtually every liquid system, it does not predict the observed dependence of temperature on the breakdown strength of the liquid.

Recently, Jones and Kunhardt have described a model focusing on the time from the voltage pulse initiation to breakdown (Jones and Kunhardt, 1995a). The features of this model start with the formation of a low-density region like a bubble. This bubble is formed by nucleation near one of the electrodes where local heating is taking place due to high electric field currents. Then, an electron avalanche develops when the density of the bubbles reach a critical value, N_c , which is 10^{20} cm^{-3}. When the local field caused by the avalanche reaches the magnitude of the applied field, it hinders growth of the avalanche. As the electron avalanche grows, the electrons heat the region as they propagate, and thus lower the density of the area that they are growing into. This then allows for the electron avalanche to begin again in a new region. This cycle of local heating, density lowering, electron avalanche growth, and retardation then propagates the front across the gap. The time lag before breakdown is broken up into four different times. These are

$$\tau_{bd} = \tau_{nuc} + \tau_{ex} + \tau_{\alpha r} + \tau_r \qquad (2.4)$$

where τ_{bd} is the time to breakdown, τ_{nuc} is the time for the heating of the liquid and the formation of a nucleation site , τ_{ex} is the time for the growth and expansion of the nucleation site until it reaches the critical density (N_c) so that electron ionization can take place, and $\tau_{\alpha r}$ is the time for the growth of the electron avalanche until the local space charge retards its growth. τ_r is the time for the interval between the retardation of the bubble in which the electron avalanche takes place and than the subsequent bridging of the gap by the propagation of the ionizing front.

Electrons ahead of the ionization front are continuously injected into the liquid side of the interface. These electrons then heat the liquid, causing nucleation

and growth, and then cause the electron avalanche to occur ahead of the front. The power deposited by these electrons is dependent on the trailing ionization column because this determines the energy flow from the electrode. Thus the resistance of the trailing column determines the heating rate of the liquid just ahead of the ionization front, and thus the speed of the ionization front. The rate of growth of the electron density at the front is determined by the ionization time, $\tau_I \approx 1/(\alpha v_d)$, where v_d is the electron drift velocity. Again with the parameters used above, the time is on the order of picoseconds. This would then lead to a growth in the ionization time τ_i. Jones concludes that the growth observed experimentally is much slower than this, and thus the heating of the liquid ahead of the ionization front needs additional time.

2.5 The Oxidation of Phenol

Phenol oxidation is a very well studied process. Phenol degradation has been observed in supercritical water (Thornton, et al., 1991, Thornton et al., 1992, Krajnc, et al., 1996), by sonication (Pétrier, et al., 1994), by ozonation (Niegowski, 1953, Eisenhauer, 1968), by UV photolysis (Sun, et al., 1993), and by pulsed streamer corona (Sharma et al., 1993). In most of these works, the oxidation of phenol was achieved through reaction with a hydroxyl radical. The hydroxyl radical electrophillically attacks the phenol to form the primary products catechol, resorcinol, and hydroquinone. The hydroxyl radical then reacts with the primary products to produce muconic and fumuric acids as well as other organic acids. These organic acids then get oxidized to form the smaller organic acids such as oxalic and formic acid. The final end products of the hydroxyl radical oxidation of phenol are carbon dioxide and water.

In the pulsed streamer corona, hydroxyl radicals are produced as well as high concentrations of hydrogen peroxide. Fenton's reaction has been used in several works (Joshi, 1994, Joshi, et al., 1995, Sharma, 1993, Sharma et al., 1993, Sun, et al., 1993, Zepp, et al., 1992) to convert hydrogen peroxide to hydroxyl radical using the following reactions

$$Fe^{++} + H_2O_2 \xrightarrow{h\nu} OH\bullet + OH^- + Fe^{+++}, \qquad (2.5)$$

which is the Fenton's reaction and

$$H_2O_2 \xrightarrow{h\nu} 2OH\bullet \qquad (2.6)$$

which is the photo-Fenton's reaction. These reactions have been shown to work best at low pH. Both reactions have been observed in UV photolysis where hydrogen peroxide is injected into the waste stream and subjected to UV light ((Sun, et al., 1993, Zepp et al., 1992).

Fenton's reaction has also been shown to occur in pulsed streamer corona (Sharma et al., 1993, Joshi et al., 1995). Without the addition of ferrous ions to promote Fenton's reaction, there was little degradation of phenol. With ferrous ions added, significant degradation of phenol occurred.

2.6 Activated Carbon

Activated carbon is a form of carbon that has been treated to have a very high porosity. The raw materials used most for the processing of activated carbon are lignite, coal, wood, coconut shells, and petroleum residues (Kinoshita, 1988). These materials are carbonized by heating them in the absence of oxygen. These particles

are then activated by chemical activation or gas activation. Chemical activation involves the addition of inorganic chemicals to the raw materials during carbonization to dehydrate the organic molecules. Gas activation requires that the carbonized substance be heated in steam to oxidize the surface sites. There is a large concentration of ash (15 –20%) left in the activated carbon after processing. This ash is usually water soluble and composed of aluminum, iron, magnesium, and calcium silicates.

The process used to make activated carbons leads to particles with very high total surface area ranging from 450 m^2/g to over 1500 m^2/g (Kinoshita, 1988, Bansal, et al., 1988). The pore size is typically in the range of 1 – 100 nm in diameter. The different pore diameters correspond to different applications. For example, the smaller pore sizes would be used in gas phase applications and the larger pore sizes would be used for liquid phase applications.

Activated carbons are used for the removal of organic pollutants from air and water (Jankowska, et al., 1991, Bansal, et al., 1988). This is due to the fact that activated carbon is a superb adsorbent. Other applications of activated carbon include solvent recovery, deodorizing, decolorizing, and gas separation. Most of these processes require that after the activated carbon has been used, it must be regenerated. This is sometimes accomplished by heating the carbon and burning off the adsorbed materials.

Activated carbon has been shown to decompose hydrogen peroxide in an electrochemical process (Bansal, et al., 1988, Jankowska, et al., 1991). This decomposition occurs both on the surface of the carbon as well as in the solution.

The rate at which this happens increases with increasing pH as well as with increasing temperature. Experimental evidence has shown that when activated carbon is given an electrical potential (i.e., as an electrode in an electrochemical system), it can oxidize ferrous ions to ferric ion as follows,

$$Fe^{2+} \rightarrow Fe^{3+} + e^{-} \qquad (2.7)$$

(Bansal, et al,. 1988). This oxidation might lessen the effects of Fenton's reaction in the solution.

Little work has been done to study reactions of organic species occurring on the surface of the activated carbon. Vidic et al. (1993) reported the polymerization of phenol on the surface of activated carbon. This occurred only for the case where molecular oxygen was present in the system. This polymerization increased the adsorption capacity of the activated carbon. The amount of polymerization of phenol adsorbed on to the surface of the activated carbon was dependent on the amount of oxygen present.

Logemann et al., (1997) uses a catalyst to promote advanced oxidation reactions on the surface of a catalyst with the brand name ECOCLEAR. The composition of the catalyst is not given but the material has high adsorptive properties. The ECOCLEAR process involves a bed of the catalyst upon which the contaminated liquid is circulated. Ozone is then bubbled into the reaction chamber. It is postulated that the ozone is adsorbed onto the catalyst surface as an $O\bullet^{-}$ radical and then reacts with an adjacent contaminant adsorbed on the surface of the ECOCLEAR. Arguments are given that the process does not use hydroxyl radicals

and that the reaction takes place on the surface of the catalyst, although the supporting evidence does not necessarily agree.

Hydroxyl radicals are easily formed at high pH but do not form as readily at lower pH. Experiments were conducted at three different pH values where at low pH, the decolorization of sulfuric acid was studied, and at neutral and high pH, the removal of COD and AOX from industrial waste streams was conducted to see if hydroxyl radicals played any part in the reaction. At the low pH, the time to reach 94% removal was 7.7 h at a 1.0 g/L ozone dose, and 16.7 h at a 1.9 g/L ozone dose. At the neutral pH, it took 3.8 h to convert 44% of the COD and 63% of the AOX at a 1.4 g/L ozone dose. At the high pH, 46% COD conversion and 81% AOX conversion were achieved in 3.1 h at an ozone dose of 1.6 g/L. It is difficult to conclude the effect of pH because more than one variable is changing from one experiment to the next, but it seems that the reaction takes place much slower at the low pH and increases as the pH is increased, indicating that hydroxyl radicals might be present in the reaction. The increase in reaction time with an increase in ozone dose at the lower pH might also indicate that the reaction does not depend on the amount of ozone present, which would contradict the proposed mechanism of reaction.

The authors also conclude that the reactions take place on the surface of the catalyst because solution temperature does not have much effect on the rate of conversion. They reported an experiment that observed the decolorization of a waste stream at 20°C and 80°C. With similar ozone doses, the color removal was 100% after 1.3 h at 80°C and 98% after 2.4 h at 20°C. This indicates that the reaction proceeds twice as fast at the higher temperatures, which might indicate that the

reactions take place in the liquid phase according to the author's arguments. The process in which this reaction takes place is difficult to evaluate with the data given, the lack of information on the catalyst, and without the analysis of the reaction products.

CHAPTER 3

EXPERIMENTAL METHODS

3.1 Pulsed Power Supply

A schematic of the pulsed power supply used is shown in Figure 1. The unit is composed of two modules: 1) a commercial transformer-rectifier, and 2) a pulse forming network. The transformer- rectifier is a Universal Voltronics 0-100 kV DC, 50 mA high voltage power supply. The transformer-rectifier set uses a 208 V, single phase alternating current input. Internal rectifiers were removed from the circuit, giving a 0-100 kV AC variable voltage output.

The second module takes the AC voltage from the transformer-rectifier set and forms a short pulsed voltage output. The transformer-rectifier high voltage first goes through a series of high voltage resistors that limits the current that goes through the rest of the circuit. A series of diodes then half-wave rectifies the alternating current source. An array of capacitors (2700 pF) stores the charge. Connected next in the circuit is a rotating rod high voltage spark gap that rotates at 1800 rpm, which aligns the rod electrode with the two sphere electrodes twice in each rotation, leading to an alignment frequency of 60 Hz. When the spark gap aligns, the charge stored in the capacitors is discharged across the gap and sent into the liquid-phase reactor. The

pulsed corona is then formed discharging from the high voltage point electrode, and the discharge grows towards the ground plane electrode.

Figure 2 shows the transformation of the voltage waveform within the pulse forming circuit. Entering the pulse forming circuit is an alternating current voltage waveform that is a typical sinusoidal wave. After leaving the diodes, the voltage waveform becomes half-wave rectified. At this point, the negative component of the sinusoidal wave is removed. During the cycle when the spark gap is not aligned, the capacitors charge. As the spark gap aligns, the capacitors discharge across the gap into the reactor. As indicated, the expected voltage pulse has a very fast rise time on the order of 20 ns, and then an exponential decay. The voltage pulse width is dependent on the type of solution in the reactor and is in the range of 1 μs to 1 ms.

3.2 Pulsed Corona Reactor

The pulsed corona reactor shown in Figure 3 was used for investigating the physical effects of the addition of the various particles to aqueous solutions. This reactor consisted of a 1 L glass vessel with an opening, ported top. The high voltage input for the discharge point electrode comes in at the top of the reactor through a glass U-tube. Inside of the reactor, the end of the high voltage wire inside the U-tube is attached to a hypodermic needle with a mechanically sharpened tip. The high-voltage pulse is discharged into the solution at this point electrode. The stainless steel ground plane is located in the solution 5 cm directly above the point electrode. The ground plate is attached to an earth ground. There is a magnetic stirrer at the bottom of the reactor vessel to ensure a well-mixed solution. This reactor did not have any cooling mechanism to keep the reactor at constant temperature. This was not needed

due to the very short duration of the experiments carried out in this reactor. The temperature of the solutions during these experiments varied only 1-3 °C.

The pulsed corona reactor shown in Figure 4 was used for the experiments investigating the chemical effects of the addition of activated carbon and various salts to aqueous solutions. The reactor consists of a 1 L glass vessel with an opening, ported top that also had an outer water jacket to keep the solution at a constant temperature. The cooling water flowed around the jacket and kept the temperature of the reactor vessel at 20.0 °C. High voltage is introduced into the reactor through a glass tube penetrating the reactor side wall. The tube enters the reactor and bends at a 90° angle at the center towards the top of the reactor. At the end of this tube, a fitted glass cap contains a mechanically sharpened 1mm diameter stainless steel wire. Again, this point electrode is connected to high voltage. The stainless steel ground plane electrode is located in the solution 5 cm directly above the point electrode. This ground electrode is attached to an earth ground. There is a magnetic stirring bar at the bottom of the reactor to keep the solution well mixed. There are three open ports on the lid of the reactor used for taking samples during the experiments.

The particles used in this study were activated carbon (obtained from Fisher Scientific, 75 – 300 μm particle size), spherical silica glass beads (obtained from Potter Industries, 110-180 μm diameter, 53-78 μm diameter, 30-60 μm diameter, and 25 μm and finer diameter particle size), porous silica gel (Supelco, Davison Grade 12 mesh size 100/120), and copper particles (Fisher, 35-40 μm diameter particle size). The activated carbon and the smallest size glass spheres were used both in an

unwashed and a washed state. The unwashed particles were used in the state that they were supplied. The washed particles were thoroughly rinsed before use. The treatment consisted of adding 50 g of the particles to 5 L of deionized water and mixing the suspended particles for two hours. The particles were then filtered using 1 μm filter paper and dried at 105 °C. This process was repeated seven times at which point the wash solution conductivity was that of deionized water, or 1 μScm^{-1}, which indicated that all of the salts on the surface of the carbon washed off.

Salts were added to some experimental solutions to achieve certain solution conductivities. Other organic species were added to the solutions and particle suspensions for testing the removal fraction using pulsed streamer corona. The salts and other chemicals used throughout the study were reagent grade potassium chloride, calcium chloride, sodium chloride, ferrous sulfate, phenol, resorcinol, hydroquinone, catechol, acetic acid, and acetonitrile (all obtained from Fisher Scientific). All chemicals were used as they were received from the manufacturer.

3.3 Experimental Procedure for Physical Effects Experiments

To investigate the physical effects of the addition of particles on the pulsed streamer corona, the following procedure was used. First, 1 L of deionized water was added to the reactor. Then the desired amount of particles and salts were added to the deionized water and the magnetic stirrer was engaged to suspend the particles and mix the salt solution. Before pulsed corona treatment, initial measurements of conductivity (Cole-Parmer Model 1484-10 conductivity meter), pH (Fisher Accumet 950 pH meter), and temperature (standard mercury thermometer) were recorded.

The reactor was then connected to the high voltage pulsed power supply,

which was engaged and set to 10 kV dial voltage. Dial voltage is the pulsed voltage that is indicated on the front of the power supply. The dial voltage is not a true measurement of the actual pulsed voltage. At 10 kV, a Tektronix TDS 460 fast digital storage oscilloscope was used to analyze voltage and current waveform characteristics. A Tektronix P6015A high voltage probe wired in parallel with the input of the pulsed power to the reactor was attached to the oscilloscope to record the voltage waveform. The reactor current waveform was measured in series with the ground using a P6021 Tektronix current probe. The reactor electric power was calculated by integration of the product of voltage and current by the oscilloscope. The waveform properties analyzed were maximum peak pulsed voltage, voltage rise time, voltage pulse width, maximum current, and power, as well as the average current read on a dc ammeter. Visual observations of the streamer properties such as length, thickness, color, and quantity were also noted.

After these measurements were taken, the voltage was increased in increments of 2.5 kV. At each voltage step, the same measurements were taken. The voltage was increased until breakdown (or sparkover) between the point and plane electrodes were achieved. At this stage, a single spark bridges the two electrodes causing the system to short circuit. At breakdown, the voltage is quickly turned off in order to not damage any of the electrical circuitry. A the conclusion of each experiment, final readings of conductivity, pH, and temperature of the solution were measured.

For the investigation of the physical effects of the added particles, the following particles and salts were used. Aqueous suspensions of particles alone (no salts added) were conducted with 1, 2, 4, and 6 g of the unwashed activated carbon, 1,

and 2 g of the washed carbon, 1, 2, and 5 g of the ≤25 μm unwashed glass spheres, 1 and 2 g of the ≤25 μm washed glass spheres, 1 and 2 g of the 30 – 60 μm glass spheres, 1 and 2 g of the 52 – 78 μm glass spheres, 1 and 2 g of the 110 – 180 μm glass spheres, 1 and 2 g of the silica gel, and 2 and 5 g of the copper particles.

Salt solutions (without particles) were made with potassium chloride at 14 and 140 μScm^{-1} (adding 1 mL and 10 mL of a 0.1 M potassium chloride stock solution to 1 L deionized water), calcium chloride at 14 and 140 μScm^{-1} (adding 0.5 mL and 5 mL of a 0.1 M calcium chloride stock solution to 1 L deionized water), and sodium chloride at 14 and 140 μScm^{-1} (adding 1 mL and 10 mL of a 0.1 M sodium chloride stock solution to 1 L deionized water). Combinations of the salt solutions and the particles were made at both concentrations of the washed activated carbon and each of the six salt solutions individually. Additionally, experiments were done with the combination of both the ≤25 μm washed glass beads and each of the six salt solutions individually. All experiments were repeated at least three times to ensure that the error was less than 5-7 % (using a 95% confidence interval, see Appendix).

3.4 Analytical Instrumentation

Samples of 1) the unwashed activated carbon, 2) the solution resulting from the suspension of the unwashed activated carbon, and 3) the solution resulting from the suspension of the unwashed glass spheres were sent to PIXE Analytical Laboratories (1380 Blounstown Highway, Tallahassee, FL, 32304) for elemental analysis. PIXE is elemental analysis using proton induced x-ray emission. The solutions for the carbon and glass leachate were obtained from the first solution in the

washing procedure mentioned above. The carbon sample was sent in the form received from the manufacturer.

Scanning electron microscopy (SEM) was conducted on several activated carbon samples in the Department of Biological Sciences, Florida State University, Tallahassee, FL. Samples of unwashed activated carbon, washed activated carbon, corona treated unwashed activated carbon, and corona treated washed activated carbon were analyzed. The corona treatment consisted of suspending 1 g of the carbon in 1 L deionized water, and treating the solution at an applied voltage of 46 kV (maximum applied voltage) for 10 minutes. The carbon was then filtered out, dried, and sent for analysis. The SEM apparatus also had an x-ray emission apparatus incorporated with the SEM. The x-ray emissions qualitatively analyze the elements present on the surface of the carbon. The x-ray emissions apparatus was not calibrated to give quantitative results of the concentrations of these elements.

3.5 Experimental Procedure for Chemical Effects Experiments

To investigate the effects of the activated carbon particles on the chemistry of the induced reactions, a Perkin-Elmer HPLC was used for the analysis. Aqueous samples were injected into a Supelcosil C18 column (25.0 cm X 4.6 mm) in a mobile phase of 0.5% acetic acid, 5.0% acetonitrile, and 94.5% deionized water. The flow rate of the mobile phase was 1.0 mL per minute. A Perkin-Elmer LC80 Spectrophotometer attached to the HPLC analyzed the separated solution at a wavelength of 280 nm. The recorded peaks were identified and quantified from a set of calibration standards of phenol and the primary oxidation byproducts catechol, hydroquinone, and resorcinol. The phenol and resorcinol were calibrated with 5, 10,

25, 50, and 100 ppm standard solutions. The catechol was calibrated with 5, 10, 25, and 50 ppm standard solutions. The resorcinol was calibrated with 5, 10, and 25 ppm standard solutions. The calibration curves for these compounds can be found in the Appendix.

The experiments focusing on the chemical aspects of the activated carbon in aqueous suspension were performed in the jacketed reactor. As stated before, the temperature of the water in the cooling jacket was kept constant at 20.0 °C. 1 L of deionized water was first added to the reactor. To the deionized water, 10 ml of a 10,000 ppm phenol solution was added to obtain a 100 ppm phenol solution in the reactor. In all of the experiments this was the starting phenol concentration. Also, 0.1348 g of ferrous sulfate ($FeSO_4 \bullet 7H_2O$) was added to the reactor on each run to promote Fenton's reaction. This addition of ferrous sulfate corresponds to a 485 mM solution which is the optimal level found experimentally by Sharma et al., (1993).

Two samples were taken before treatment and injected in to the HPLC. The initial solution was sampled to measure the conductivity, pH, and temperature before the experiment. If particles were used in the experiment, they were added at this point. The reactor was then attached to the high voltage and then the power was turned on and the applied voltage was set to the treatment voltage level. During the trial, ~2 mL liquid samples were taken out of the reactor at 1, 2, 4, 6, 8, 10, and 15 minutes treatment time. This was done by placing a syringe having Tygon tubing at the end inside one of the sampling ports on the reactor lid. The tubing was lowered under the ground electrode and the sample was taken. The sample was then transferred to a sample bottle by removing the Tygon tubing and placing a syringe

filter (0.6 μm pore size) on the end of the syringe, and then injecting the sample into the bottle. The samples were then analyzed by the HPLC within two hours of sampling.

During the corona treatment, measurements of the maximum peak voltage, voltage rise time, voltage pulse width, maximum current, and power were recorded from the oscilloscope. After fifteen minutes, the corona was turned off. Post-corona measurements of the conductivity, pH, and the temperature of the solution were then recorded.

There were five different experimental conditions used to determine the chemical effects of adding carbon particles to the pulsed streamer corona reactor. The initial phenol concentration for all of the experiments was 100 ppm and the ferrous sulfate concentration was 0.1348 g/L for all of the experiments. First, an experiment was conducted to determine the rate of adsorption of the phenol on to the surface of the activated carbon. For this, 1 g/L of the washed activated carbon was suspended in deionized water in the reactor and pulsed corona was not used. This allows for adsorption to occur with no reactions taking place. Two experimental conditions were investigated without the addition of activated carbon to determine the rate of reaction of the phenol and the formation of byproducts without any interaction with the activated carbon particles. These were conducted at the two corona treatment voltages of 46 kV and 57 kV. Finally, two experimental conditions combined the corona-induced reactions and the adsorption and possible surface reactions of the activated carbon. 1 g/L washed activated carbon was suspended in deionized water in the reactor and the corona treatment voltages were 46 kV and 57

kV. At each experimental condition, 3 trials were made to ensure that the error was less than 5-7 % (using 95% confidence interval, see Appendix).

3.6 Experimental Procedures for Adsorption Experiments

Experiments were performed to measure the adsorption equilibrium constant for the adsorption of phenol onto the washed activated carbon. This was done with 25, 50, and 100 ppm phenol solutions, and with 1 g/l washed activated carbon suspended in solution. An initial sample of each phenol solution was injected into the HPLC before adding the washed activated carbon. After adding the washed activated carbon, the particles were mixed and suspended in the solution for one hour. During this time, the solution was kept at 20.0 °C using the jacketed reactor. After one hour, a final sample was injected into the HPLC for analysis.

CHAPTER 4

MODEL FORMULATION AND SOLUTION

Reaction and diffusion in porous media is of continuing interest for chemical engineers. The processing of many materials involves heterogeneous reactions taking place on the surface of catalysts. These problems also occur in various organs, tissues, and other cellular materials. Different models have been developed to analyze the problem. One model used a set of random spheres to estimate the structure of the porous media. Another model was developed to represent the porous particle as a random set of capillary tubes modeling the pores in the catalyst.

Due to the complex nature of the porous catalysts, a volume averaging technique was developed by Whitaker (1967), and expanded by Ochoa, et al. (1986), Ryan, et al. (1981), Whitaker (1987), and Whitaker, (1991). This technique begins with phase averaging the species continuity equation in the catalyst pores. The resulting volume averaged equations could be solved to determine a profile of the phase average concentration within the particle. One advantage of this method is that the specific geometry of the internal pores is not needed except to determine the effective diffusion. In the present work, the governing phase averaged equations are again averaged in the cross section of the particle using the appropriate length scale.

This requires a solution of the closure problem. The closure problem first relates the phase averaged concentration to the cross-sectional area average concentration and a concentration deviation variable. The equation for the deviation variable is then solved. Finally, the resulting set of ordinary differential equations is solved analytically to find the cross-sectional area averaged concentration as a function of time.

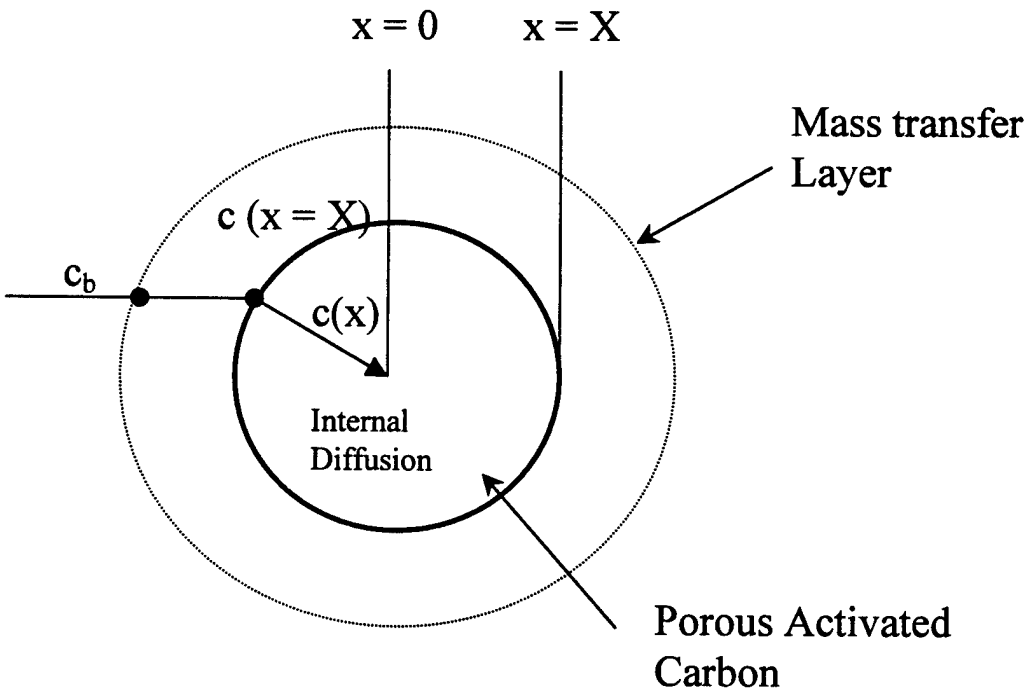
4.1 Problem Definition

The reaction and diffusion problem will provide a theoretical representation of the experimental system that combines the reactions induced by the pulsed streamer corona in the bulk as well as the surface reaction, mass transfer, and adsorption associated with the activated carbon particles. For the model, only one reactive species is considered, although generalization to the multicomponent case is under development. Phenol will represent this species in the experimental system.

The phenol is in the bulk liquid phase initially, and the solution is well mixed so that the phenol concentration is uniform throughout the reactor. At time 0, activated carbon particles are suspended in the reactor and the pulsed corona treatment begins. The particles are evenly distributed throughout the reactor. A boundary layer forms around the particle and becomes a mass transfer resistant layer. The phenol diffuses from the bulk phase through the mass transfer layer, and then through the particle. The aqueous phase pulsed corona produces reactive species in the bulk and possibly on the surface that react with the phenol. For the model, these reactions are assumed to be first-order and irreversible. Reactions are assumed to

take place on the surface of the activated carbon as well. Again, these reactions are considered to be first-order and irreversible.

Three cases will be considered. First, the case with no mass transfer will be solved. The first case will also consider the reaction term in the closure problem. The second case will assume the reaction term in the closure term to be negligible, while neglecting mass transfer. The second case will be solved in both rectangular geometry as well as spherical geometry. The third case will consider the mass transfer resistant case without the reaction term in the closure problem. A comparison of the three cases will also be given.



4.2 Case I – Reaction in Closure, No Mass Transfer

For a first approximation, many identical particles are suspended in a well-mixed solution containing one species, c. The resulting material balances are the species continuity equations in the bulk phase,

$$V\frac{dc_b}{dt} = -AD\frac{\partial c}{\partial x}\Big|_X - k_b c_b V \qquad (4.1)$$

where c_b is the concentration in the bulk solution, and k_b is the reaction rate in the bulk phase, D is the effective diffusion coefficient in the particle phase, V is the fluid volume, and A is the external surface area of all the particles. The value of A then represents the surface area of all the particles suspended in the bulk solution. The first term in Equation (4.1) is the accumulation term, the second term is the mass flux from the bulk phase to the particle phase, and the third term is the reaction in the bulk phase. The species continuity equation in the particle phase is

$$\frac{\partial c}{\partial t} = D\frac{\partial^2 c}{\partial x^2} - k_p c \qquad (4.2)$$

where c is the concentration in the particle, and k_p is the effective reaction rate in the particle. The first term in Equation (4.2) is the accumulation term, the second is the diffusion through the particle, and the third is the reaction term in the particle.

The boundary and initial conditions are as follows

$$c\big|_{x=X} = Kc_b\big|_{x=X} \qquad (4.3)$$

$$\frac{\partial c}{\partial x}\Big|_{x=0} = 0 \qquad (4.4)$$

$$c_b\,(t=0) = c_{b0} \qquad (4.5)$$

$$c\,(t = 0) = 0 \tag{4.6}$$

where K is the adsorption equilibrium constant. Equation (4.3) is the adsorption of the phenol from the bulk fluid to the carbon particle. The second boundary condition is the no flux condition at the center of the particle. The initial conditions show the initial phenol concentration in the bulk liquid, and initially there is no phenol present on the activated carbon.

The first step in solving Equations (4.1) and (4.2) is to non-dimensionalize both of these Equations utilizing the following non-dimensional variables

$$S = \frac{x}{X} \tag{4.7}$$

$$\tau = \frac{tD}{X^2} \tag{4.8}$$

Substituting Equations (4.7) and (4.8) into (4.1) and (4.2) gives the following equations

$$\frac{dc_b}{d\tau} = -\gamma \frac{\partial c}{\partial s}\Big|_1 - \phi_b c_b \tag{4.9}$$

$$\frac{\partial c}{\partial \tau} = \frac{\partial^2 c}{\partial s^2} - \phi_p c \tag{4.10}$$

where the following definitions have been used

$$\phi_b = \frac{k_b X^2}{D} \tag{4.11}$$

$$\phi_p = \frac{k_p X^2}{D} \tag{4.12}$$

$$\gamma = \frac{AX}{V} \tag{4.13}$$

The initial conditions (4.5) and (4.6) remain the same and the boundary conditions are now

$$c\big|_1 = Kc_b\big|_1 \tag{4.14}$$

$$\frac{\partial c}{\partial s}\Big|_0 = 0 \tag{4.15}$$

Equation (4.10) represents the concentration at a particular point in the particle. A macroscopic averaging technique is used to simplify the particle phase equations. The following is the definition of the macroscopic average

$$\langle c \rangle = \int_0^1 c\,ds \tag{4.16}$$

Applying this average to Equation (4.10) gives

$$\frac{\partial < c >}{\partial \tau} = \frac{\partial c}{\partial s}\Big|_1 - \phi_p < c > \tag{4.17}$$

Equations (4.17) and (4.9) are now solved using a closure technique. To do this we relate the average concentration in the particle to the point concentration by using Gray's decomposition (Gray, 1975) according to

$$c = < c > + \tilde{c} \tag{4.18}$$

where $\tilde{c}$ is the point deviation from the average. We now use this identity to subtract Equation (4.17) from Equation (4.10) to get

$$0 = \frac{d^2\tilde{c}}{ds^2} - \frac{d\tilde{c}}{ds}\Big|_1 - \phi_p \tilde{c} \tag{4.19}$$

This equation takes into account the fact that the partial differential with respect to s of $< c >$ is zero, and assumes that the time derivative of the deviation variable is negligible. This assumption is valid when (Whitaker, 1991, Ryan et al., 1981)

$$\frac{tD}{R^2} \gg 1 \tag{4.20}$$

which in our case is satisfied. For t = 900 s, D = 3.3 X 10^{-8} m^2/s, and R = 0.0002 m (values corresponding to those used in experiments, see Appendix), the left-hand side of Equation (4.20) is 750. Applying the average of Equation (4.18), the following equation results

$$< \tilde{c} >= 0 \tag{4.21}$$

The following boundary equation results from the previous boundary Equation (4.15)

$$< c > + \tilde{c}|_1 = Kc_b \tag{4.22}$$

At this point we propose the following solution for the deviation variable (Ochoa, et al., 1986),

$$\tilde{c} = < c > f(s) + g(s) \tag{4.23}$$

Applying this to Equation (4.19) gives

$$0 = < c > \frac{d^2 f}{ds^2} + \frac{d^2 g}{ds^2} - < c > \frac{df}{ds}\Big|_1 - \frac{dg}{ds}\Big|_1 - \phi_p < c > f - \phi_p g \tag{4.24}$$

First we will solve the g-field of this equation. The g-field separates in the following way

$$0 = \frac{d^2 g}{ds^2} - \frac{dg}{ds}\Big|_1 - \phi_p g \tag{4.25}$$

with the following equations resulting from the previous boundary equations

$$g|_1 = Kc_b \tag{4.26}$$

$$\frac{dg}{ds}|_0 = 0 \tag{4.27}$$

and that average of the g-field is zero (Ochoa, et al., 1986)

$$< g >= 0 \tag{4.28}$$

The general solution to Equation (4.25) is

$$g(s) = A_1 e^{\sqrt{\phi_p}s} + B_1 e^{-\sqrt{\phi_p}s} - \frac{1}{\phi_p}\frac{dg}{ds}|_1 \tag{4.29}$$

Boundary condition (4.27) gives

$$A_1 = B_1 \tag{4.30}$$

Boundary condition (4.26) gives

$$A_1 = \frac{Kc_b + \frac{1}{\phi_p}\frac{dg}{ds}|_1}{2\cosh\sqrt{\phi_p}} \tag{4.31}$$

Finally, the condition in (4.28) gives

$$\frac{dg}{ds}|_1 = -\psi Kc_b \tag{4.32}$$

where

$$\psi = \frac{\phi_p \tanh\sqrt{\phi_p}}{\tanh\sqrt{\phi_p} - \sqrt{\phi_p}} \tag{4.33}$$

The f-field is solved in a similar manner. The equation for the f-field is

$$\frac{d^2 f}{ds^2} - \frac{df}{ds}|_1 - \phi_p f = 0 \tag{4.34}$$

with the following condition (Ochoa, et al., 1986)

$$< f >= 0 \tag{4.35}$$

and the following boundary equations

$$1 + f(1) = 0 \tag{4.36}$$

$$\frac{df}{ds}\Big|_0 = 0 \tag{4.37}$$

Again, the general solution for an equation of this form is

$$f(s) = A^* e^{\sqrt{\phi_p}s} + B^* e^{-\sqrt{\phi_p}s} - \frac{1}{\phi_p}\frac{df}{ds}\Big|_1 \tag{4.38}$$

Applying Equation (4.37) to the previous equation gives

$$A^* = B^* \tag{4.39}$$

And from Equation (4.36) the integration constant is

$$A^* = \frac{\frac{1}{\phi_p}\frac{df}{ds}\Big|_1 - 1}{2\cosh\sqrt{\phi_p}} \tag{4.40}$$

Finally the following equation results from Equation (4.35)

$$\frac{df}{ds}\Big|_1 = \psi \tag{4.41}$$

in which ψ is defined as Equation (4.33).

Now that the solutions have been given for the g-field and the f-field, the two results can be combined to obtain

$$\frac{d\bar{c}}{ds}\Big|_1 = \psi < c > -\psi K c_b \tag{4.42}$$

Putting this back into Equations (4.9) and (4.17), the following set of differential equations are obtained

$$\frac{d<c>}{d\tau} = (\psi - \phi_p)<c> - \psi K c_b \tag{4.43}$$

$$\frac{dc_b}{d\tau} = -\gamma\psi <c> + (\gamma K\psi - \phi_b)c_b \tag{4.44}$$

Before presenting the general solution for the system of equations, the following definitions will help simplify the end results

$$W \equiv \psi - \phi_p \tag{4.45}$$

$$Y \equiv -K\psi \tag{4.46}$$

$$X \equiv -\gamma\psi \tag{4.47}$$

$$Z \equiv -(K\gamma\psi - \phi_b) \tag{4.48}$$

$$Q \equiv \tfrac{1}{2}(W - Z) \tag{4.49}$$

$$T \equiv \frac{1}{2}\sqrt{(Z+W)^2 + 4XY} \tag{4.50}$$

With these definitions, the general solution to Equations (4.43) and (4.44) are

$$<c>(\tau) = C_1^* e^{(Q+T)\tau} + C_2^* e^{(Q-T)\tau} \tag{4.51}$$

$$c_b(\tau) = C_1 e^{(Q+T)\tau} + C_2 e^{(Q-T)\tau} \tag{4.52}$$

Using the initial conditions in (4.5) and (4.6), the following equations are obtained

$$C_1 + C_2 = c_{b0} \tag{4.53}$$

$$C_1^* = -C_2^* \tag{4.54}$$

The other two boundary equations necessary to solve Equations (4.51) and (4.52) arise when Equations (4.41) and (4.42) are solved at $\tau = 0$ to get

$$\left.\frac{d<c>}{d\tau}\right|_{\tau=0} = Y c_{b0} \tag{4.55}$$

$$\frac{dc_b}{d\tau}\Big|_{\tau=0} = -Zc_{b0} \tag{4.56}$$

Now the conditions given in Equations (4.53) - (4.56) are applied to Equations (4.51) and (4.52) to obtain the final solution of

$$c_b(\tau) = \left[\frac{c_{bo}}{2T}(T-Q-Z)\right]\left\{e^{(Q+T)\tau} - e^{(Q-T)\tau}\right\} + c_{bo}e^{(Q-T)\tau} \tag{4.57}$$

$$< c > (\tau) = \frac{Yc_{b0}}{2T}\left(e^{(Q+T)\tau} - e^{(Q-T)\tau}\right) \tag{4.58}$$

4.3 Case II – No Reaction in Closure, No Mass Transfer (Rectangular Geometry)

The following derivation is similar to the one above but the reaction rate is assumed to be negligible in the closure problem (Ochoa, et al., 1986, Ryan, et al., 1981). The problem is identical to Equations (4.1) – (4.18), but the difference begins with Equation (4.19). Equation (4.19) can now be rewritten as

$$0 = \frac{d^2\tilde{c}}{ds^2} - \frac{d\tilde{c}}{ds}\Big|_1 \tag{4.59}$$

with the condition

$$< \tilde{c} >= 0 \tag{4.60}$$

and the boundary equation

$$< c > + \tilde{c}\Big|_1 = Kc_b \tag{4.61}$$

Again, the proposed solution for the deviation variable is

$$\tilde{c} = < c > f(s) + g(s) \tag{4.62}$$

Applying Equation (4.62) to Equation (4.59) the following equation results

$$0 = < c > \frac{d^2 f}{ds^2} + \frac{d^2 g}{ds^2} - < c > \frac{df}{ds}\Big|_1 - \frac{dg}{ds}\Big|_1 \tag{4.63}$$

First we will solve the g-field of this equation. The g-field separates in the following way

$$0 = \frac{d^2 g}{ds^2} - \frac{dg}{ds}\Big|_1 \tag{4.64}$$

with the condition

$$< g >= 0 \tag{4.65}$$

and the following boundary equations

$$g\Big|_1 = Kc_b \tag{4.66}$$

$$\frac{dg}{ds}\Big|_0 = 0 \tag{4.67}$$

The general solution to Equation (4.64) is the following

$$g(s) = \frac{dg}{ds}\Big|_1 \frac{s^2}{2} + A_1 s + B_1 \tag{4.68}$$

From boundary Equation (4.67),

$$A_1 = 0 \tag{4.69}$$

Solving Equation (4.68) with the boundary condition in Equation (4.66) gives

$$B_1 = Kc_b - \frac{1}{2}\frac{dg}{ds}\Big|_1 \tag{4.70}$$

Finally the boundary Equation (4.65) results in

$$\frac{dg}{ds}\Big|_1 = 3Kc_b \tag{4.71}$$

A similar technique solves for the f-field. The equation for the f-field is

$$\frac{d^2 f}{ds^2} - \frac{df}{ds}\Big|_1 = 0 \tag{4.72}$$

with the condition

$$< f >= 0 \tag{4.73}$$

and the boundary equations

$$1 + f(1) = 0 \tag{4.74}$$

$$\frac{df}{ds}\Big|_0 = 0 \tag{4.75}$$

The general solution to Equation (4.72) is

$$f(s) = \frac{df}{ds}\Big|_1 \frac{s^2}{2} + A^* s + B^* \tag{4.76}$$

Applying the boundary condition in Equation (4.75) gives

$$A^* = 0 \tag{4.77}$$

and the following results from applying boundary Equation (4.74)

$$B^* = -1 - \frac{1}{2}\frac{df}{ds}\Big|_1 \tag{4.78}$$

Finally, applying boundary condition (4.73) the following solution is derived

$$\frac{df}{ds}\Big|_1 = -3 \tag{4.79}$$

From the combination of Equation (4.79) and (4.71) as in the previous case gives

$$\frac{d\tilde{c}}{ds}\Big|_1 = -3 < c > +3Kc_b \tag{4.80}$$

Putting this solution back into Equations (4.9) and (4.17) gives the following system of differential equations

$$\frac{d < c >}{d\tau} = (-3 - \phi_p) < c > +3Kc_b \tag{4.81}$$

$$\frac{dc_b}{d\tau} = 3\gamma < c > -(3\gamma K + \phi_b)c_b \tag{4.82}$$

For these differential equations, the following definitions are different than the ones shown in the first case

$$W \equiv (-3 - \phi_p) \tag{4.83}$$

$$Y \equiv 3K \tag{4.84}$$

$$X \equiv 3\gamma \tag{4.85}$$

$$Z \equiv (3\gamma K + \phi_h) \tag{4.86}$$

For this case, Equations (4.83) – (4.86) can be inserted into Equations (4.49) - (4.59) to obtain the solution for this case.

From the solutions from Case I (where the reaction term is solved within the closure problem) the limiting case is

$$\lim \psi (k_p \rightarrow 0) = -3 \tag{4.87}$$

This limiting value applied to Equations (4.44) – (4.48) gives terms identical to Equations (4.83) – (4.86). For very small values of k_p, the surface phase reactions are negligible in the closure problem.

The effect of the reaction term in the closure can be seen further in Figures 5, 6, and 7. These figures compare the theoretical results for Case I and Case II. Figure 5 compares the two cases with k_p=0.00001 sec^{-1}. At this small surface reaction rate, the two cases are identical. At this small of a reaction rate, the assumption that the surface reaction rate is negligible in the closure problem is valid. Figure 6 shows the comparison of Case I and Case II for a surface reaction rate of 0.001 sec^{-1}. Again, the two cases match up almost identically indicating that at this rate constant, the assumption in Case II is still valid. Figure 7 shows the comparison of the two cases

when the particle surface reaction rate is increased to 0.1 sec^{-1}. At this reaction rate, the assumption that the reaction rate is negligible in the closure is still valid. The two cases predict a similar concentration profiles. The validity of Case II depends on the surface reaction rate on the particle, which is valid when the rate is less than 0.1 sec^{-1}. Above this, the two cases considered begin to deviate from each other, although the particle reaction rate is high enough to cause both the bulk and particle concentrations to go to zero very rapidly (figure not shown).

4.4 Case II – No Reaction in Closure, No Mass Transfer (Spherical Geometry)

The derivation for this case begins with the species continuity equation in the bulk phase given in Equation (4.1) and in the particle phase given by

$$\frac{\partial c}{\partial t} = D\frac{1}{r^2}\frac{\partial}{\partial r}\left(r^2\frac{\partial c}{\partial r}\right) - k_p c \tag{4.88}$$

where r is the radial term. The initial conditions are identical to those in Equations (4.5) and (4.6) and the boundary equations are

$$c\big|_{r=R} = Kc_b\big|_{r=R} \tag{4.89}$$

$$\frac{\partial c}{\partial r}\Big|_{r=0} = 0 \tag{4.90}$$

where R is the radius of the particle. Equation (4.88) must now be non-dimensionalized. This is done using the definitions

$$S = \frac{r}{R} \tag{4.91}$$

$$\tau = \frac{tD}{R^2} \tag{4.92}$$

Applying these definitions to Equations (4.1) and (4.88) gives Equations (4.9) and

$$\frac{\partial c}{\partial \tau} = D\frac{1}{s^2}\frac{\partial}{\partial s}\left(s^2\frac{\partial c}{\partial s}\right) - \phi_p c \tag{4.93}$$

which use the definitions

$$\phi_h = \frac{k_h R^2}{D} \tag{4.94}$$

$$\phi_p = \frac{k_p R^2}{D} \tag{4.95}$$

$$\gamma = \frac{AR}{V} \tag{4.96}$$

and have initial conditions (4.5) and (4.6) and the boundary Equations in (4.14) and (4.15). A macroscopically averaged particle equation is used to simplify Equation (4.93) and is defined as

$$< c >= \int_0^1 c s^2 ds \tag{4.97}$$

Applying Equation (4.97) to (4.93) gives the following

$$\frac{\partial < c >}{\partial \tau} = \frac{\partial c}{\partial s}\Big|_1 - \phi_p < c > \tag{4.98}$$

As done previously, Gray's decomposition (Equation (4.18)) is used and Equation (4.98) is subtracted from Equation (4.93) to give

$$0 = \frac{1}{s^2}\frac{\partial}{\partial s}\left(s^2\frac{\partial \tilde{c}}{\partial s}\right) - \frac{\partial \tilde{c}}{\partial s}\Big|_1 \tag{4.99}$$

This equation again neglects the time variation in the deviation variable (Equation (4.20)). The boundary equations for Equation (4.99) are given in Equations (4.21) and (4.22). A solution to Equation (4.98) is given by

$$\tilde{c} =< c > f(s) + g(s) \tag{4.100}$$

Applying this to Equation (4.98) gives

$$0 = \frac{1}{s^2}\frac{\partial}{\partial s}\left(s^2 < c > \frac{df}{ds}\right) + \frac{1}{s^2}\frac{\partial}{\partial s}\left(s^2 \frac{dg}{ds}\right) - < c > \frac{df}{ds}\Big|_1 - \frac{dg}{ds}\Big|_1 \qquad (4.101)$$

The reaction terms in Equation (4.101) are again neglected in the closure problem.

First, the g-field of this equation will be solved. The g-field of Equation (4.101) separates into

$$0 = \frac{1}{s^2}\frac{\partial}{\partial s}\left(s^2 \frac{dg}{ds}\right) - \frac{dg}{ds}\Big|_1 \qquad (4.102)$$

with the condition

$$< g >= 0 \qquad (4.103)$$

and the boundary equations

$$g\Big|_1 = Kc_b \qquad (4.104)$$

$$\frac{dg}{ds}\Big|_0 = 0 \qquad (4.105)$$

The general solution to Equation (4.102) is the following

$$g(s) = \frac{dg}{ds}\Big|_1 \frac{s^2}{6} - A_1 s^{-1} + B_1 \qquad (4.106)$$

From boundary Equation (4.105),

$$A_1 = 0 \qquad (4.107)$$

Solving Equation (4.106) with boundary condition (4.104) gives

$$B_1 = Kc_b - \frac{1}{6}\frac{dg}{ds}\Big|_1 \qquad (4.108)$$

Finally the condition in Equation (4.103) results in

$$\frac{dg}{ds}|_1 = 9Kc_h \tag{4.109}$$

The equation for the f-field is separated from Equation (4.101) to give

$$\frac{1}{s^2}\frac{\partial}{\partial s}\left(s^2\frac{df}{ds}\right) - \frac{df}{ds}|_1 = 0 \tag{4.110}$$

with the condition

$$< f >= 0 \tag{4.111}$$

and the boundary equations

$$1 + f(1) = 0 \tag{4.112}$$

$$\frac{df}{ds}|_0 = 0 \tag{4.113}$$

The general solution to Equation (4.110) is

$$f(s) = \frac{df}{ds}|_1 \frac{s^2}{6} - A^* s^{-1} + B^* \tag{4.114}$$

Applying the boundary Equation in (4.113) gives

$$A^* = 0 \tag{4.115}$$

and the following results from applying boundary Equation (4.112)

$$B^* = -1 - \frac{1}{6}\frac{df}{ds}|_1 \tag{4.116}$$

Finally, applying boundary condition (4.111) the following solution is derived

$$\frac{df}{ds}|_1 = -9 \tag{4.117}$$

From the combination of Equation (4.117) and (4.109) as in the previous case gives

$$\frac{d\tilde{c}}{ds}\Big|_1 = -9 < c > +9Kc_b \tag{4.118}$$

Putting this solution back into Equations (4.9) and (4.98) gives the following system of differential equations

$$\frac{d < c >}{d\tau} = (-9 - \phi_p) < c > +9Kc_b \tag{4.119}$$

$$\frac{dc_b}{d\tau} = 9\gamma < c > -(9\gamma K + \phi_b)c_b \tag{4.120}$$

For these differential equations, the following definitions are different than the ones shown in the first case

$$W \equiv (-9 - \phi_p) \tag{4.121}$$

$$Y \equiv 9K \tag{4.122}$$

$$X \equiv 9\gamma \tag{4.123}$$

$$Z \equiv (9\gamma K + \phi_b) \tag{4.124}$$

For this case, Equations (4.121) – (4.124) can be inserted into the Equations (4.49) - (4.58) to obtain the solution for this case.

Figure 8 compares the solution obtained for the rectangular and spherical case of the model derivation where the reaction term is assumed to be negligible in the closure problem. As seen in this figure, the is almost no difference in the solution when the geometry of the problem is changed from rectangular to spherical. Even though the constants for the spherical case differ from the constants for the rectangular case by a factor of 3, the final solution combines the constants in a way to

show almost no difference between the two. All further references to Case II shall refer to the solution with rectangular coordinates.

4.5 Case III – No Reaction in Closure, Mass Transfer

The previous two cases considered the problem without mass transfer resistance of the reactive species from the bulk solution to the carbon particle. When a particle is suspended in a liquid, a thin boundary layer forms around particle. In this layer, mass transfer limits the diffusion through the region. This case will include the effects of mass transfer resistance for the case of a mono-component system and as in Case II, the reaction term will be left out of the closure problem.

The material balance in Equation (4.1) and the species continuity equation in Equation (4.2) govern the behavior in this system. The mass transfer resistance is incorporated into the boundary equation

$$-AD\frac{dc}{dx}\Big|_{x=X} = AK_{mt}(c(X) - Kc_b) \qquad (4.125)$$

where K_{mt} is the mass transfer coefficient. The other boundary equations and initial conditions in Equations (4.4) – (4.6) remain the same. The non-dimensional form of Equation (4.125) is given as

$$-\frac{AD}{R}\frac{dc}{ds}\Big|_1 = AK_{mt}(c|_1 - Kc_b) \qquad (4.126)$$

Applying the definition of the average, Equation (4.126) using the non-dimensional terms in Equations (4.7) and (4.8) gives

$$-\frac{AD}{R}\frac{d\tilde{c}}{ds}\Big|_1 = AK_{mt}(< c > +\tilde{c}|_1 - Kc_b) \qquad (4.127)$$

The equation for the g-field is

$$0 = \frac{d^2 g}{ds^2} - \frac{dg}{ds}\Big|_1 \tag{4.128}$$

with the condition

$$< g >= 0 \tag{4.129}$$

and the boundary equations

$$g\Big|_1 = \frac{KK_{mf} c_b - \frac{D}{R}\frac{dg}{ds}\Big|_1}{K_{mf}} \tag{4.130}$$

$$\frac{dg}{ds}\Big|_0 = 0 \tag{4.131}$$

The general solution to Equation (4.128) is the following

$$g(s) = \frac{dg}{ds}\Big|_1 \frac{s^2}{2} + A_1 s + B_1 \tag{4.132}$$

Boundary Equation (4.131) gives

$$A_1 = 0 \tag{4.133}$$

and from the boundary Equation (4.130)

$$B_1 = Kc_b - \frac{dg}{ds}\Big|_1 \left(\frac{D}{RK_{mf}} + \frac{1}{2}\right) \tag{4.134}$$

Finally the boundary condition in Equation (4.129) results in

$$\frac{dg}{ds}\Big|_1 = \frac{3RKK_{mf} c_b}{K_{mf} R + 3D} \tag{4.135}$$

Similarly the equation for the f-field is

$$\frac{d^2 f}{df^2} - \frac{df}{ds}\Big|_1 = 0 \tag{4.136}$$

with the condition

$$< f >= 0 \tag{4.137}$$

and the boundary equations

$$f\big|_1 = \frac{-\frac{D}{R}\frac{df}{ds}\big|_1 - K_{ml}}{K_{ml}} \tag{4.138}$$

$$\frac{df}{ds}\big|_0 = 0 \tag{4.139}$$

The general solution to Equation (4.136) is

$$f(s) = \frac{df}{ds}\big|_1 \frac{s^2}{2} + C_1^* s + C_2^* \tag{4.140}$$

Applying the condition in Equation (4.139) we obtain

$$A^* = 0 \tag{4.141}$$

and applying boundary Equation (4.138) gives

$$B^* = \frac{df}{ds}\big|_1 \left(-\frac{1}{2} - \frac{D}{RK_{ml}}\right) - 1 \tag{4.142}$$

Finally, applying the boundary condition in Equation (4.137) the following solution is derived

$$\frac{df}{ds}\big|_1 = -\left(\frac{3RK_{ml}}{RK_{ml} + 3D}\right) \tag{4.143}$$

Combining Equations (4.135) and (4.143) gives

$$\frac{d\bar{c}}{ds}\big|_1 = \left(\frac{-3RK_{ml}}{RK_{ml} + 3D}\right) < c > + \left(\frac{3KK_{ml}R}{K_{ml}R + 3D}\right) c_b \tag{4.144}$$

Inserting this solution back into Equations (4.9) and (4.17) gives the following system of differential equations

$$\frac{d<c>}{d\tau} = \left(\frac{-3RK_{mt}}{RK_{mt}+3D} - \phi_p\right)<c> + \left(\frac{3KK_{mt}R}{K_{mt}R+3D}\right)c_b \tag{4.145}$$

$$\frac{dc_b}{d\tau} = \left(\frac{AR^2 3K_{mt}}{VRK_{mt}+3VD}\right)<c> - \left(\frac{3AR^2 KK_{mt}}{VRK_{mt}+3VD} + \phi_b\right)c_b \tag{4.146}$$

For these differential equations, the following definitions are

$$W \equiv \left(\frac{-3RK_{mt}}{RK_{mt}+3D} - \phi_p\right) \tag{4.147}$$

$$Y \equiv \left(\frac{3KK_{mt}R}{K_{mt}R+3D}\right) \tag{4.148}$$

$$X \equiv \left(\frac{AR^2 3K_{mt}}{VRK_{mt}+3VD}\right) \tag{4.149}$$

$$Z \equiv \left(\frac{3AR^2 KK_{mt}}{VRK_{mt}+3VD} + \phi_b\right) \tag{4.150}$$

$$Q \equiv \tfrac{1}{2}(W-Z) \tag{4.151}$$

$$T \equiv \frac{1}{2}\sqrt{(Z+W)^2 + 4YX} \tag{4.152}$$

These constants in Equations (4.147) – (4.150) reduce to those in Equations (4.83) – (4.86) when K_{mt} gets large. These constants are then used in Equations (4.51) – (4.58) to obtain the complete solution to the problem.

As stated in Table 1, Case I reduces to the limiting case of Case II as k_p goes to zero and Case III reduces to the limiting case of Case II as K_{mt} gets very large. Figures 9, 10, and 11 show the comparison between Case II and Case III when the mass transfer coefficient is varied keeping all of the other parameters identical. Figure 9 compares the two cases with a mass transfer coefficient of 1 m/s. The two

sets of curves are virtually identical. A mass transfer coefficient of 0.001 m/s is shown if Figure 10. Again, the model predicts results that seem identical for both Case II and Case III. Only when the mass transfer coefficient is decreased to 1×10^{-6} m/s is there a difference in the two cases, as shown in Figure 11. Case II is therefore a valid approximation at low values of k_p under 10 sec^{-1} and for mass transfer coefficients above 0.001 m/s. For the experimental conditions in the pulsed streamer corona reactor, the mass transfer resistance is estimated to be 4×10^{-6} m/s (Frössling, 1938, Sitaraman, et al., 1963, see Appendix) and therefore Case III will be used to compare the theoretical model to the experimental results.

Figure 12 shows the effect of the surface reaction rate on the bulk phase concentration. These results were calculated using the solution for Case III using a mass transfer resistance coefficient of 4×10^{-6} m/s. The range of surface reaction rate constants is from 0.0001 sec^{-1} to 10 sec^{-1} differing by powers of 10. At the two lowest surface reaction rate constants, 0.0001 sec^{-1} and 0.001 sec^{-1}, the bulk phase concentration is limited by the slow surface reactions. The curves for these values represent the bulk phase reactions, the adsorption, and the mass transfer to the particle. The surface reaction is slow enough that the particle is saturated with the reacting species. As the surface reaction rate is increased to 0.01 sec^{-1}, the reaction rate is fast enough to show a decrease in the bulk concentration. As the surface reaction rate increases to 0.1, 1, and 10 sec^{-1}, there is a decrease in the bulk phase concentration from previous values of the surface reaction rate due to faster reactions on the particle. The bulk concentration, however, remains the same for these three values of the surface phase reaction rate. At these rates, the system is mass transfer

limited. The reacting species is not getting to the particle fast enough, and then reacts almost instantaneously on the surface of the particle.

CHAPTER 5

EXPERIMENTAL RESULTS & DISCUSSION

5.1 Particle Effects on Breakdown Voltage

Figure 13 shows the voltage waveform patterns for the solutions containing 100 mL pure deionized (DI) water, 1 g/L unwashed activated carbon particles in 1000 mL DI water and 1 g/L ≤25μm unwashed glass spheres in 1000 mL DI water. All three of these waveform patterns were recorded at an applied voltage of 46 kV. These waveforms show that the voltage decay time for the carbon and glass in water suspension cases is greater than for the case of the DI water. The voltage waveform for both the glass spheres and carbon particle cases are very similar to each other and show no significant differences. Figure 14 shows the current pulse for the deionized water case, which has a peak current of 45 A. The decay of the current pulse oscillates due to the capacitance and inductance of the circuit.

Figure 15 summarizes the breakdown voltage for all the experiments with particles present in suspension conducted in this study as a function of the quantity of particles. The presence of unwashed activated carbon in suspension clearly has a distinct effect on the breakdown voltage, and the dependence of this breakdown voltage on the amount of activated carbon is also very important. The ≤25 μm

unwashed glass spheres in suspension was the only other particle type to show an increase in breakdown voltage with an increase in particle quantity, although the magnitude of the increase for the glass beads is significantly less than that of the activated carbon. Suspensions with larger glass spheres showed a decrease in the effect of particle quantity as seen in this figure. The presence of any quantity of copper dust or silica gel in suspension had no effect on the breakdown voltage in the range studied, although they also showed a slightly smaller breakdown voltage than the deionized water. The presence of washed activated carbon did not have any effect on the aqueous suspension breakdown voltage.

Qualitative observations were also made noting the size, quality, and quantity of the streamers produced in suspension for varying concentrations of all types of particles. In comparison to the no particle case, the addition of unwashed activated carbon particles to the DI water in the reactor increased the length of the observed streamers. The streamers also had a magenta color in the presence of the carbon particles. The glass spheres and the silica gel particles in suspension produced longer streamers than the case without particles. The number of streamers observed were smaller and the intensity of the streamers was lower for the glass spheres and the silica gel particle cases compared to the unwashed carbon particle case. For the smallest glass spheres ($\leq$25 μm and finer), the corona discharge was clouded from view due to the large number of particles in suspension. This was also true for the case of copper dust in suspension, where only the glow of the corona was observable.

The most significant finding of these results is the increased breakdown voltage due to the addition of the unwashed activated carbon and the addition of the

smallest diameter unwashed glass spheres to DI water. The main physical properties of the particles include surface area, dielectric constant, and solution conductivity, each that might contribute to the effects seen in the different particle suspensions.

An increased breakdown voltage of aqueous suspensions containing unwashed activated carbon particles was thought to be explained by the electronic nature of the carbon particle. By the electronic nature, both the particle conductivity and dielectric constant are considered. Activated carbon is a relatively good conductor compared to the glass spheres and the silica gel particles. Copper dust particles were used to investigate a highly conductive particle in the pulsed streamer corona reactor. The presence of copper particles lowered the voltage at which breakdown occurred compared to the case of DI water alone, in contrast to the opposite effect for the presence of the carbon particles. This difference in breakdown voltages for conducting particles would predict that the conductivity of the particle itself does not contribute to the breakdown voltage as greatly as initially thought.

The voltage waveforms shown in Figure 13 are similar to previous studies (Clements et al., 1985) where a rapid, nanosecond rise was followed by an exponential voltage decay. Clements observed that the voltage decay time decreased with increasing solution conductivity. Clements also showed an increase in voltage decay time of 500 - 1000 μs when the conductivity of the solution was decreased from 10 μS/cm to 1 μS/cm at an applied voltage of 25 kV. The same pattern is observed in the voltage waveforms in Figure 13. For the case of DI water alone (the lowest conductivity case), the decay time of the voltage was the longest of the three. The conductivity of the solutions increased with the addition of carbon particles and

glass spheres, thus the voltage decay time decreased. The conductivity of the solutions containing glass spheres and the unwashed carbon particles was 22 μScm^{-1} and 80 μScm^{-1} respectively. The waveforms corresponding to solutions containing glass spheres and the unwashed carbon particles had similar voltage decay time.

Clements et al. (1985) obtained photographs that showed that the number of streamers varied with the solution conductivities. At the lower conductivities, they observed more streamers than at the higher conductivities. This pattern was not observed in the present study with the addition of particles to aqueous solutions. For the case of the addition of unwashed carbon particles, the conductivity of the solution increased with increasing concentrations of particles. The addition of unwashed activated carbon particles to the solution also resulted in an increased number of observed streamers. In Clements work, the conductivity was increased from 1 μScm^{-1} to 10 μScm^{-1} using solutions of KOH. The addition of glass spheres and silica gel particles in the present work did not change the number of streamers compared to the case of DI water alone. The difference here between the Clements work and the present work is due to the nature of the different particles.

5.2 Scanning Electron Microscopy Results

As shown in Figure 16, the surface of unwashed activated carbon particles were observed using scanning electron microscopy. Numerous pores are present on the surface of the unwashed activated carbon. Also, white "dust" particles can be noticed all over the surface of the particles. This dust could be the ash remaining from the processing of the activated carbon. Attached to the SEM apparatus is an x-ray emissions apparatus that can scan a very small area of the sample. An overall

scan of an unwashed activated carbon particle (not focusing in on a single dust particle but an area that included several dust particles on the carbon surface) showed that the elements potassium, silicon, sulfur, and chlorine were present on the surface. The instrument was not calibrated to give quantitative results, but it could only determine that the elements were there in a high enough concentration for the equipment to observe it (detectable limit is not known). An emissions scan was then specifically focused on one of the dust particles and the elemental result was similar to the overall scan of the surface. The emissions data indicates that the elemental properties of the dust particles are the same as those of the unwashed activated carbon particles and cannot be salt crystals.

Figure 17 shows the surface of a washed activated carbon particle sample. There is no observable change in the pore structure of the activated carbon particles after washing. The amount of dust particles present on the surface of the activated carbon decreases with washing. X-ray emission analysis indicated the presence of potassium on both a wide area scan and a spot scan of one of the dust particles. This indicates that the cleaning process removes most of the potassium from the surface of the activated carbon. The decrease in the dust particles could be the result of the water solubility of the ash (which is primarily silicates of aluminum, magnesium, and iron).

SEM pictures of the unwashed and washed activated carbon after a 10 minute 46 kV treatment are shown in Figures 18 and 19, respectively. After the pulsed corona treatment, there is no noticeable difference in the pore structure or any pore diameter change in the surface of the carbon. In both cases, there is a large reduction

in the number of the dust particles on the surface of the activated carbon. From the x-ray emissions analysis, there was no potassium on either sample. The only element observed on both samples was silicon.

5.3 PIXE Analysis

PIXE (proton induced x-ray emissions) analysis was performed on 1) the unwashed activated carbon, 2) the solution resulting from a suspension of the unwashed activated carbon, and 3) the solution resulting from a suspension of the unwashed ≤25 μm glass spheres. These results are shown in Table 3. The unwashed activated carbon had levels that were above 10 ppm by weight of phosphorous, sulfur, potassium, calcium, copper, and strontium. Potassium accounted for almost 1% of the total weight of the unwashed activated carbon particle sample. When the unwashed activated carbon particle sample was suspended in deionized water, potassium was the highest concentration element in the aqueous phase solution. In addition, the carbon leachate has high concentrations of sodium, silicon, phosphorous, chlorine, potassium, and calcium, all above 1 ppm by weight. In the solutions formed from the suspension of the unwashed glass spheres were high levels of sodium, silicon, sulfur, chlorine, and calcium in concentrations above 1 ppm by weight, but interestingly, no potassium.

To compare to the results of the PIXE analysis and the electrical breakdown studies, varied experimental conditions were used to look at the effects of the different salt solutions by themselves and also in combination with the washed activated carbon and the washed glass spheres. From the PIXE analysis of the carbon leachate, potassium and sodium had the highest concentration and calcium also had

one of the highest concentrations in the solution. The glass sphere leachate had a high concentration of sodium. Both solutions had a significant concentration of chlorine. The salts used in the pulsed corona experiments were potassium chloride, calcium chloride, and sodium chloride. These salts were then investigated in solution both with and without washed activated carbon and washed glass sphere suspensions.

5.4 Particle Effects on Reactor Power Consumption

Figure 20 shows the results for power consumption under pulsed corona treatment for a combination of the calcium chloride solution at a constant conductivity and different concentrations of washed activated carbon. The experimental conditions used were 140 μScm^{-1} calcium chloride solution and three washed activated carbon concentrations of no particles, 1 g/L, and 2 g/L. For all three of the curves, as the applied voltage (peak voltage on the oscilloscope) is increased, the reactor power consumption increased as expected. At the highest applied voltage of 67 kV, the reactor power consumption was around 2000 mJ/pulse. At the higher applied voltages, the combination of the 2 g/L washed activated carbon and the 140 μScm^{-1} calcium chloride solution showed slightly lower power consumption.

A similar graph is shown in Figure 21. This shows the reactor power consumption for pulsed corona treatment of no particles, 1 g/L, and 2 g/L washed activated carbon in combination with a 140 μScm^{-1} sodium chloride solution. Again, as the applied voltage increases, the reactor power consumption increases for all cases. At an applied voltage of 67 kV, the power consumption for all conditions is slightly over 2000 mJ/pulse. This result is almost identical to that of the calcium chloride solutions.

Figure 22 shows the power consumption for pulsed corona treatment of the combination of different concentrations of washed activated carbon and potassium chloride solutions. The potassium chloride concentration was held constant to give 140 μScm^{-1} and the particle concentrations were 0 g/L, 1 g/L, and 2 g/L washed activated carbon. For the case of no particles, the power consumption at the higher applied voltages was over 2000 mJ/pulse. This is similar to all of the calcium chloride and sodium chloride cases mentioned previously. The curves for the 1 g/L and 2 g/L washed activated carbon with the potassium chloride solution had a lower slope and also showed a reactor power consumption of under 1000 mJ/pulse at the higher applied voltages. The power consumption for the combination of the potassium salt and the washed carbon is less than half of all the other cases tried. It does not seem that the amount of washed activated carbon in the range studied has any effect on the power consumption, as long as both the washed activated carbon and the potassium chloride solution are present in the solution.

The next figure, Figure 23, gives a comparison of the pulsed corona experiments with no particles and salt solutions of similar conductivities. The curves for no particles with 140 μScm^{-1} conductivity solutions of potassium chloride, sodium chloride, and calcium chloride are shown. All three of these conditions gave almost identical results. At the higher applied voltages above 60 kV, the reactor power consumption is slightly over 2000 mJ/pulse. This shows that without any added particles, the power consumption is similar for all of the cases.

Figure 24 gives the power consumption for the three different salt solutions in combination with 1 g/L washed activated carbon. The curves for the 140 μScm^{-1}

sodium chloride solution with carbon and the 140 μScm^{-1} calcium chloride solution with carbon are similar. At the higher applied voltage, they both have high power consumption of over 2000 mJ/pulse. The only experimental condition to have significantly lower power consumption is the case of the 1 g/L washed activated carbon in combination with the 140 μScm^{-1} potassium chloride solution. As stated above, the reactor power consumption is under 1000 mJ/pulse at the highest applied voltage for the combination of the potassium salt and the washed activated carbon. When the carbon concentration is increased to 2 g/L, similar results are achieved, as shown in Figure 25.

The trend of lower power consumption for pulsed corona treatment of the combination of potassium chloride and washed activated carbon is also noticed at a lower salt solution conductivity as shown in Figures 26 and 27. Figure 26 shows the reactor power consumption at different applied voltages for 1 g/L washed activated carbon in combination with either 14 μScm^{-1} sodium chloride solution, 14 μScm^{-1} calcium chloride solution, or 14 μScm^{-1} potassium chloride solution. Figure 27 shows the same three solution conditions, but the washed activated carbon concentration is increased to 2 g/L. For the experiments containing the sodium and calcium salts with the two carbon concentrations, the power was about 500 mJ/pulse at the higher applied voltages. The reason the power is lower at lower conductivities (14 μScm^{-1} vs. 140 μScm^{-1}) is that the resistivity of the water is increased, the current (V=IR) is reducer, which lowers the reactor power consumption. The power consumption for the potassium salt with the carbon increased to 130 mJ/pulse and 220 mJ/pulse at the higher applied voltages for the 1 g/L and 2 g/L washed activated,

carbon respectively. Again, the power consumption in the reactor is lower for the combination of the washed activated carbon and the potassium chloride solution, compared to carbon and either of the other two salts. The reason for the difference in power consumption for the 1 g/L washed activated carbon with the potassium chloride solution and the 2 g/L washed activated carbon with the potassium chloride solution is not known at this time.

Figure 28 shows the power consumption for pulsed corona experiments using suspensions of 1 g/L and 2 g/L unwashed activated carbon in deionized water, and compares this to suspensions of 1 g/L and 2 g/L washed activated carbon in a 140 μScm^{-1} potassium chloride solution. Solutions containing suspensions of the unwashed activated carbon showed power characteristics higher than those of the washed activated carbon particles suspended in the KCl solution at the higher voltages, although the power characteristics were lower than those of the salt solutions without any particles. The higher power consumption of the unwashed activated carbon suspensions compared to the washed activated carbon suspensions, both in potassium chloride, may be due to the additional salts that are present in the unwashed activated carbon.

Figure 29 shows the power consumption for the combination of the washed ≤ 25 μm diameter glass spheres and the three higher conductivity salt solutions. This figure shows that the calcium chloride, sodium chloride, and potassium chloride salts in combination with the glass spheres have similar reactor power consumption. At the higher applied voltages, the reactor power reaches 2000 mJ/pulse. This result is similar to that of the salt solutions by themselves, and both the combination of the

sodium chloride and calcium chloride salts with the washed activated carbon. A reduced power was observed for the combination of the potassium chloride and the washed activated carbon compared to the combination of the potassium chloride and the ≤ 25 μm diameter washed glass spheres. Again, the reduced power consumption is specific to only the combination of the washed activated carbon and the potassium chloride salt.

Activated carbon is a well-known adsorbent for a range of organic and inorganic compounds. It can also adsorb some inorganic ions and it may affect reactor power through reduction of current carrying species. It is clear that washed activated carbon in aqueous suspension does not reduce reactor power in the presence of any salt species except salts of potassium. These results are highly reproducible and cannot be accounted for by changes in the surface or pore structure of the activated carbon as observed by scanning electron microscopy. In addition, particles of other types such as porous silica gel with large internal surface area do not affect the reactor performance through changes in power levels.

One method for the commercial production of activated carbon requires chemical activation at high temperatures and pressures in the presence of potassium hydroxide or potassium chloride, sulfate, or bicarbonate salts (Bansal, et al., 1988). The activation process creates a high surface area pore structure in which the surface of the carbon particles consists of stacks of flat aromatic sheets crosslinked in a random manner. Carbon readily interacts with oxygen and to a lesser degree hydrogen, nitrogen, and sulfur, through resonance-stabilized unpaired electrons. A number of acidic surface groups are also present. Potassium is also known to form

graphite intercalation compounds by penetrating the lattice of graphitic materials (Brandt, et al., 1988). These graphite intercalation compounds of potassium are well studied; however, the structure of activated carbon in general does not contain as extensive a lattice structure as graphite. The exact natures of the interaction of potassium with activated carbon and its effect on the electrical properties of a high voltage discharge are not known. This may lead to further work to investigate how the potassium interacts with the activated carbon.

5.5 Phenol Removal

The rate of adsorption of phenol onto washed activated carbon in deionized water suspension is shown in Figure 30. The experimental conditions for this figure are a starting concentration of 100 ppm phenol, 485 mM ferrous sulfate, and 1 g/L washed activated carbon. No voltage was applied to the reactor. Phenol removal from the solution was 74%. The amount removed represents the adsorption of the phenol to the surface of the activated carbon. Under these conditions, there are no byproducts formed. This indicates that there are no reactions on the surface of the carbon when there is no applied voltage.

Figure 31 shows the phenol removal results for the experiments with no particles in suspension added at an applied pulsed treatment oltage of 46 kV. The concentrations of the different species are all normalized to 1 by dividing all of the concentrations by 100 ppm. As indicated in the figure, 28% of the phenol is removed in 15 minutes of pulsed corona exposure. Concurrently, 10 ppm catechol, 2 ppm resorcinol, and 1 ppm of hydroquinone are formed. This accounts for 84% (by moles) of the carbon initially present. The remaining 16% of the carbon is assumed

to be other less complex oxidation products of the phenol such as formic acid, oxalic acid, and other organic acids.

For the above experimental case of 46 kV applied pulsed corona voltage and no carbon particles in suspension, the average power in the reactor was 800 mJ/pulse, (Table 4). This corresponds to a contaminant removal efficiency of 2.3 g/kWhr calculation in Appendix). The solution conductivity increased during the run from an initial conductivity of 120 μScm^{-1} to a final conductivity of 176 μScm^{-1}. This rise in the conductivity can be justified by the conversion of the ferrous ions (Fe^{2+}) to the ferric ions (Fe^{3+}) in the Fenton's reaction.

Figure 32 shows the results for the degradation of phenol at 57 kV pulsed corona voltage with no particles present in suspension. Under these conditions, 40% of the phenol is oxidized, mostly to 16 ppm catechol, 5 ppm hydroquinone, and 2 ppm resorcinol. These primary byproduct compounds account for 80% (by moles) of the initial carbon. Again, the remaining carbon has be accounted for in other phenol oxidation products not analyzed in this study. There is a higher conversion of phenol at higher voltages (57 kV vs. 46 kV), and higher concentrations of the oxidation products are produced at the higher applied voltage. It has been shown previously (Joshi, 1994) that at higher voltages, there are an increased number of radical species that initiate the phenol oxidation.

The power consumption and solution conductivity of the experiment at 57 kV pulsed corona exposure with no added particles in suspension is found in Table 4. The conductivity of the solution went from an initial value of 120 μScm^{-1} to a final value of 200 μScm^{-1}. This is a higher final conductivity at 57 kV than the previous

case of 46 kV (176 μScm^{-1}). At 57 kV, more hydrogen peroxide is produced, and therefore more of the ferrous ions are converted to ferric ions. Ferric ion production leads to a higher concentration of the hydroxyl radicals to increase the conversion of the phenol. The reactor power consumption under these conditions is 1100 mJ/pulse, which is much higher than the previous case at 46 kV as expected. The removal efficiency at 57 kV is 2.4 g/kWh, comparable to the removal efficiency at 46 kV.

Figure 33 shows the phenol removal for the cases of 1) 46 kV and no particles added, 2) no applied voltage and1 g/L washed activated carbon, and 3) the combination of 46 kV applied voltage with 1 g/L washed activated carbon. As stated previously, after 15 minutes, the experimental condition of 46 kV applied voltage and no carbon resulted in the removal of 28% of the phenol from the bulk solution, while the experimental condition of no corona and 1 g/L washed activated carbon showed a 76% phenol removal. The combination of 46 kV corona treatment and 1 g/L washed activated carbon resulted in 78% phenol removal from the bulk solution. A slight increase in the removal is observed using a combination of corona and compared to carbon by itself.

Although it seems in the above experiment that most of the phenol is being adsorbed onto the surface of the carbon, Figure 34 indicates that there are significant oxidation products being formed. Analysis shows that 6 ppm catechol, 1 ppm hydroquinone, and 1 ppm resorcinol are formed. These levels are slightly lower than for the case of 46 kV alone (no particles). Catechol, resorcinol, and hydroquinone all adsorb quite readily to the activated carbon and it is assumed that there is a significant level of these compounds on the activated carbon after 15 minutes.

The reactor power consumption for the combination of 46 kV pulsed corona treatment and washed activated carbon in suspension was 830 mJ/pulse, which is higher than that for the corona alone (Table 4). The power efficiency was 6.27 g/kWhr for this case, much higher than the case using only pulsed corona treatment. The conductivity of the solution increased from an initial value of 120 μScm^{-1} to a final value of 141 μScm^{-1}. This ending conductivity is lower for the combination of the carbon and corona than for the corona alone. This might indicate that either less hydrogen peroxide is being produced in the pulsed streamer corona with the addition of the activated carbon, the carbon is converting the ferric ion back to the ferrous ion, or that ions are being adsorbed on to the activated carbon.

The experimental results combining pulsed corona treatment in the presence of washed activated carbon particles suggests the possibility of surface reactions occurring on the activated carbon. The activated carbon adsorbs 76% of the phenol in the bulk solution, reducing the amount of phenol in the bulk phase. Similar reduction in the oxidation products should be seen if only bulk phase reactions are occurring. From the oxidation products measured in the bulk phase, there was only a small decrease in the amount of oxidation, not a 76% decrease in byproducts expected for only bulk phase reactions. Some of these products have been adsorbed onto the surface of the carbon. Preliminarily, these results indicate possible surface reactions.

Figure 35 shows the results of 1) 57 kV pulsed corona treatment with no washed activated carbon particles in suspension, 2) no corona with carbon particles, and 3) 57 kV applied voltage with carbon particles. With the 57 kV corona treatment alone, the phenol removal is 40%, while for the 1 g/L washed activated carbon alone,

the phenol removal is 76%. For the combination of both the 57 kV corona treatment and the 1 g/L washed activated carbon, the phenol removal is increased to 89%. There is a greater enhancement of the combination of the carbon and corona at 57 kV than at 46 kV.

Figure 36 shows the oxidation products formed with the combination of 57 kV corona treatment and 1 g/L washed activated carbon. After the 15-minute treatment time, phenol concentration drops from 100 ppm to 11 ppm, and catechol formation is 6 ppm, hydroquinone formation is 2 ppm, and resorcinol formation is 4 ppm. Again, there will be a significant amount of each of these species adsorbed on to the carbon, causing a reduction of the amount f the byproducts able to be detected in the solution. The total amount of oxidation products is similar (and possibly higher) to that of the bulk phase reactions alone, indicating that the adsorbed phenol is also reacting. This result strengthens the notion of surface reactions occurring on the activated carbon.

The power consumption and conductivity change for the combination of 57 kV applied voltage and 1 g/L washed activated carbon are given in Table 4. For this experimental condition, the reactor power consumption is 1370 mJ/pulse. The overall power efficiency for this case was 4.33 g/kWhr. The conductivity of the solution increased from 120 μScm^{-1} to 170 μScm^{-1} after the 15-minute treatment. The final conductivity is lower for the combination of both the 57 kV applied voltage and the 1 g/L washed activated carbon than for the 57 kV corona treatment without particles. Again, this could be due to reduced hydrogen peroxide formation resulting in a lower conversion of ferrous ions to ferric ions, or that the activated carbon catalyzes the reaction of ferric ions to ferrous ions or adsorption of the ions by the activated carbon.

Figure 37 gives the summary for all of the experiments where catechol was formed. The case of 46 kV pulsed corona treatment with no carbon present shows a production of 11 ppm catechol over the 15 minute treatment time. For the 57 kV case with no carbon, the catechol increased from 0 ppm to 16 ppm over the 15-minute interval. Similarly, for the case of 46 kV pulsed corona treatment with 1 g/L washed activated carbon, the catechol continuously increased to 6 ppm over the 15-minute treatment time. Unlike the following three conditions, the 57 kV applied voltage with the 1 g/L washed activated carbon experiment shows an increase in the catechol concentration to 7 ppm at 8 minutes, which then decreases to 6 ppm at 15 minutes. This final condition indicates an increase in the overall rate of reaction of the degradation of the catechol.

Similar trends are seen in the concentration of resorcinol for the four different experiments as seen in Figure 38. The formation of resorcinol in the cases of 46 kV with no carbon, 57 kV with no carbon, and 46 kV with 1 g/L washed activated carbon all increased continuously over the 15-minute treatment time to 2.1 ppm, 2.3 ppm, and 1.5 ppm, respectively. The case of 57 kV corona treatment with 1 g/L washed activated carbon gave a resorcinol concentration of 1 ppm after 8 minutes, which then decreased to 0.5 ppm after 15 minutes.

Figure 39 shows the hydroquinone concentration for the four experimental cases. The overall trend for all experimental cases for pulsed corona treatment with washed activated carbon was for hydroquinone to increase continuously over the 15-minute treatment time. A summary of the phenol primary oxidation products at 57 kV applied voltage and 1 g/L washed activated carbon is given in Figure 40. This

figure shows the increase in the concentration for both the catechol and the resorcinol over the first 8 minutes of the experiment and then a decrease in both concentrations over the final 7 minutes of the experiment. Contrary to this, the hydroquinone continues to increase over the entire 15 minutes of the experiment.

If the activated carbon increased the formation of the hydroxyl radicals in the bulk phase, this would increase the rates of reaction for all of the species and not just two of the three. Surface reactions might explain the selective increase in the degradation of catechol and resorcinol. Hydroquinone, catechol, and resorcinol all adsorb onto the carbon at similar rates. The mechanism of the surface reactions would have to be one that targets both the catechol and the resorcinol to increase the overall rates of reaction and not target the hydroquinone. Further analysis of the products other than catechol, hydroquinone, and resorcinol needs to be done to obtain the true mechanism of the surface reactions.

5.6 Comparison of Experimental and Theoretical Results

To compare the theoretical model to the experimental results, several constants need to be determined. Figure 41 shows the experimental results that determine the adsorption equilibrium constant for phenol on the washed activated carbon. This constant is obtained from the slope of this curve over the concentrations of interest. For this work, the value of 424 (ppm bulk)/(ppm surface) was used.

Another constant in the theoretical model that can be experimentally determined is the kinetic rate of reaction for the phenol oxidation in the bulk phase. This is accomplished by using the experimental data obtained from the phenol breakdown for the 46 kV and 57 kV pulsed corona treatment voltages without any

carbon particles added to the solution. The rate of reaction is assumed to be a first-order reaction. Figures 42 and 43 show the natural logarithm of the concentration divided by the initial concentration versus time. The slope of the best-fit line is then the reaction rate constant. At 46 kV the phenol reaction rate constant is 0.0004 sec^{-1}, and at 57 kV the phenol reaction rate constant is 0.0006 sec^{-1}. Although at 57 kV the first-order rate constant is a good fit to the data, the first-order fit for the 46 kV case is not as good and may be accounted for by the slower initiation reactions.

Other parameters used in the theoretical model were the activated carbon particle radius, the total outer surface area of the activated carbon particles, the volume of the reactor, and the effective diffusivity. The manufacturer provided the total surface area for the activated carbon. The effective diffusivity was estimated (Satterfield, 1970, see Appendix) from typical parameters for activated carbon (most properties were not given by the manufacturer). The values used in the model were 0.0002 m for the particle diameter, 0.024 m^2 for the total outer surface area, 0.001 m^3 for the volume of the reactor, 3.3×10^{-8} m^2s^{-1} for the effective diffusivity, and 4×10^{-6} m/s (Frössling, 1938, Sitaraman, et al., 1963, see Appendix) for the mass transfer resistance coefficient.

Figures 44 and 45 show the results of the fit of the theoretical and experimental cases for the 46 kV and 57 kV pulsed corona treatments without any added particles. The adsorption equilibrium constant (K), in this model was set to 0. In both cases, the experimental data and the theoretical model match very well. This shows that the first-order reaction rate approximation is valid and the results from the model are valid.

The goal of comparing the theoretical model to the experimental data is to determine whether or not there are reactions taking place on the surface of the activated carbon. The only parameter in the theoretical model that can vary is the kinetic reaction rate on the particle surface. All of the other parameters are set at the values mentioned above. To fit the theoretical model to experiments, adjustments were made to the value of k_p until the experimental data and the theoretical model matched as closely as possible. Figure 46 show the best-fit theoretical curve and the experimental data for the combination of 46 kV pulsed corona exposure with 1 g/L washed activated carbon. The value of k_P that was used to determine the best fit for the model was 0.00045 sec^{-1}. The model fit shows that the particle surface reaction rate is in the same order of magnitude of the bulk phase reactions. The model also predicts that after 15 minutes treatment time, the concentration of the phenol on the surface of the carbon particles is around 50 ppm.

Figure 47 shows the experimental data for the 57 kV pulsed corona voltage with 1 g/L washed activated carbon, and the best-fit curve predicted by the theoretical model. The particle surface reaction rate from the model is 0.00175 sec^{-1}. At the higher applied voltage (57 kV), the surface reaction rate is three times larger than the bulk phase reaction rate. For smaller rates of surface phase reactions, theoretical results over 15 minutes would be higher then the values obtained experimentally. The model also predicted a phenol concentration on the surface to be approximately 35 ppm for these conditions. The theory deviates from the experimental values because the model accounts only for the reaction with phenol and no other reactive species. In reality, the primary phenol byproducts also react with the reactive species

induced by the corona. Expanding the model to the multicomponent version should alleviate this problem.

This leads to the conclusion that surface phase reactions are occurring on the carbon particles. These surface reactions are induced by the pulsed streamer corona because they only occur when the pulsed corona treatment is turned on. The combination of bulk phase reactions and surface phase reactions will lead to the enhanced removal and breakdown of the organic contaminants found in the reactor. The surface phase reactions on the activated carbon particles will lead to the in-situ regeneration of the activated carbon. The process itself will clean the contaminants off of the activated carbon surface.

CHAPTER 6

CONCLUSIONS

This study has shown that the presence of activated carbon in aqueous suspension has a dramatic qualitative and quantitative effect on the nature of the pulsed electrical discharge and the removal of phenol. The addition of unwashed activated carbon to deionized water can increase the possible operating pulsed voltage in the reactor from 40 kV to over 100 kV by increasing the voltage at which breakdown occurs. In contrast, the addition of washed activated carbon particles had no effect on the breakdown voltage. The smallest ($\leq$25 μm) glass spheres also showed the trend of increasing the breakdown voltage, but to a smaller degree than that of the unwashed activated carbon. The larger size glass spheres did not have any effect on the breakdown voltage. The addition of high surface area silica gel particles to deionized water in a pulsed streamer reactor does not show effects comparable to that of the activated carbon. The addition of highly conductive copper particles also failed to have effects comparable to the activated carbon; they were found to slightly lower the sparkover voltage from that found with deionized water.

PIXE analysis showed very high levels of potassium on the unwashed activated carbon in concentrations of 1% by weight. In the leachate solution from the

unwashed activated carbon, there were high concentrations of potassium, sodium, calcium, and chloride. The leachate solution from the unwashed glass spheres had high levels of sodium and chlorine. Results from SEM and x-ray emissions showed that the unwashed activated carbon contained potassium on the surface, and after the carbon was washed, the element potassium was not present. Also, SEM showed "dust" particles that appeared on the unwashed activated carbon but the number of these dust particles decreased upon washing and corona treatment.

When the solution conductivity of deionized water reactor samples was increased by the addition of various salts, the breakdown voltage was increased. The addition of washed activated carbon particles to the salt solutions gave the same breakdown voltage as the salt solution alone. This leads to the conclusion that the breakdown voltage is controlled by the conductivity of the solution and not by the type of particle present.

There was a significant physical effect of the presence of activated carbon in suspension, however. The combination of washed activated carbon and a potassium chloride solution gave a power consumption that was 50% less than any other combinations at the higher applied voltages. This phenomenon is both particle specific as well as salt specific. The unwashed activated carbon also showed lower power consumption, but not as low as the washed activated carbon together with the potassium salt.

The chemical effects showed that without activated carbon particles in suspension, phenol removal in 15 minutes is 26% for a 46 kV corona treatment and 40% for the 57 kV corona treatment. For these cases, catechol, resorcinol, and

hydroquinone formation occurred. Without the activated carbon present, the pathway for removal is through oxidation reaction. When the activated carbon is present and there is no corona treatment, the amount of phenol adsorbed onto the washed activated carbon is 76% in 15 minutes. For the combination of the washed activated carbon and pulsed corona treatment, the phenol removal was enhanced to 78% and 89% for 46 kV and 57 kV pulsed corona treatments, respectively. These cases showed significant primary phenol byproduct formation through catechol, resorcinol, and hydroquinone. For both cases, adsorption and reactions are taking place.

An enhanced removal of phenol occurred in the case of the combination of washed activated carbon and pulsed streamer corona. Analysis of the phenol breakdown products indicates possible reactions occurring on the surface of the activated carbon. These surface reactions are specific to increasing the rate of reaction for the catechol and the resorcinol but not the hydroquinone. It has also been shown that with the combination of corona treatment and activated carbon, the removal of the phenol is enhanced through adsorption as well as reactions induced on the surface of the carbon and in the bulk solution. With the surface reactions, the contaminants that are adsorbed onto the carbon are ultimately removed and the carbon is regenerated.

The first-order reaction rate constants for the phenol oxidation without carbon present are 0.0004 sec^{-1} and 0.0006 sec^{-1} for applied voltages of 46 kV and 57 kV, respectively. The phenol-washed activated carbon adsorption equilibrium constant is 454 (ppm bulk)/(ppm on surface).

The comparison between the experimental data and the theoretical model

indicates that surface reactions are taking place. At 46 kV, the surface reaction rate constant of phenol breakdown is 0.00045 sec^{-1}, which is the same order of magnitude as the bulk phase reaction rate. At 57 kV, the surface reaction rate constant of phenol breakdown is 0.00175 sec^{-1}, which is 3 times larger than the bulk phase reaction rate.

CHAPTER 7

DIRECTIONS FOR FURTHER STUDY

Future work can proceed in several different ways. These would include further work on the modeling of the chemical reactions and more experiments looking at the chemical and physical aspects of aqueous phase pulsed streamer corona with the addition of the carbon particles.

To this point, the reaction and diffusion model presented included only one component. This model can be extended to a two component system where the two reactions taking place are in series. This model could then be extended to include i-components. After this, a more rigorous model needs to address the actual pathways of the phenol reactions. The reactions that occur on the carbon particle surface also need to be included, if different than those occurring in the bulk phase. As mentioned before, the breakdown of phenol leads to several primary byproducts by means of parallel reactions. The model needs to be modified to include parallel reactions instead of series reactions to better account for the true nature of phenol oxidation.

To further investigate the chemical effects of the added carbon particles, more experiments need to be done to look at the breakdown of phenol. The present work observed the addition of washed activated carbon only. The degradation of phenol

now needs to be investigated with the addition of unwashed activated carbon as well as the addition of the potassium ions to a suspension of unwashed carbon particles in aqueous phenol. This might help in understanding the role of the potassium ions that leach off of the unwashed activated carbon as well as isolating the effects of the potassium and the activated carbon.

Further, the induced Fenton's reaction was conducted at an optimal value obtained from Sharma (1993). This value was optimized for an initial concentration of 1 ppm. This might be the optimal value for starting at a higher level of phenol, such as that 100 ppm which this study uses as an initial concentration. The iron concentration needs to be re-evaluated for this phenol concentration.

The problems that exist with comparing the experimental data to the theoretical model are that we assumed that the bulk reactions under pulsed corona conditions remain the same with and without the addition of carbon particles, and that the adsorption equilibrium remains the same with and without the corona discharge. These assumptions need to be validated experimentally. To do so, a chemical compound needs to be found that adsorbs onto the carbon but does not react under the oxidizing conditions of pulsed corona treatment. This will enable us to determine if the adsorption equilibrium constant is affected by the corona. Next, there needs to be a way to determine the effects of the added particles on the bulk phase reactions. This could be possible if there was an oxidizable compound that did not adsorb onto the carbon, or if there was a suitable particle other than the carbon that could be added to the reactor to simulate the physical effects of the added carbon particles but

with out the adsorption effects. This would determine if there are any changes in the bulk phase reactions with and without the added carbon particles.

Another point of interest would be to consider both the physical and the chemical behavior of different forms of activated carbon. The variations of the activated carbon could include different pore sizes, different total surface area, and most importantly, activated carbon made by different means of activation. The activated carbon used in these experiments was activated by treatment with potassium hydroxide. Many other chemicals are used in the activation of carbon. These could lead to studying ions other than potassium that might increase the power efficiency. Also, different pore sizes could change the diffusion and reaction rates inside the particle and possibly enhance the phenol decomposition.

The reactor used in this study needs to be optimized to obtain the highest removal of phenol using the least amount of power. Variations in the amount of carbon, the ferrous ion concentration, the potassium ion concentration, the applied voltage, and the flow of oxygen should be investigated. If the power efficiency of this process can be increased to 20 g/kWhr, this process would be economical at the industrial level (Creyghton, 1997b). The optimization can be extended to the design of a flow reactor. This flow reactor could have multiple pulsed corona points where some discharge points have oxygen flowing through the corona (for ozone formation) and others have no oxygen flowing through the needles (hydrogen peroxide formation). These multiple discharges could control the ratio of ozone and hydrogen peroxide formation. Optimization of this ratio could lead to high power efficiencies.

Different experimental techniques could also be used to make observations not yet attained. One of these is the ultra-high speed photography. This could be used to measure the velocity of the streamer propagation as well as observing the interaction of the streamers with the particles. Monochronometers could detect the light emitted by the plasma. This technique could help in identifying different reactive species produced in the plasma as well giving local electron temperatures.

Now that it has been shown that there is a significant effect of the combination of the potassium ion and the carbon particles, a theoretical interpretation of these results needs to be obtained. This would begin with all of the governing equations of an electrical discharge in a three-phase system. These equations would then need to be solved under unique sets that would account for all species (liquid, gas, solid, and plasma) and for all of the reactive species created by the discharge. In combination with this, a steamer propagation model would also need to be included to show the interaction of the streamer with the carbon particles. This combined with the experimental results should answer some of the remaining question regarding the role of the activated carbon in the pulsed streamer corona.

Table 1.

Comparison of the Constants for the 3 Model Cases

	No mass transfer case rxn in closure	no mass transfer case no rxn in closure (rectangular coords.)	no mass transfer case no rxn in closure (spherical coords.)	mass transfer case no rnx in closure
W	$\psi - \phi_p$	$(-3 - \phi_p)$	$(-9 - \phi_p)$	$\left(\frac{-3RK_{ml}}{RK_{ml} + 3D} - \phi_p\right.$
Y	$-K\psi$	3K	9K	$\left(\frac{3KK_{ml}R}{K_{ml}R + 3D}\right)$
X	$-\gamma\psi$	3γ	9γ	$\left(\frac{AR^2 3K_{ml}}{VRK_{ml} + 3VD}\right)$
Z	$-(K\gamma\psi - \phi_b)$	$(3\gamma K + \phi_b)$	$(9\gamma K + \phi_b)$	$\left(\frac{3AR^2 KK_{ml}}{RVK_{ml} + 3VD} + \phi_b\right)$

$$\psi = \frac{\phi_p \tanh\sqrt{\phi_p}}{\tanh\sqrt{\phi_p} - \sqrt{\phi_p}}$$ where the limit as $k_p \rightarrow 0$ is -3

$$\gamma = \frac{AX}{V}$$

Table 2.

Summary of Experimental Results (Physical Effects)

Particle	Concentration (g/L)	Breakdown (kV)	Surface Area (m^2)	Conductivity (μScm^{-1})
none	0	49 kV	0	1
Activated Carbon	1 g/L	57 kV	575 m^2	80
Activated Carbon	2 g/L	64 kV	1150 m^2	130
Activated Carbon	4 g/L	75 kV	2300m^2	400
Activated Carbon	6 g/L	85 kV	5750m^2	650
Glass Beads ≤25 μm	1 g/L	51 kV	0.194m^2	22
Glass Beads ≤25 μm	2 g/L	57 kV	0.388m^2	30
Glass Beads ≤25 μm	5 g/L	64 kV	0.970m^2	70
Glass Beads 30-60 μm	1 g/L	49 kV	0.103m^2	-
Glass Beads 30-60 μm	2 g/L	51 kV	0.0206m^2	-
Glass Beads 53-78 μm	1 g/L	49 kV	0.074m^2	12
Glass Beads 53-78 μm	2 g/L	49 kV	0.148m^2	15
Glass Beads 53-78 μm	5 g/L	49 kV	0.378m^2	25
Glass Beads 110-180 μm	1 g/L	49 kV	0.033 m^2	15
Glass Beads 110-180 μm	2 g/L	49kV	0.066 m^2	8
Glass Beads 110-180 μm	5 g/L	49 kV	0.148 m^2	10
Silica Gel	1 g/L	46 kV	750m^2	2
Silica Gel	2 g/L	46 kV	1500m^2	3
Copper Dust	2 g/L	46 kV	-	3
Copper Dust	5 g/L	46 kV	-	3

Table 3.

Elemental Analysis (PIXE) of Activated Carbon and Glass Spheres

Element	Carbon (ppm)	Carbon Leachate (ppm)	Glass Sphere Leachate (ppm)
Sodium	bdl*	12	39
Silicon	86	4.90	9.39
Phosphorous	247	4.20	bdl*
Sulfur	1040	bdl*	9.89
Chlorine	129	2.63	5.07
Potassium	9210	157	bdl*
Calcium	397	3.07	6.39
Chromium	2.6	bdl*	0.188
Manganese	4.7	bdl*	bdl*
Nickel	bdl*	bdl*	0.016
Iron	0.069	0.069	0.061
Copper	19	0.050	0.030
Zinc	1.56	0.122	0.100
Rubidium	17	0.294	bdl*
Molybdenum	6.66	bdl*	bdl*
Selenium	bdl*	bdl*	0.022
Strontium	13	bdl*	bdl*

* below detection limit

Table 4.

Summary of Experimental Results (Chemical Effects)

Condition	46 kV No Carbon	57 kV No Carbon	46 kV 1 g/L Washed Carbon	57 kV 1 g/L Washed Carbon
Initial Conductivity	120 µS/cm	120 µS/cm	120 µS/cm	120 µS/cm
Final Conductivity	176 µS/cm	200 µS/cm	141 µS/cm	170 µS/cm
Phenol Removed	28%	40%	78%	89%
Power per Pulse	800 mJ/pulse	1100 mJ/pulse	830 mJ/pulse	1370 mJ/pulse
Power Efficiency	2.3 g/kWhr	2.4 g/kWhr	6.3 g/kWhr	4.3 g/kWhr

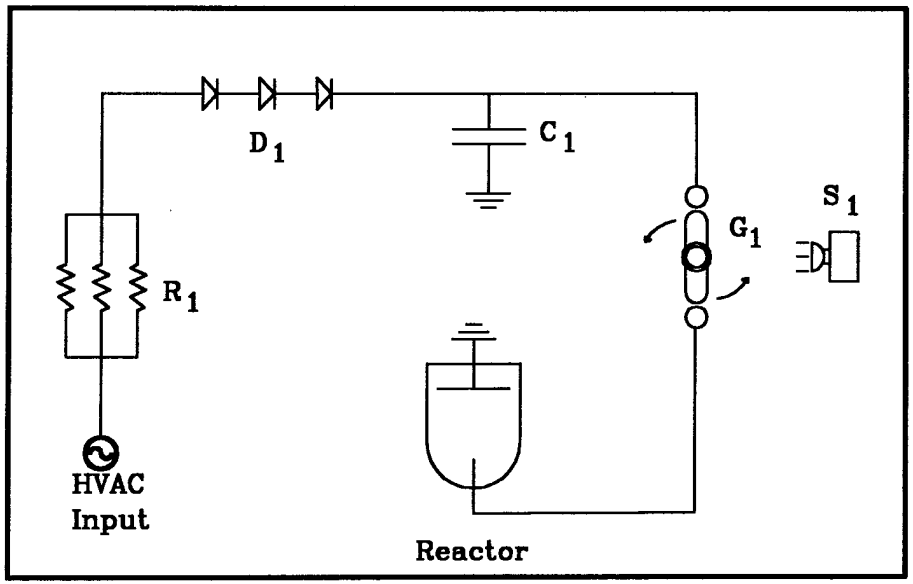


Figure 1
Pulsed Power Supply Circuit Diagram

HVAC = 0 – 100 kV, 0 – 28 mA

R_1 = 333 kΩ

D_1 = 60 kV, 12 A max

C_1 = 2900 pF

G_1 = Rotating Spark Gap, 1800 RPM, 60 discharges / sec

S_1 = Strobe Lamp

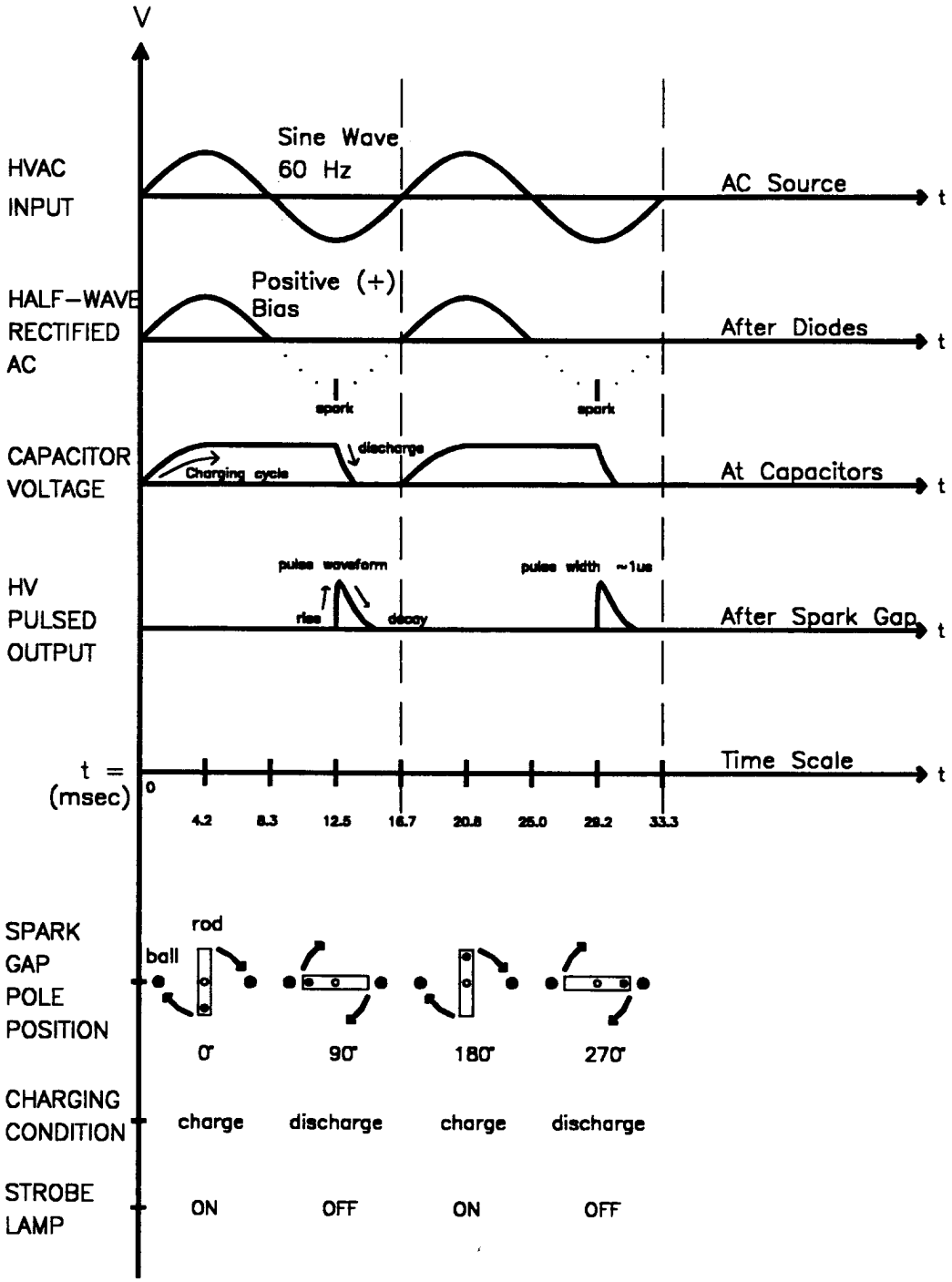


FIGURE 2

PULSED POWER SUPPLY

VOLTAGE VS. TIME WAVEFORMS

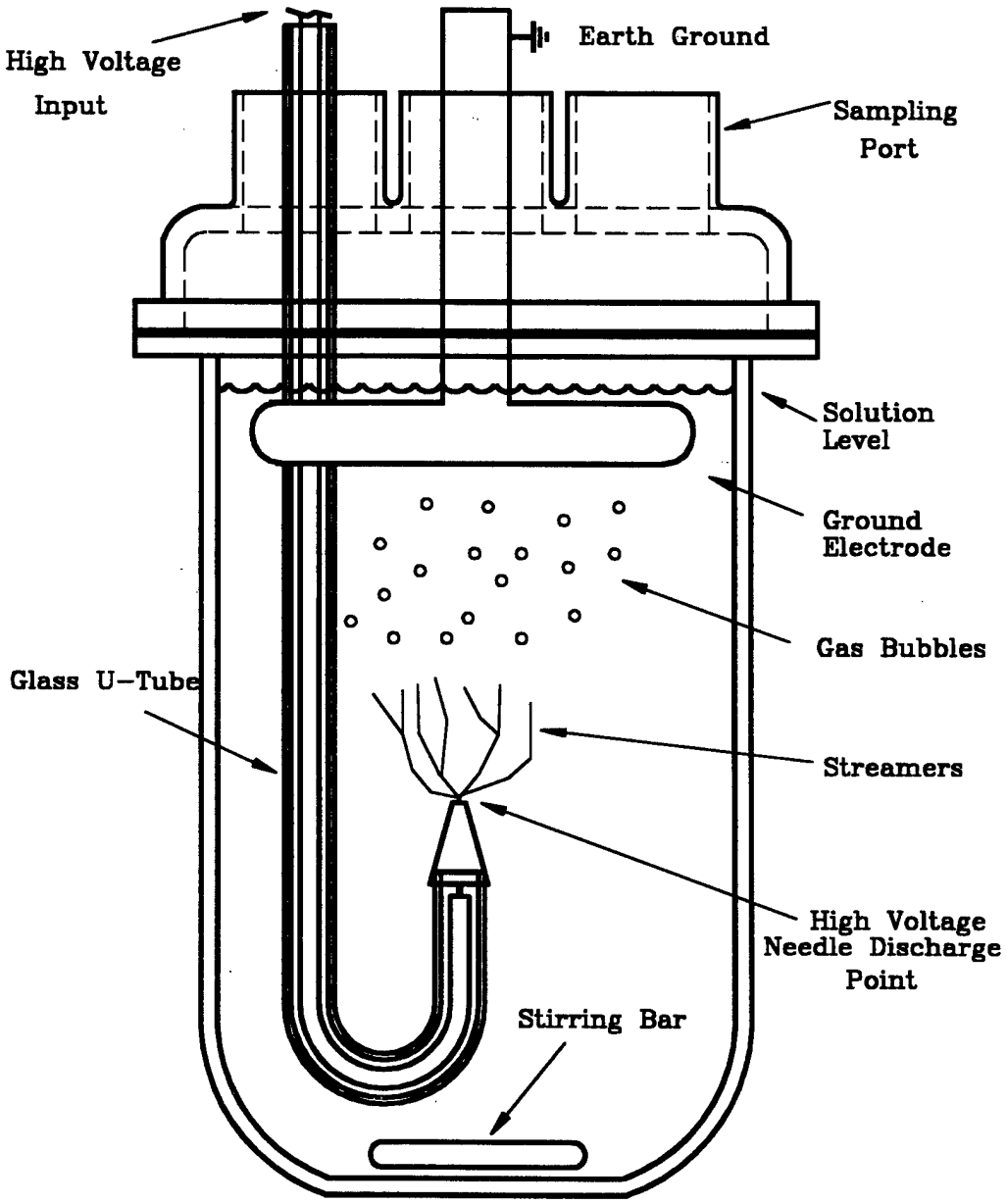


Figure 3
Liquid Phase Reactor I
(without jacket)

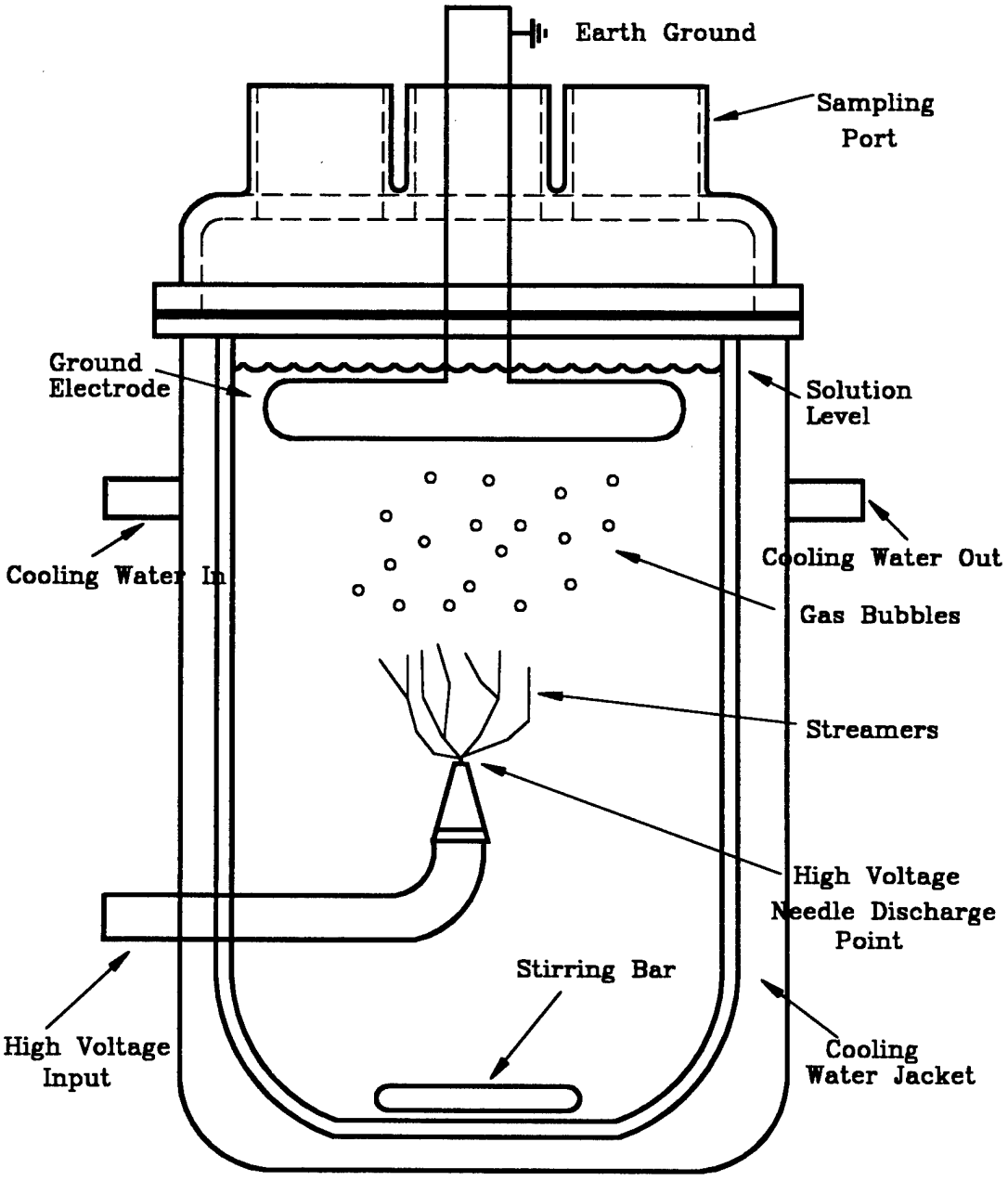


Figure 4
Liquid Phase Reactor II
(Jacketed Reactor)

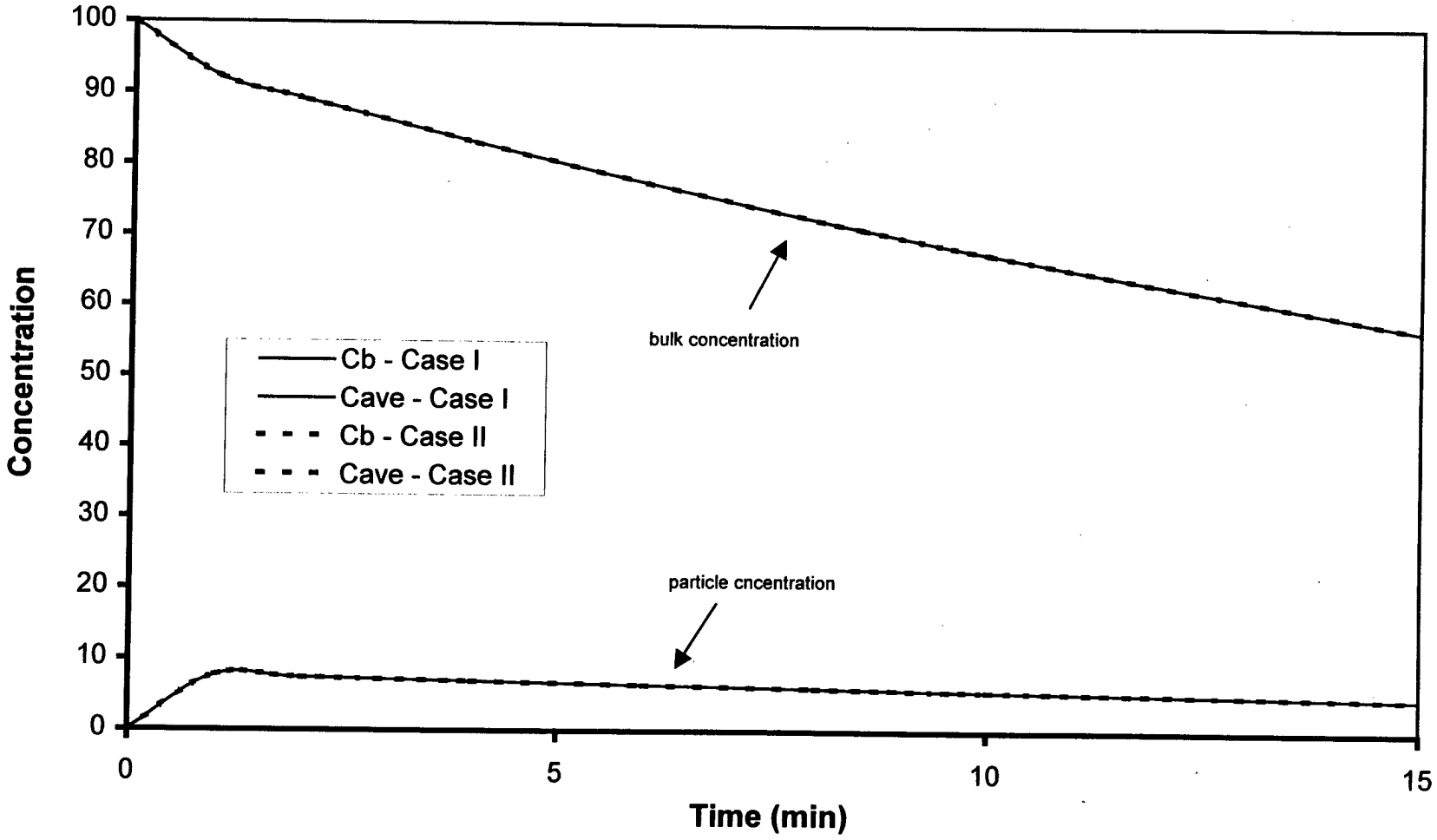


Figure 5. The Effects of Surface Reactions on the Closure Problem ($k_p = 10^{-5}$ sec^{-1})

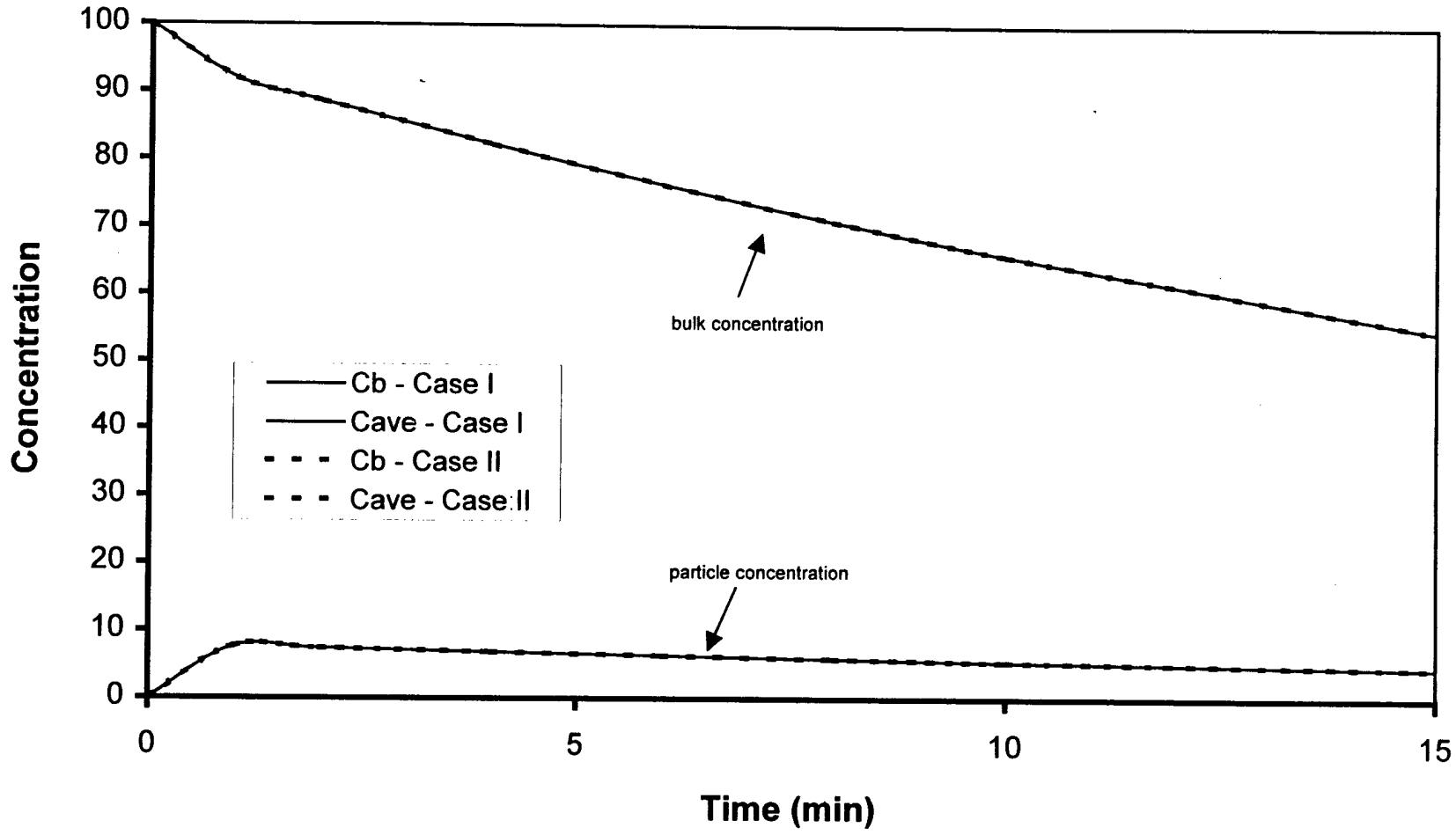


Figure 6. The Effects of Surface Reactions on the Closure Problem ($k_p = 10^{-3}$ sec^{-1})

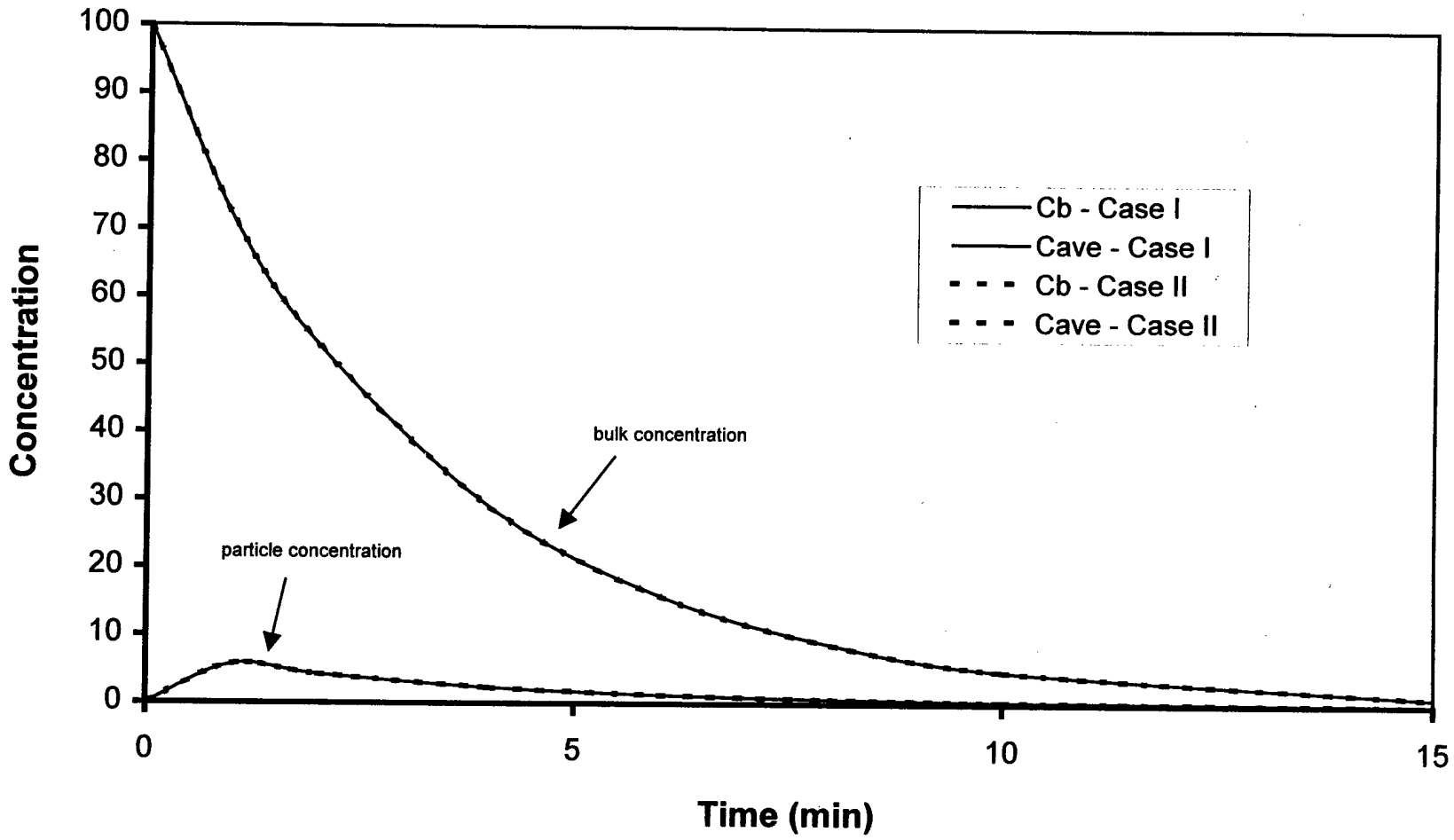


Figure 7. The Effects of Surface Reactions on the Closure Problem ($k_p = 10^{-1}$ sec^{-1})

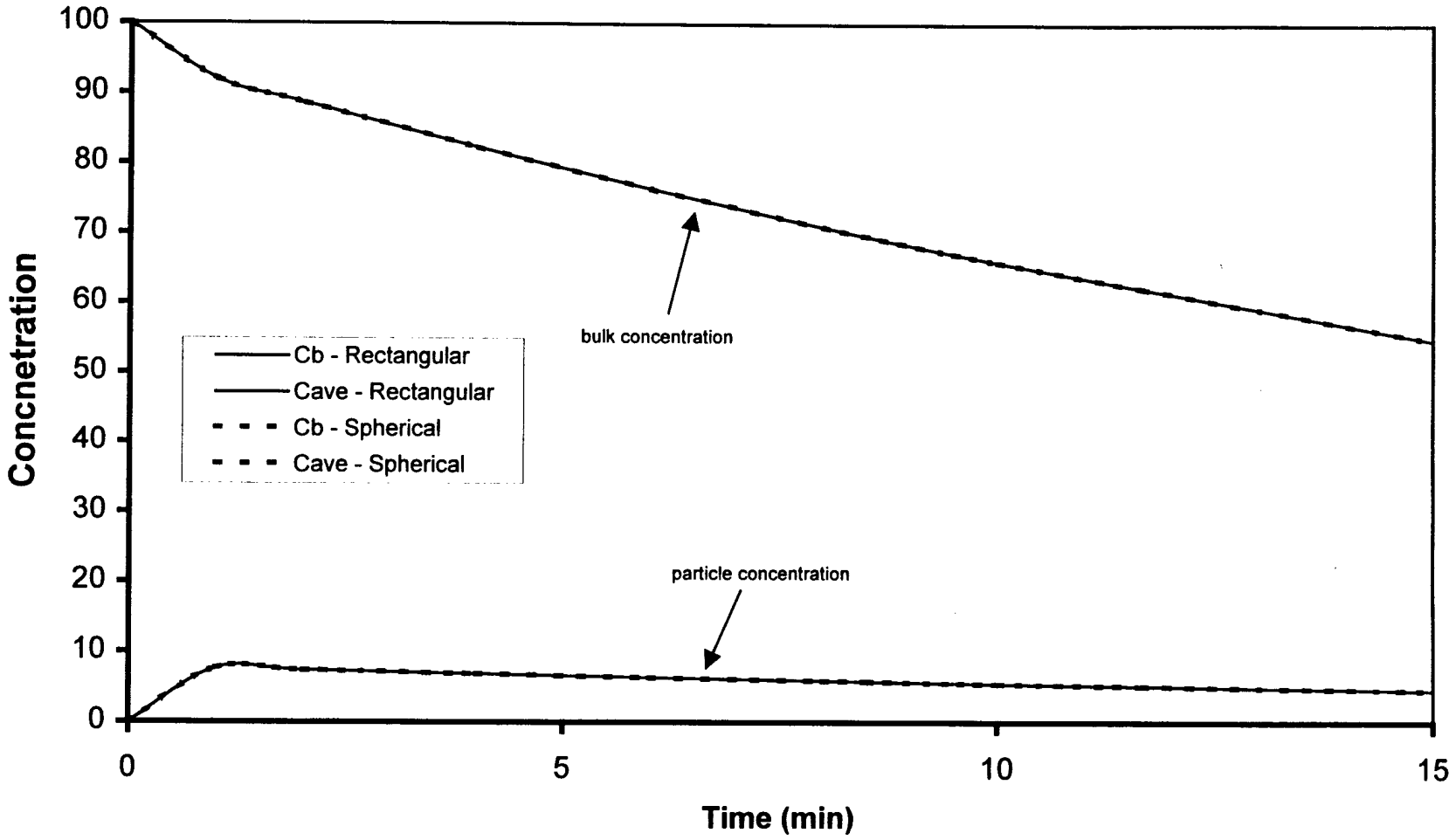


Figure 8. Rectangular vs Spherical Geometry in Model Formulation

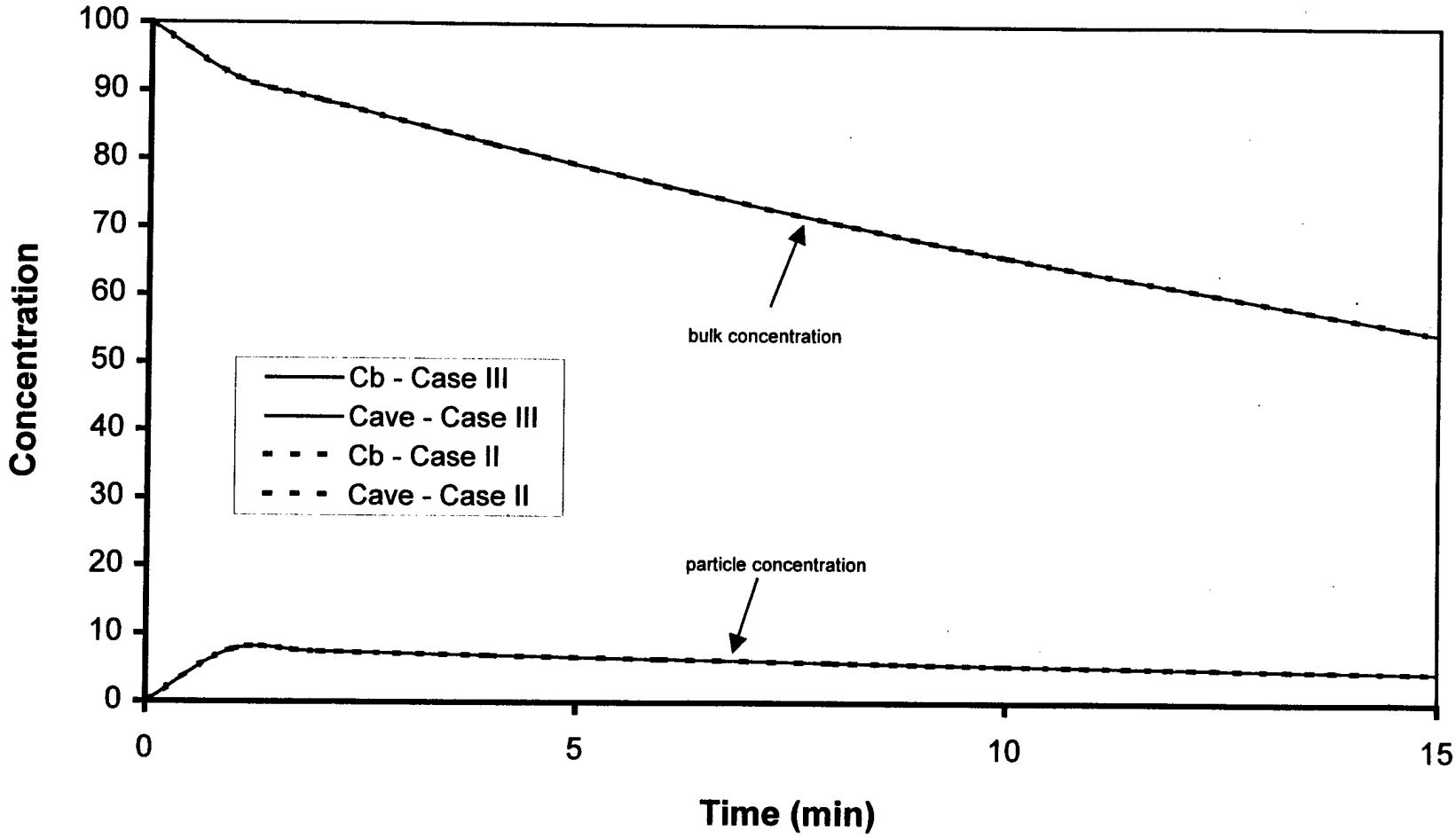


Figure 9. The Effect of Mass Transfer Resistance on the Theoretical Model (K_{mt} = 1 m/s)

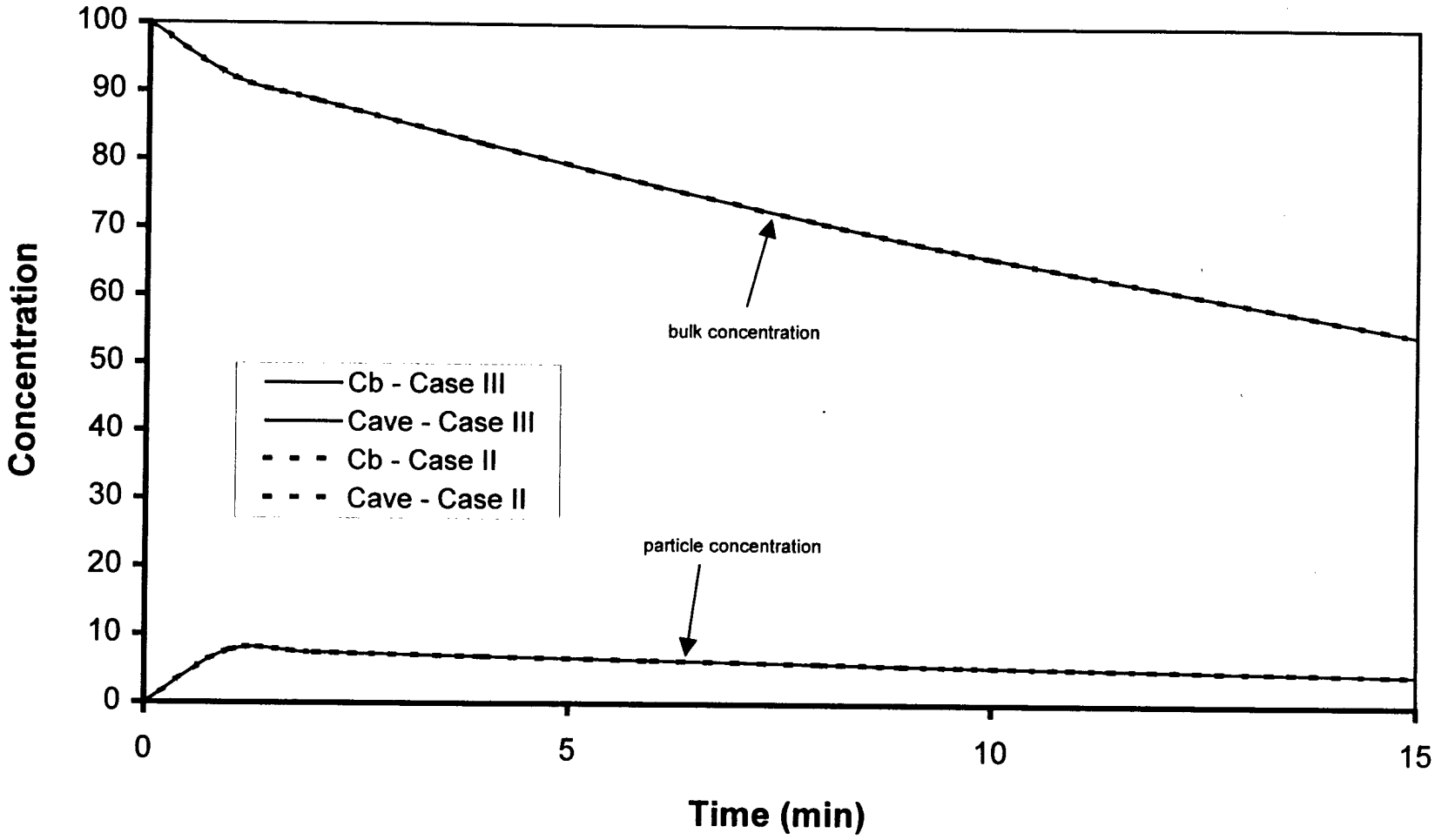


Figure 10. The Effect of Mass Transfer Resistance on the Theoretical Model ($K_{mt} = 10^{-3}$ m/s)

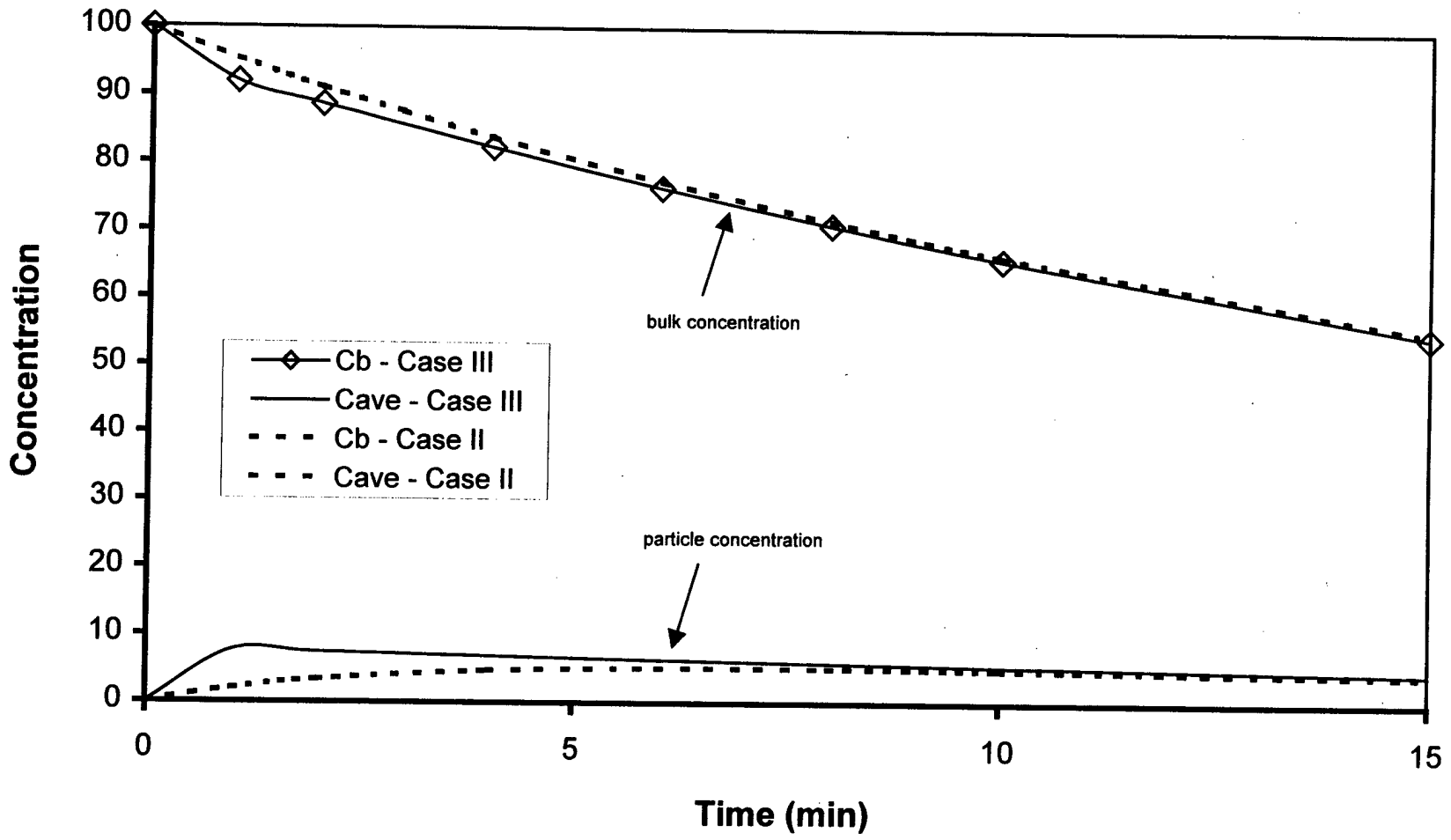


Figure 11. The Effect of Mass Transfer Resistance on the Theoretical Model ($K_{mt} = 10^{-6}$ m/s)

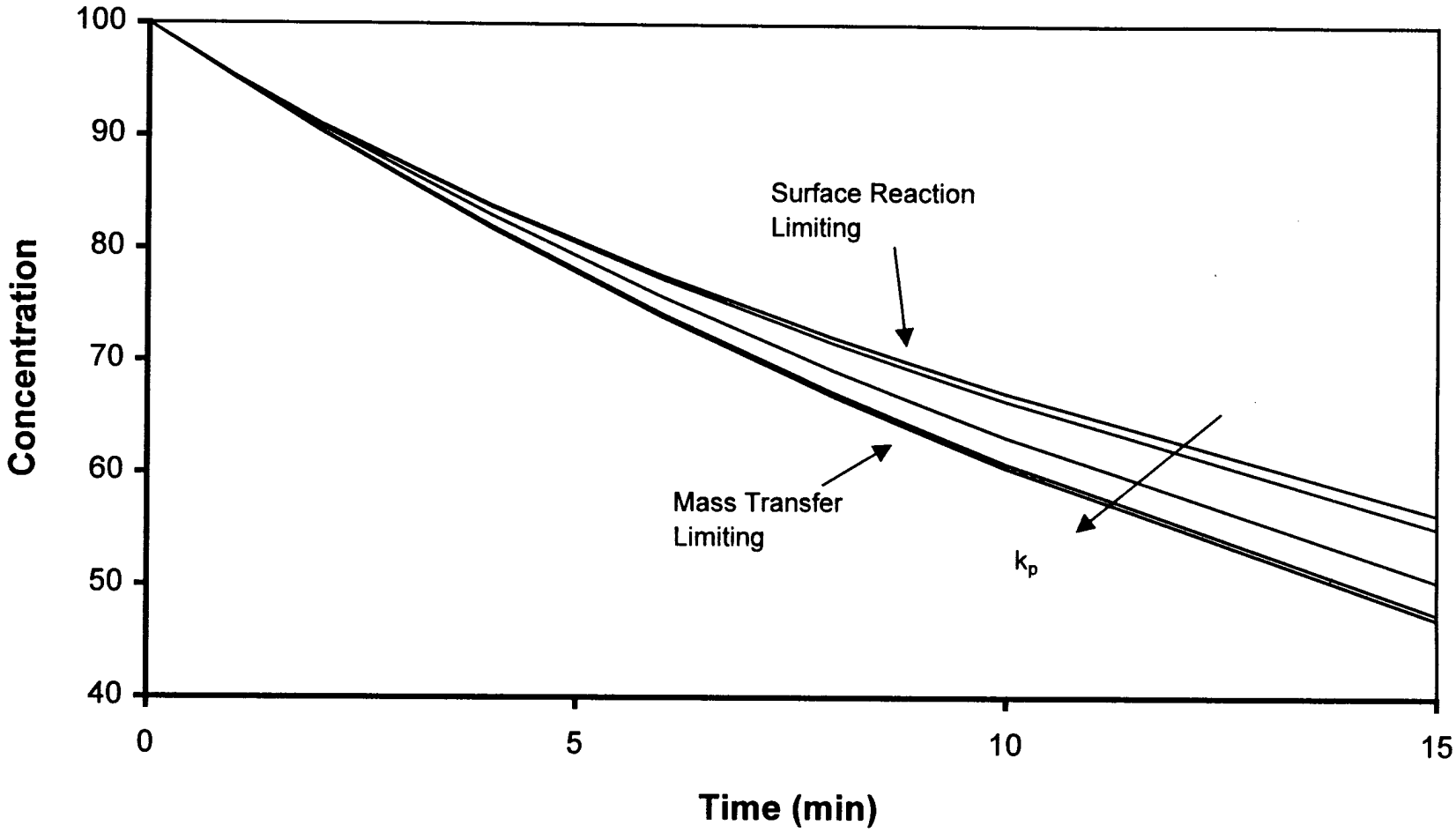


Figure 12. The Effect of the Surface Reaction Rate on the Bulk Solution Concentration

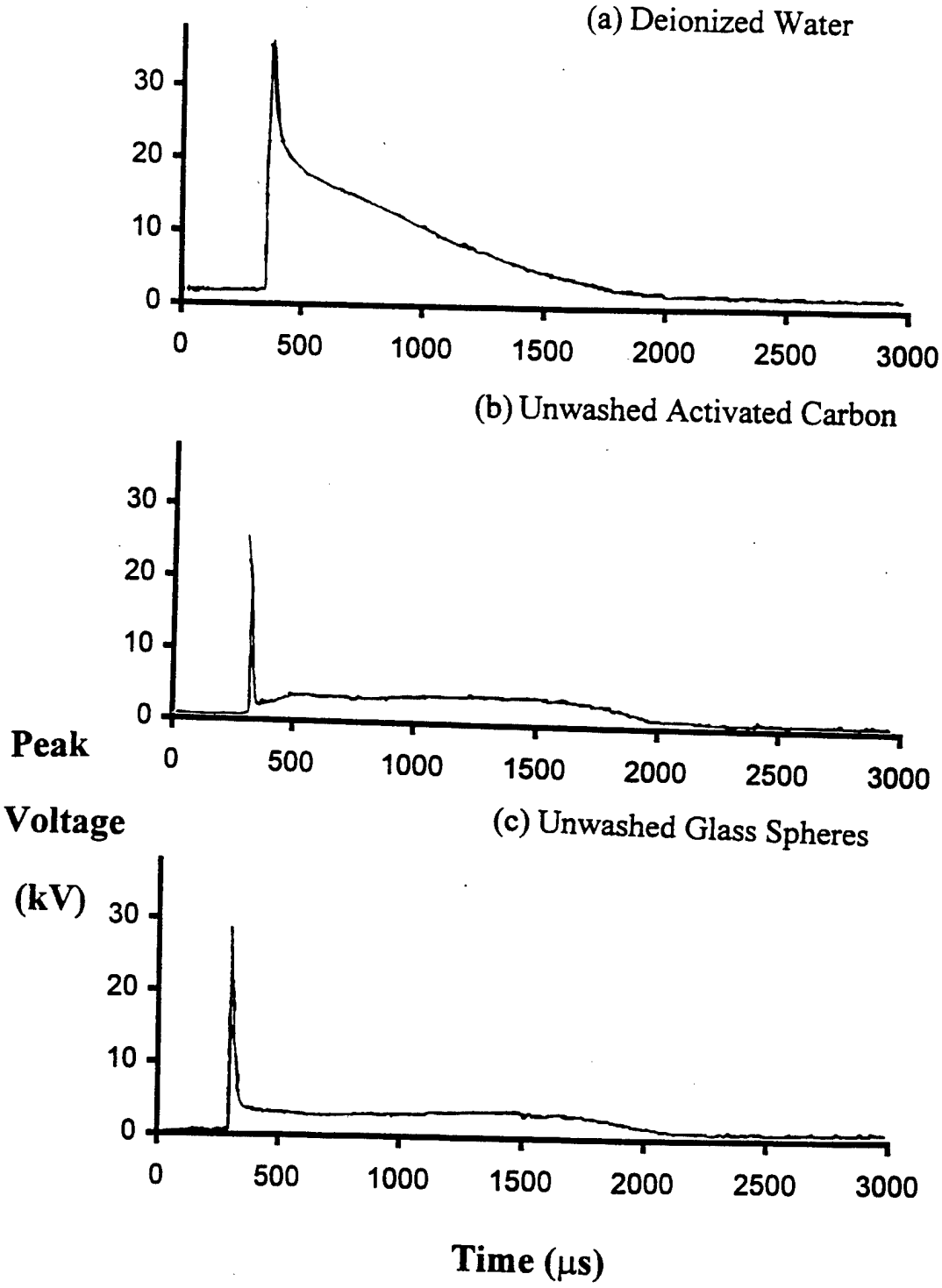


Figure 13. Voltage Waveforms for Various Solutions

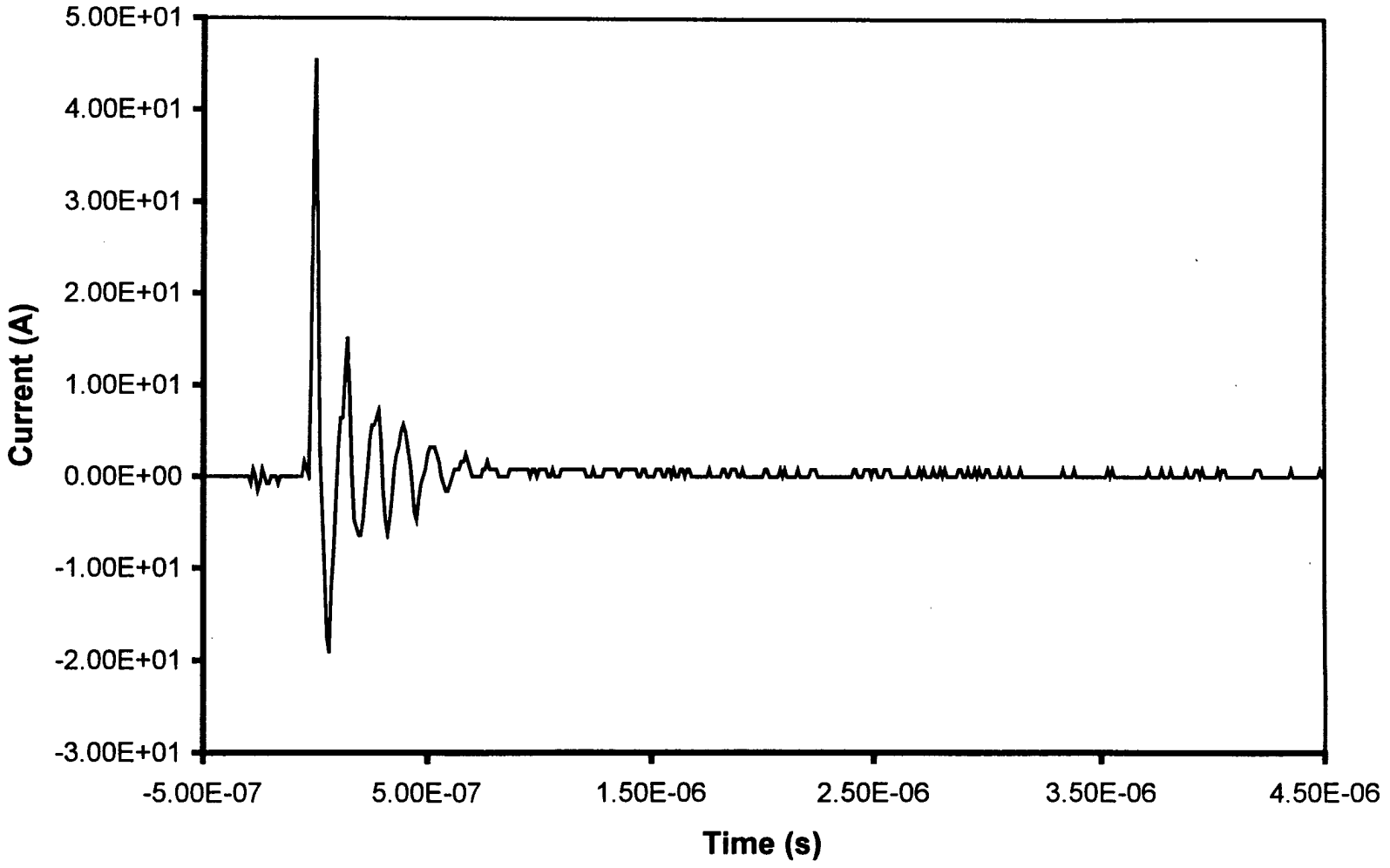


Figure 14. Current Waveform for Deionized Water

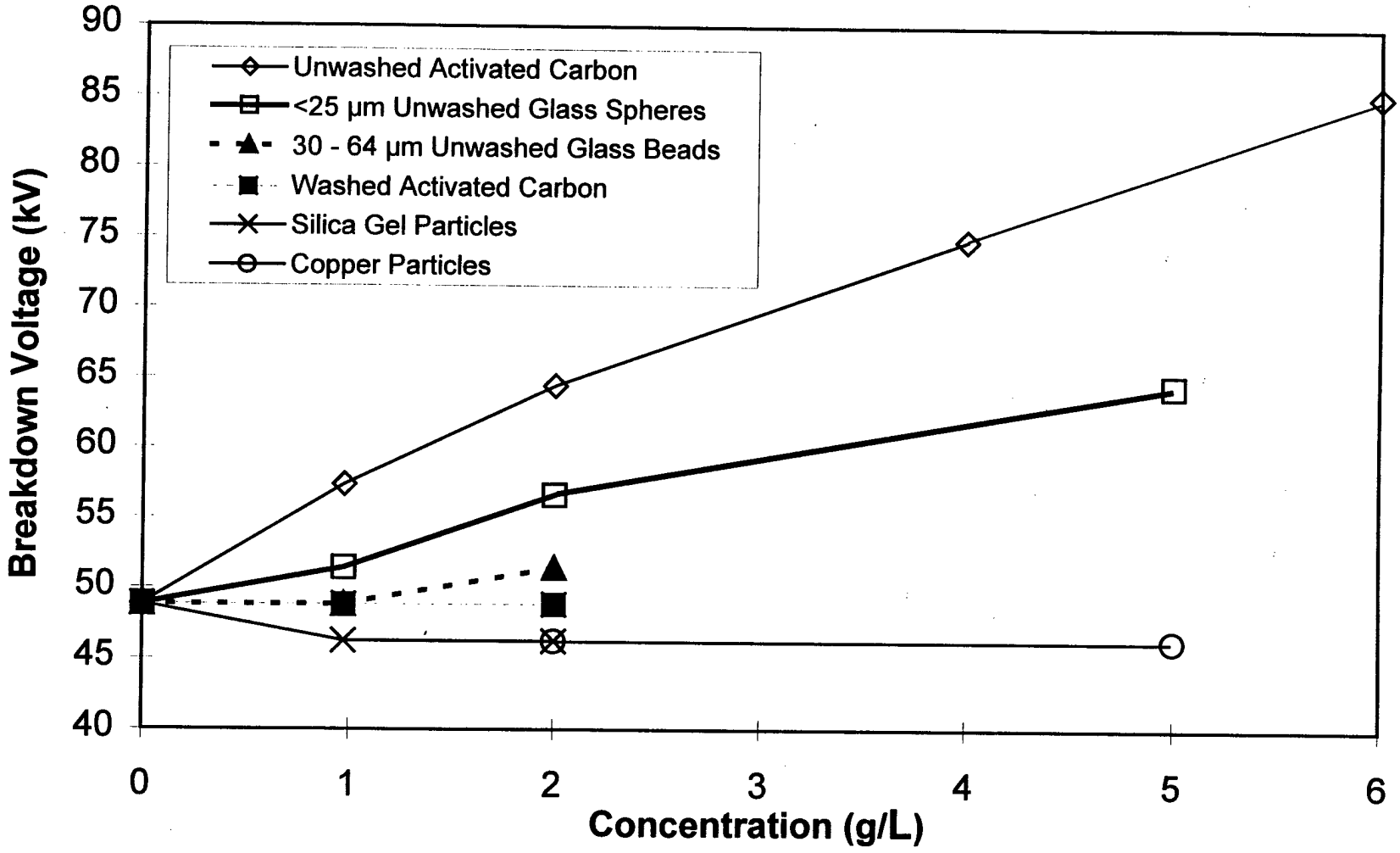


Figure 15. The Effect of Particle Concentration on Breakdown Voltage

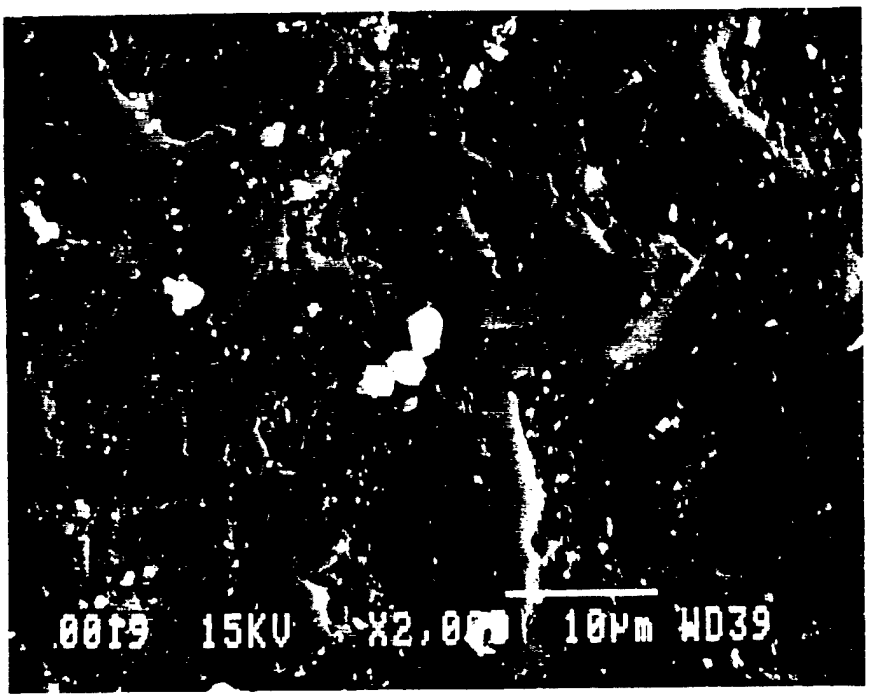


Figure 16. Unwashed Activated Carbon

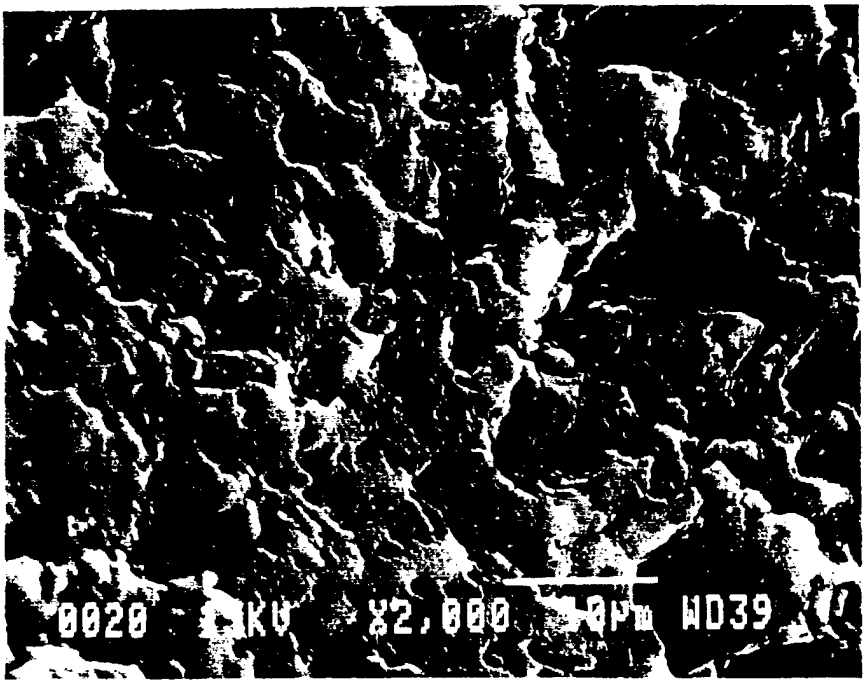


Figure 17. Washed Activated Carbon

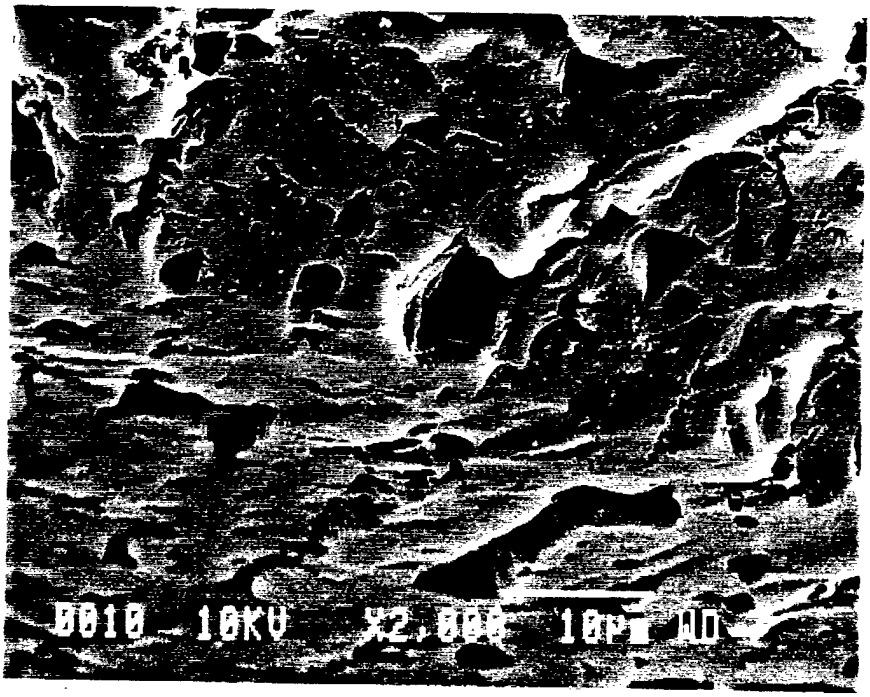


Figure 18. Unwashed Corona Treated Activated Carbon

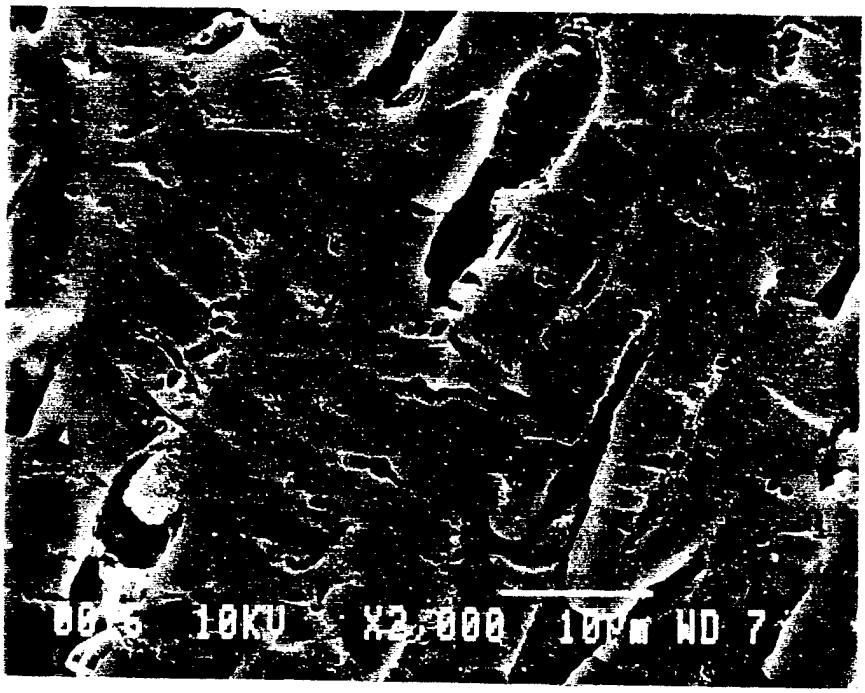


Figure 19. Washed Corona Treated Activated Carbon

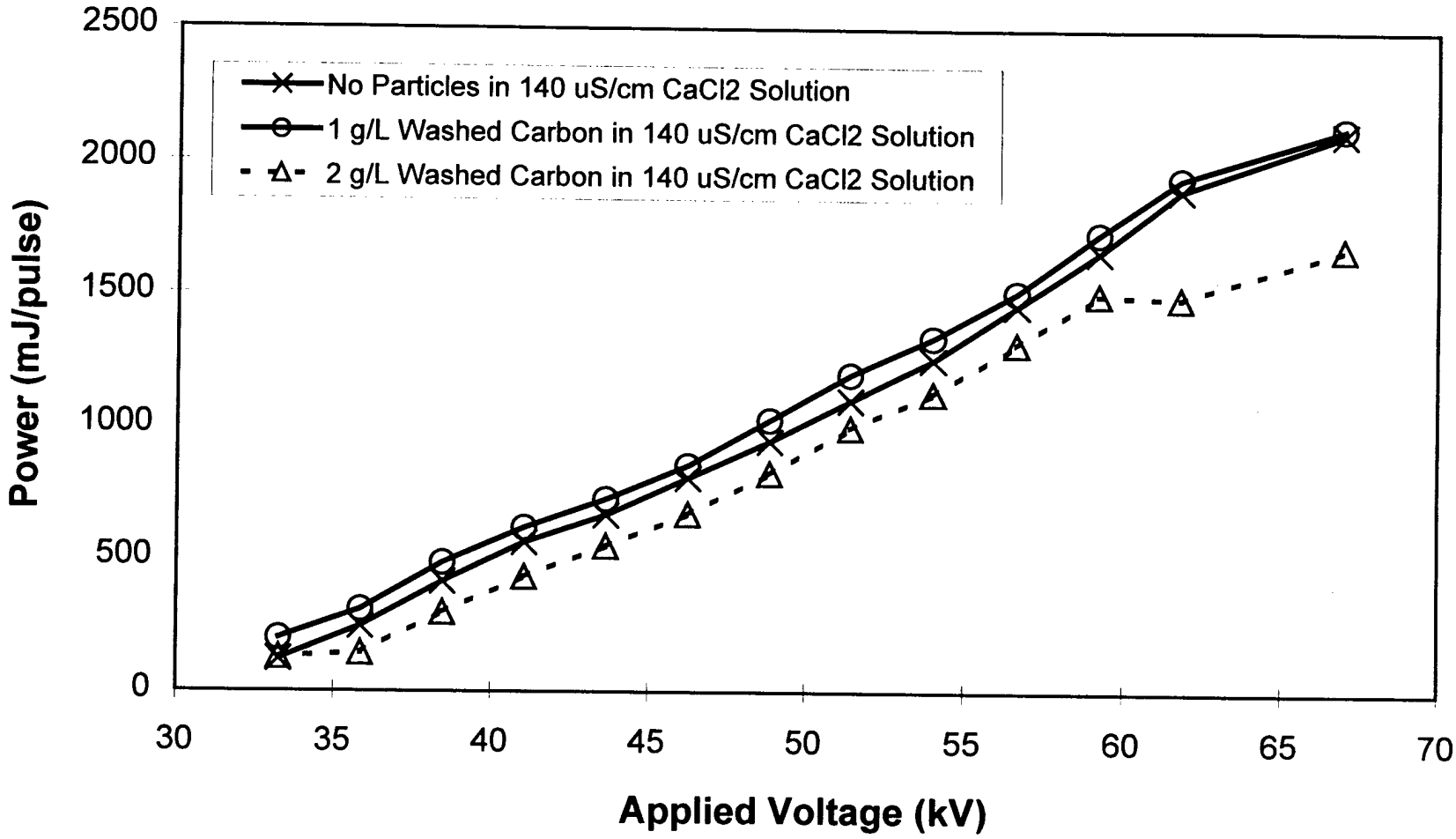


Figure 20. The Effect of Washed Activated Carbon in a $CaCl_2$ Solution on the Reactor Power Consumption

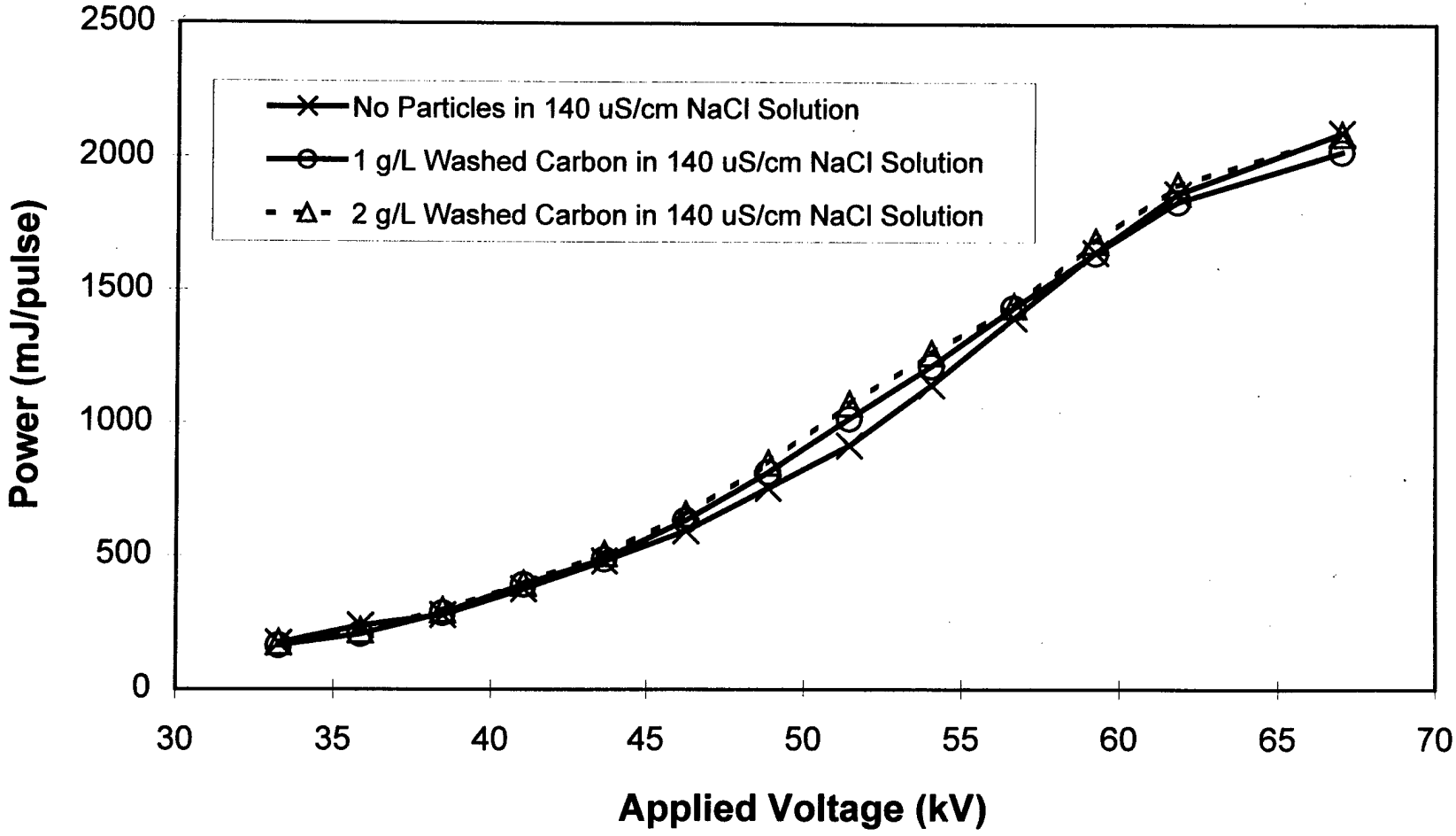


Figure 21. The Effect of Washed Activated Carbon in a NaCl Solution on the Reactor Power Consumption

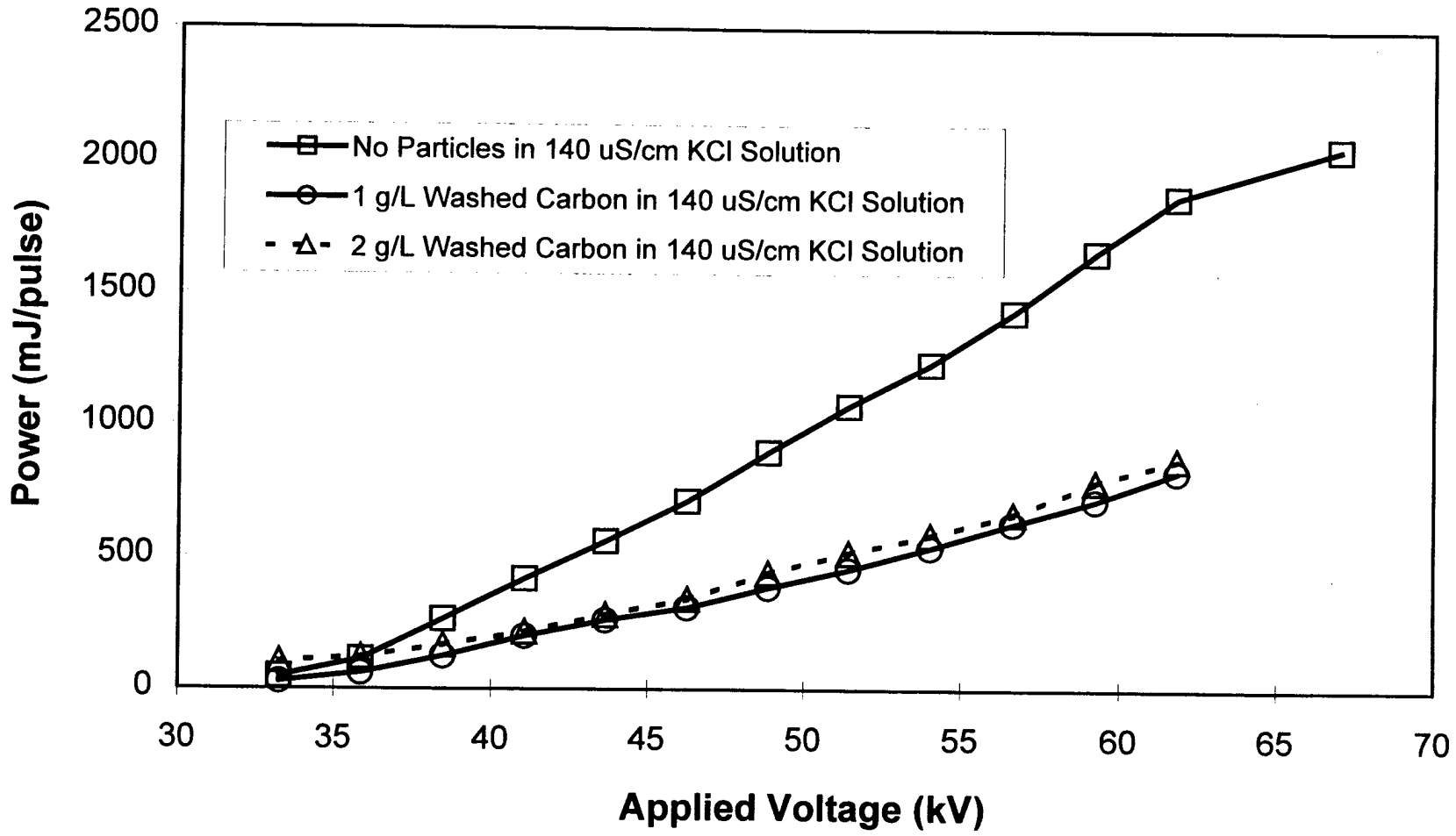


Figure 22. The Effect of Washed Activated Carbon in a KCl Solution on the Reactor Power Consumption

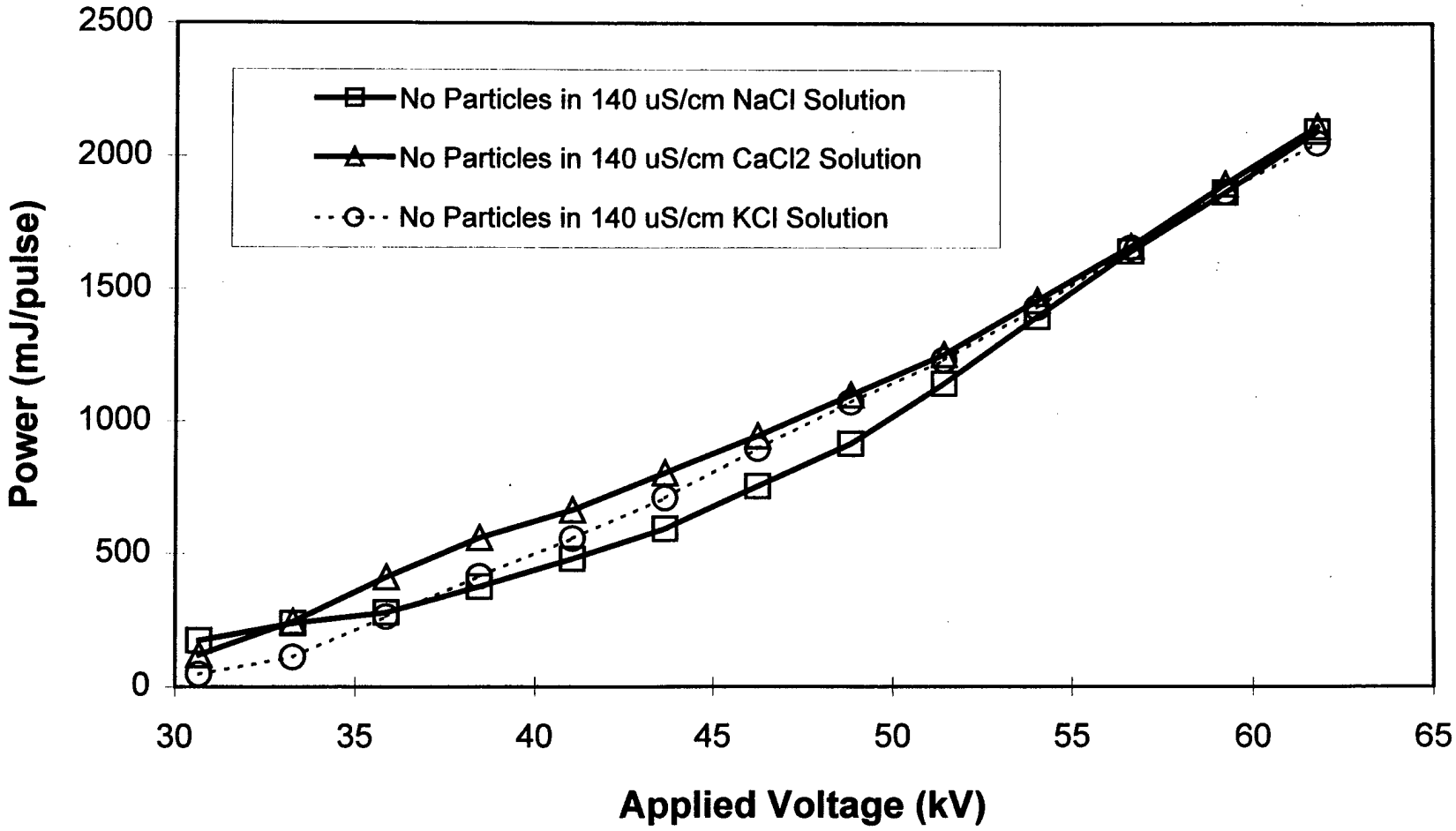


Figure 23. The Effect of Different Salt Solutions on the Reactor Power Consumption

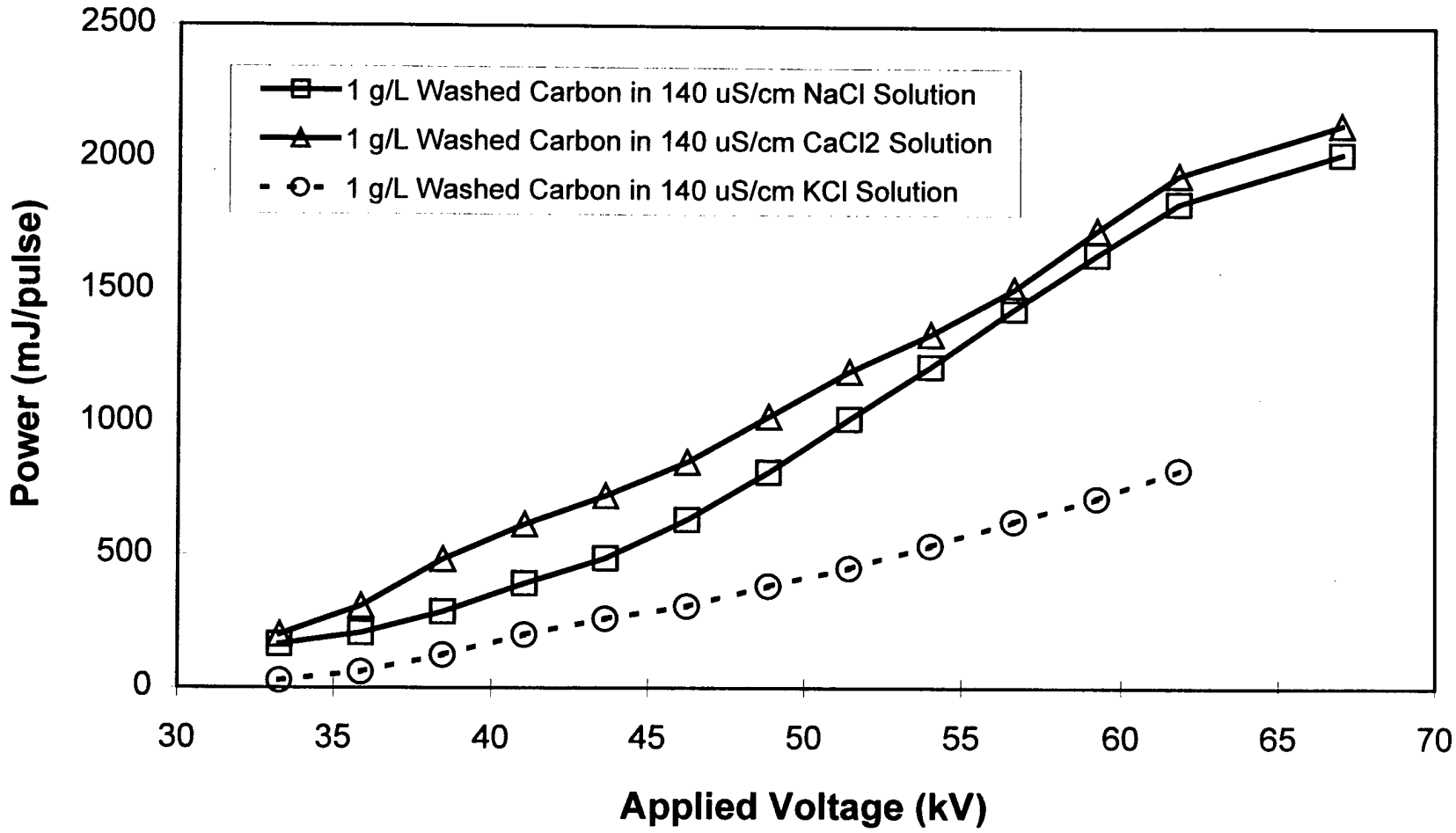


Figure 24. The Effect of Different Salt Solutions and 1 g/L Washed Activated Carbon on the Reactor Power Consumption

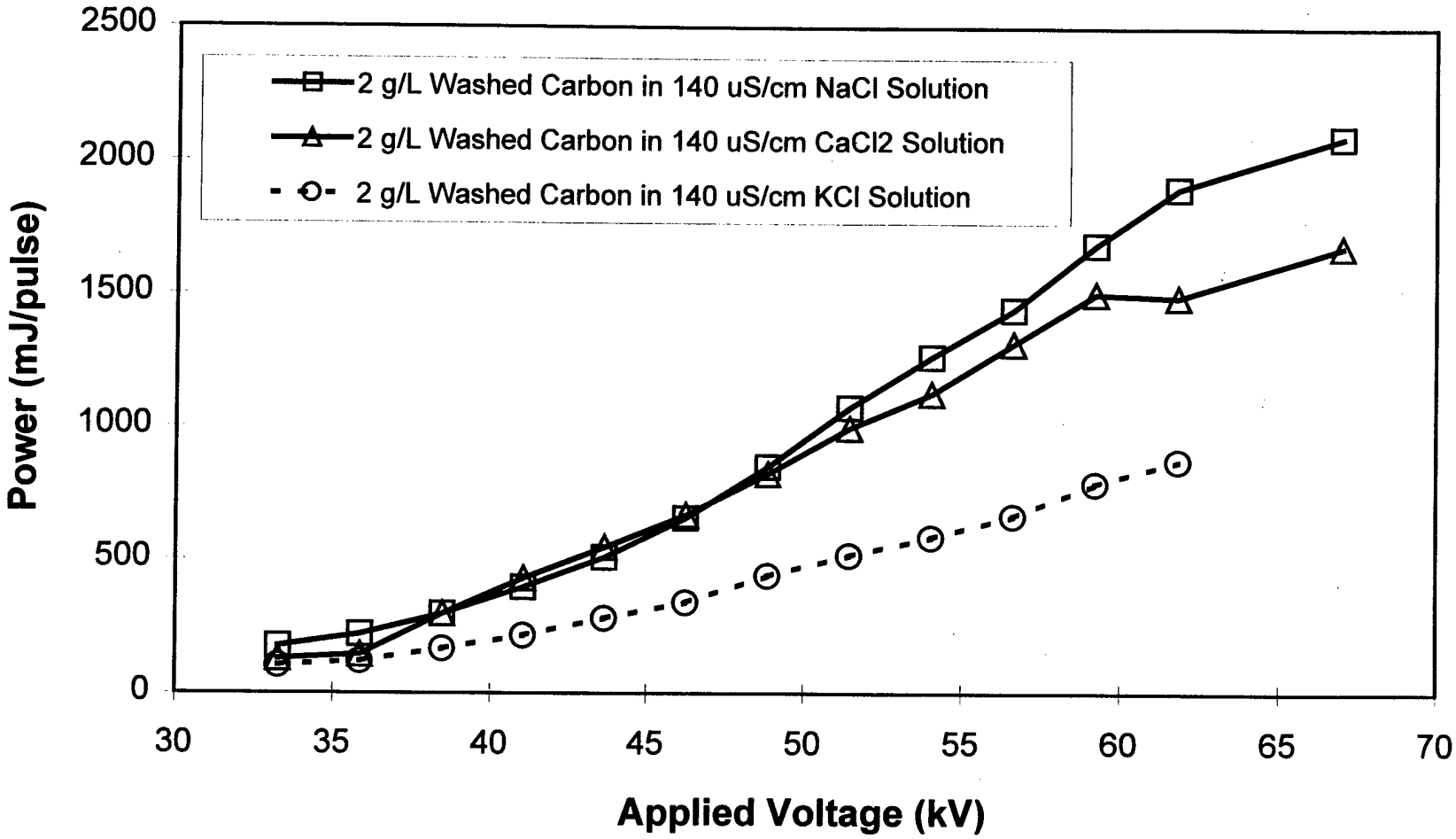


Figure 25. The Effect of Different Salt Solutions and 2 g/L Washed Activated Carbon on the Reactor Power Consumption

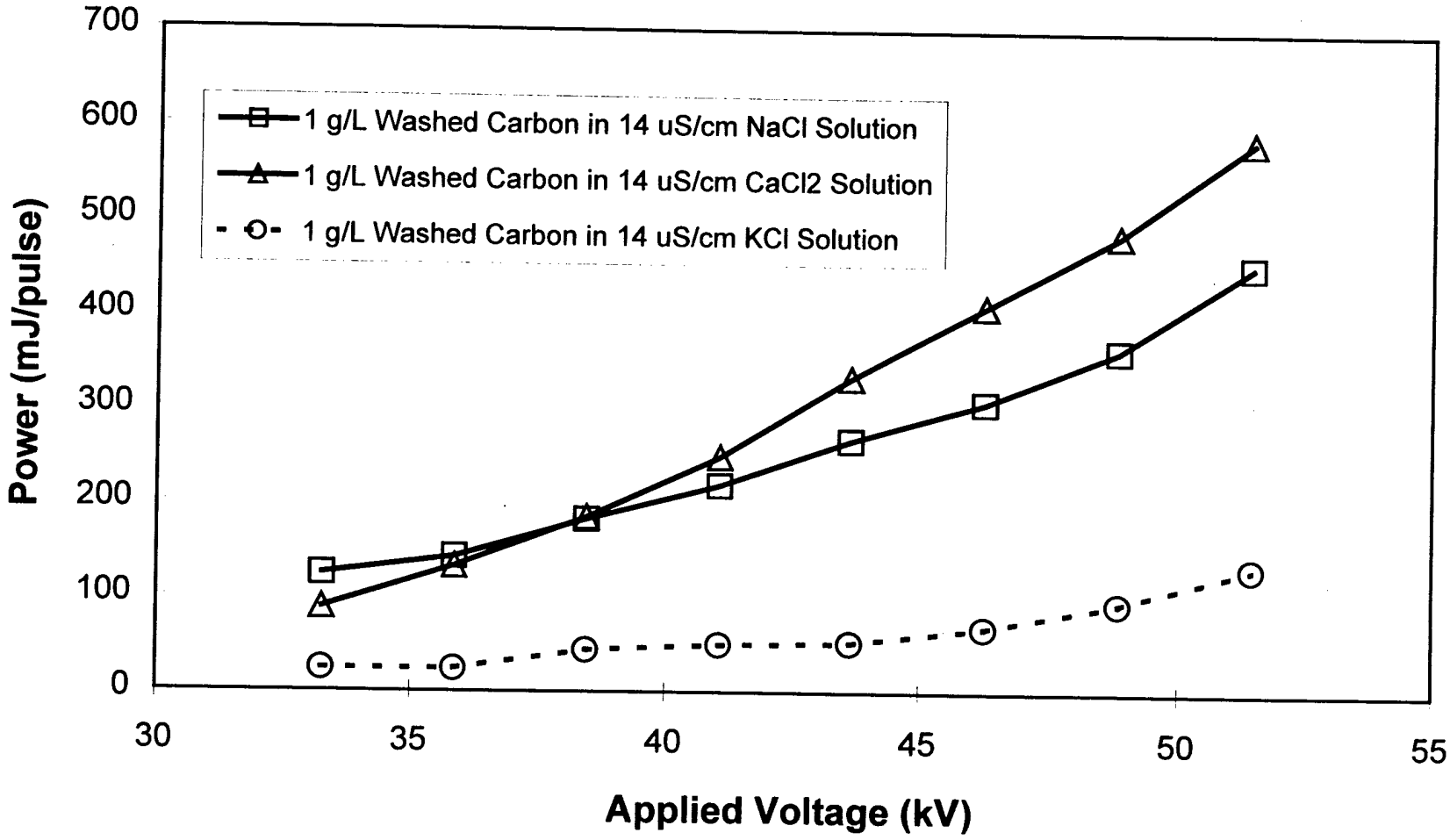


Figure 26. The Effect of Different Salt Solutions and 1 g/L Washed Activated Carbon on the Reactor Power Consumption

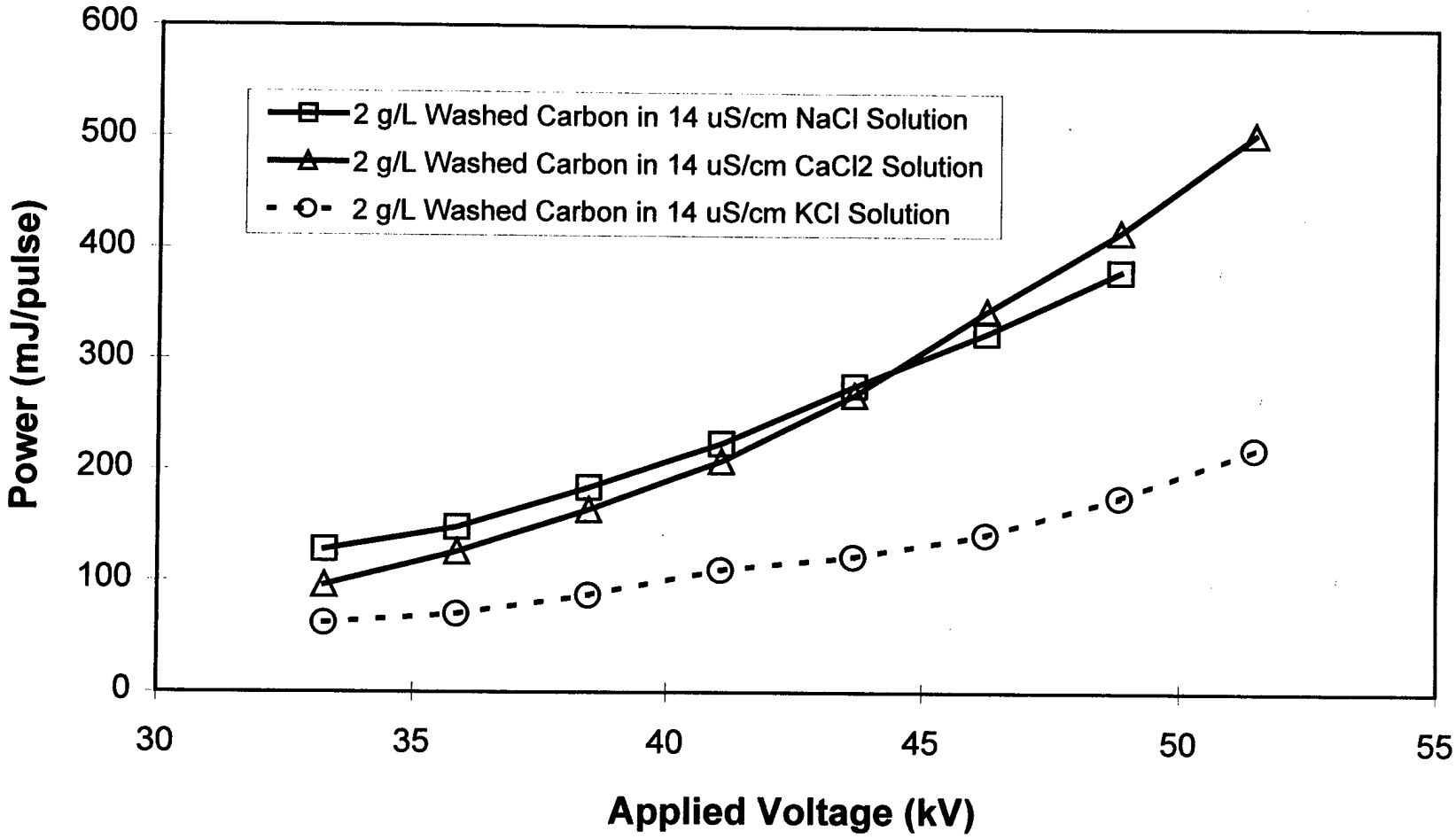


Figure 27. The Effect of Different Salt Solutions and 2 g/L Washed Activated Carbon on the Reactor Power Consumption

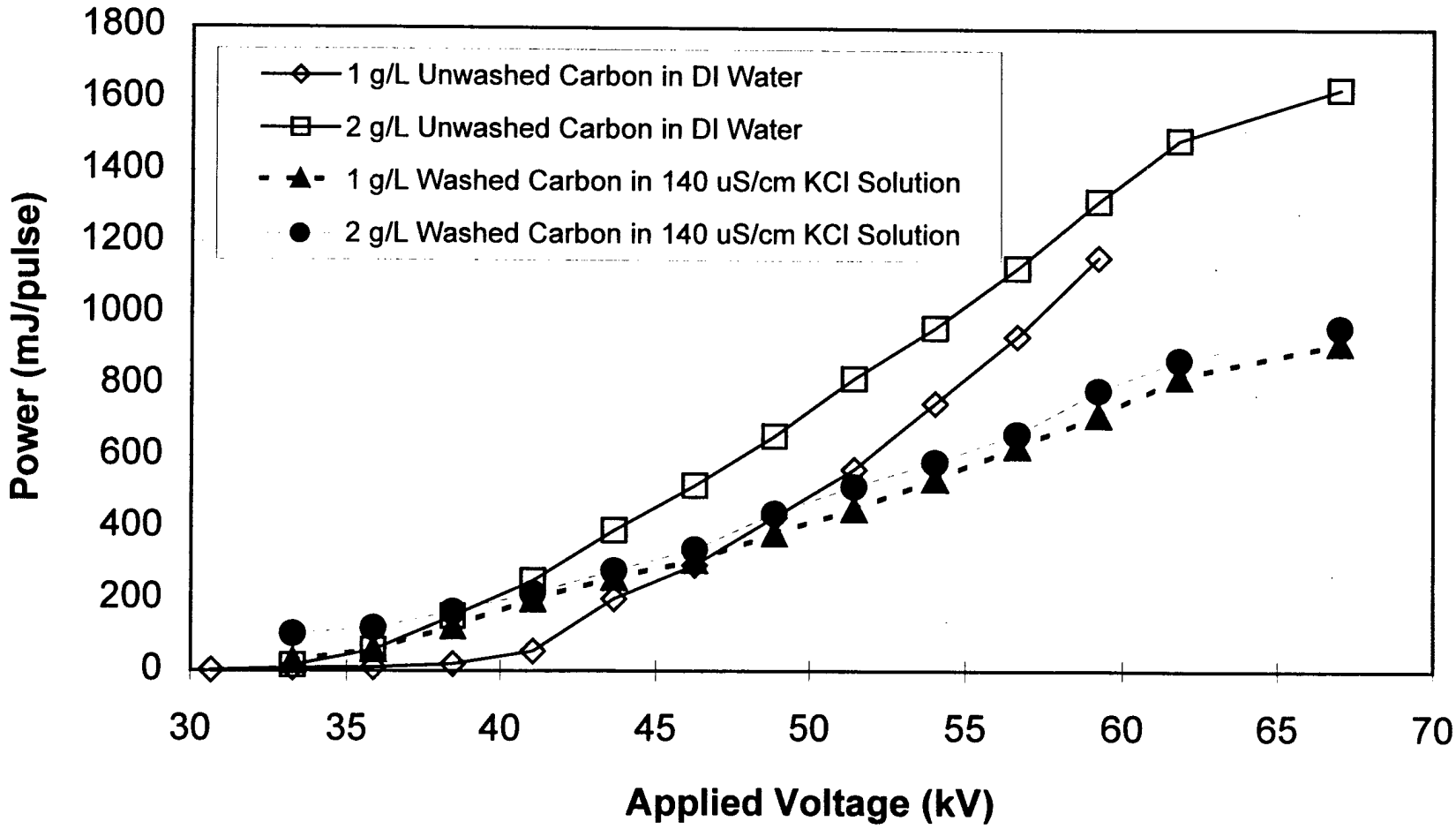


Figure 28. The Comparison of Unwashed Activated Carbon and Washed Activated Carbon in a KCl Solution on the Reactor Power Consumption

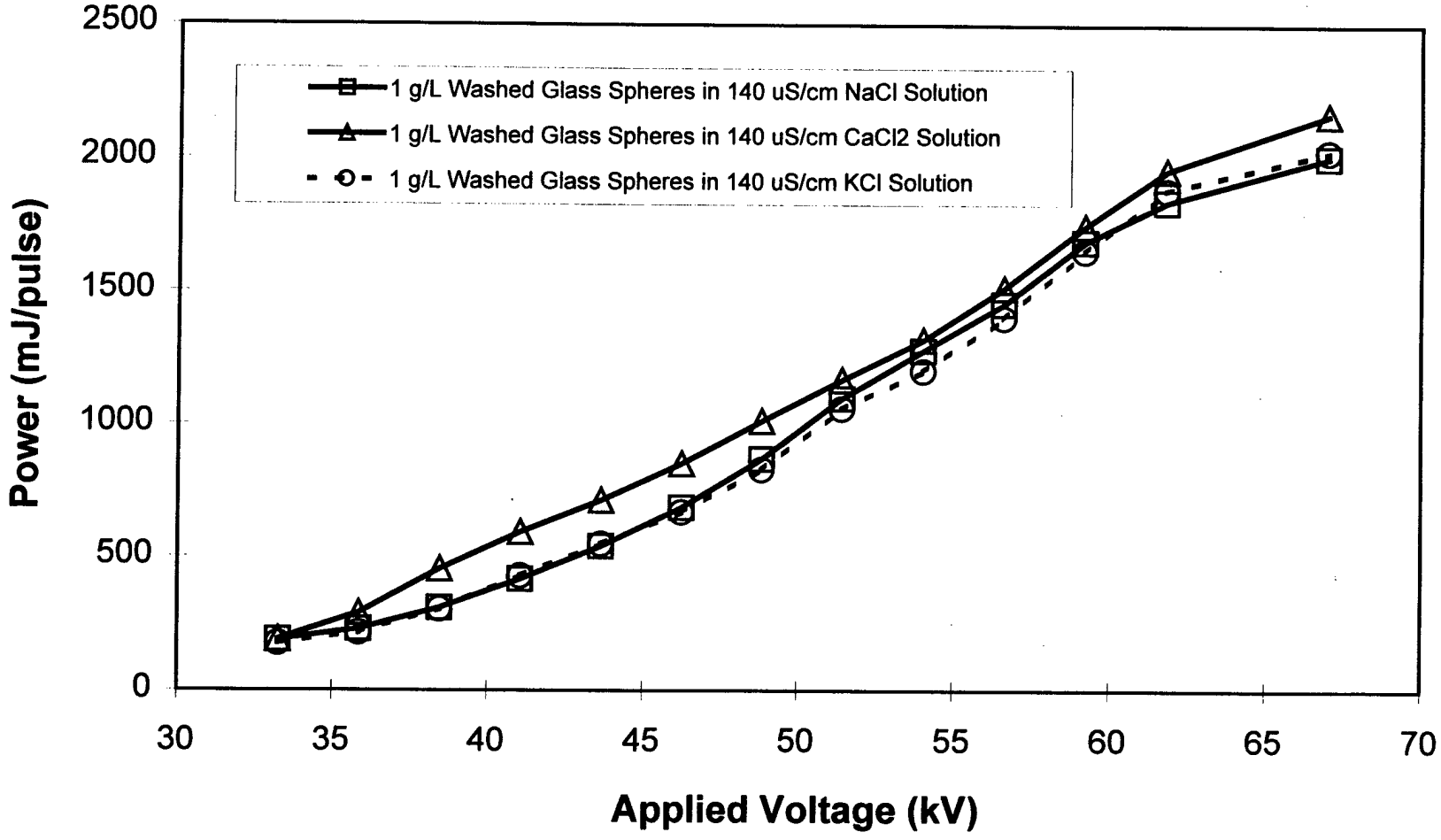


Figure 29. The Effect of Different Salt Solutions and 1 g/L Washed Glass Spheres on the Reactor Power Consumption

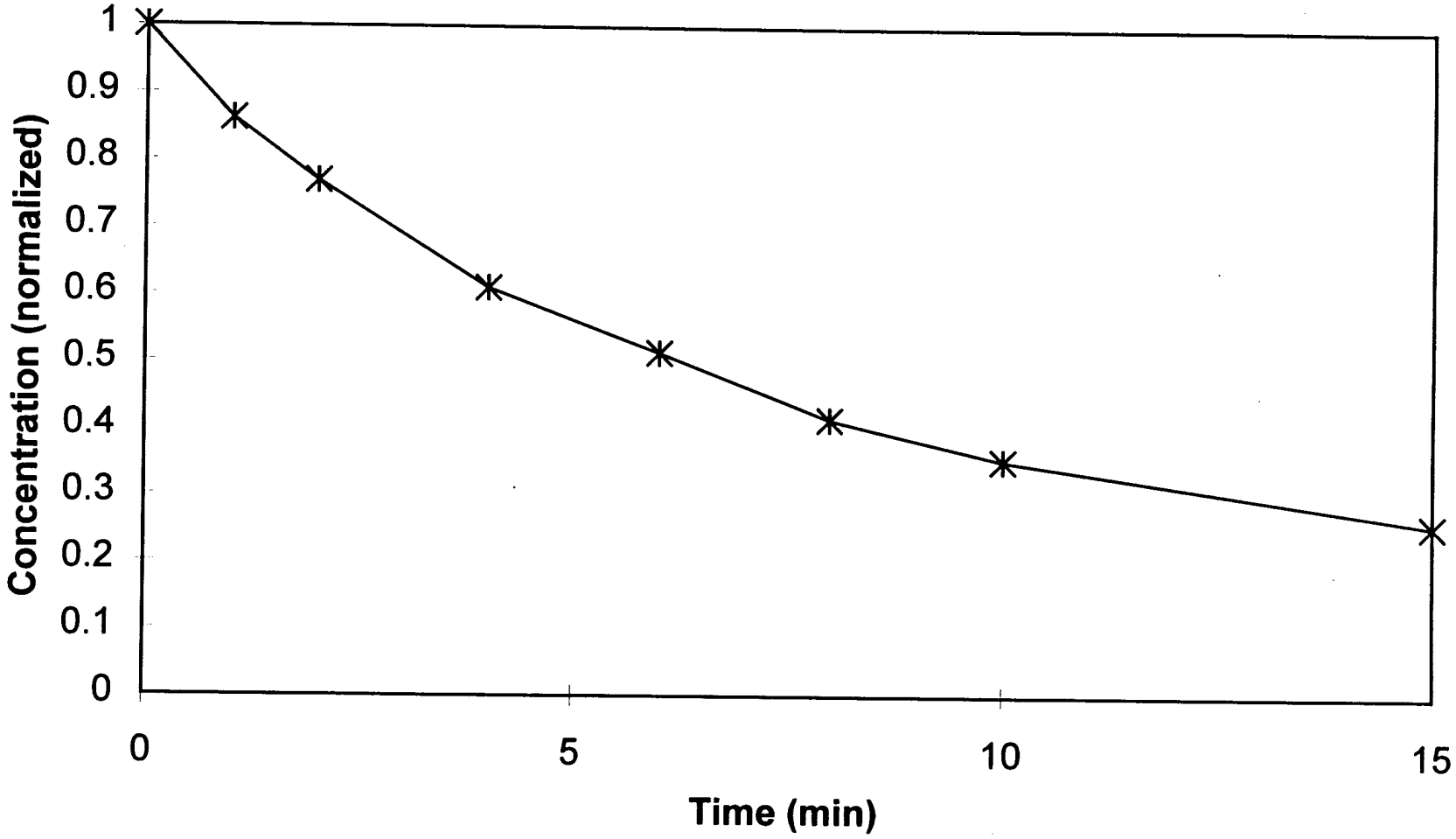


Figure 30. The Rate of Phenol Adsorption onto 1 g/L Washed Activated Carbon

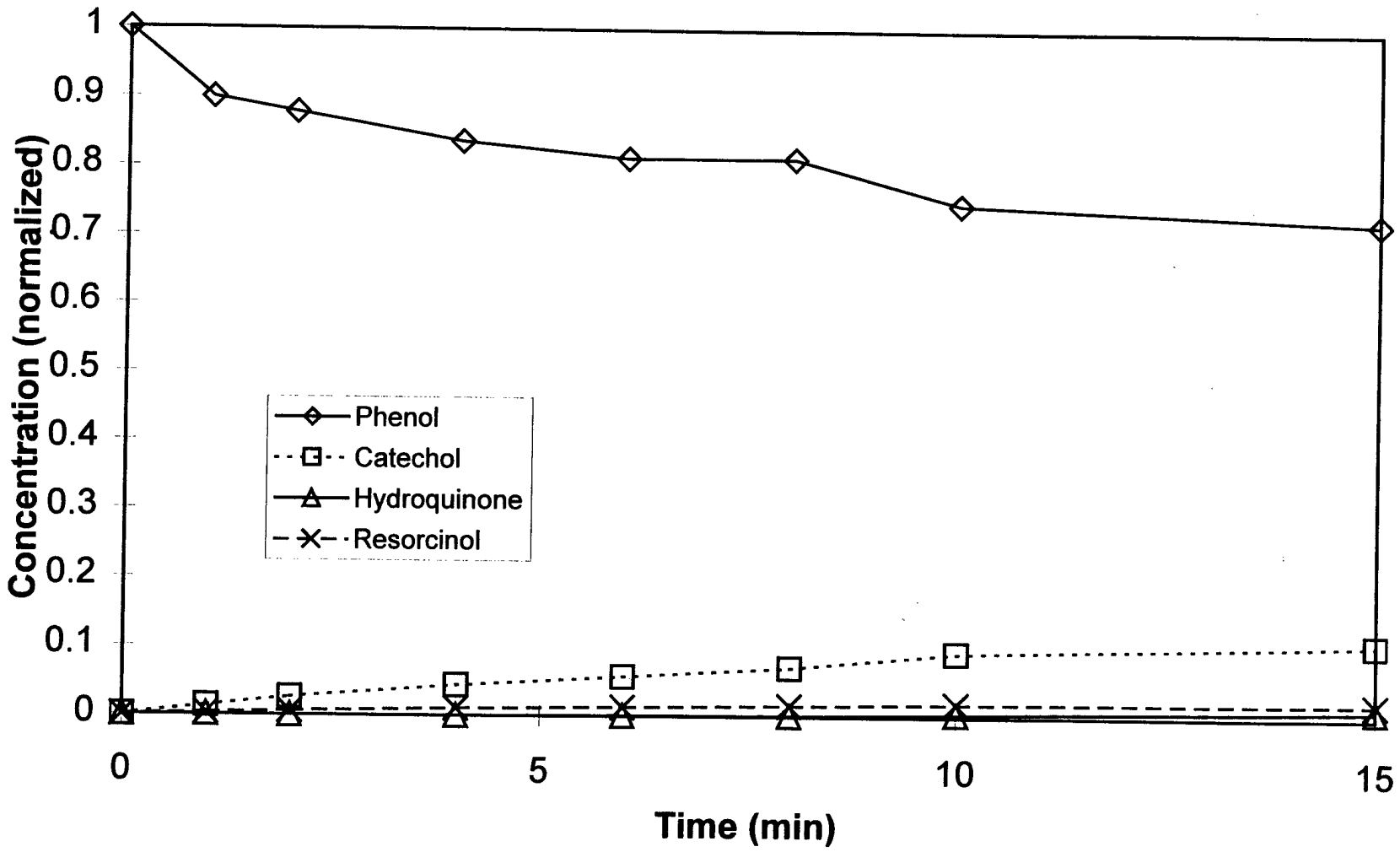


Figure 31. The Degradation of Phenol at 46 kV

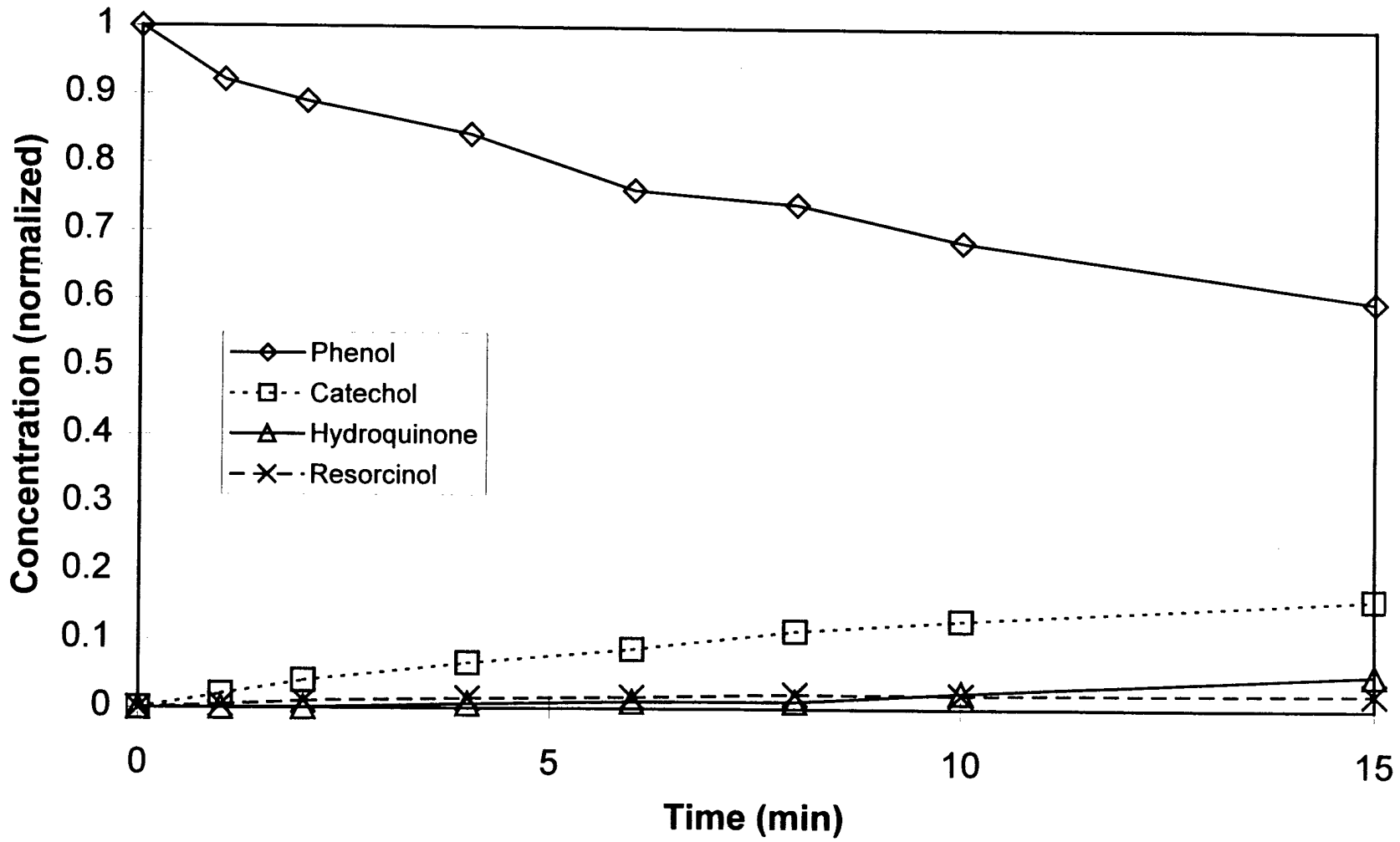


Figure 32. The Degradation of Phenol at 57 kV

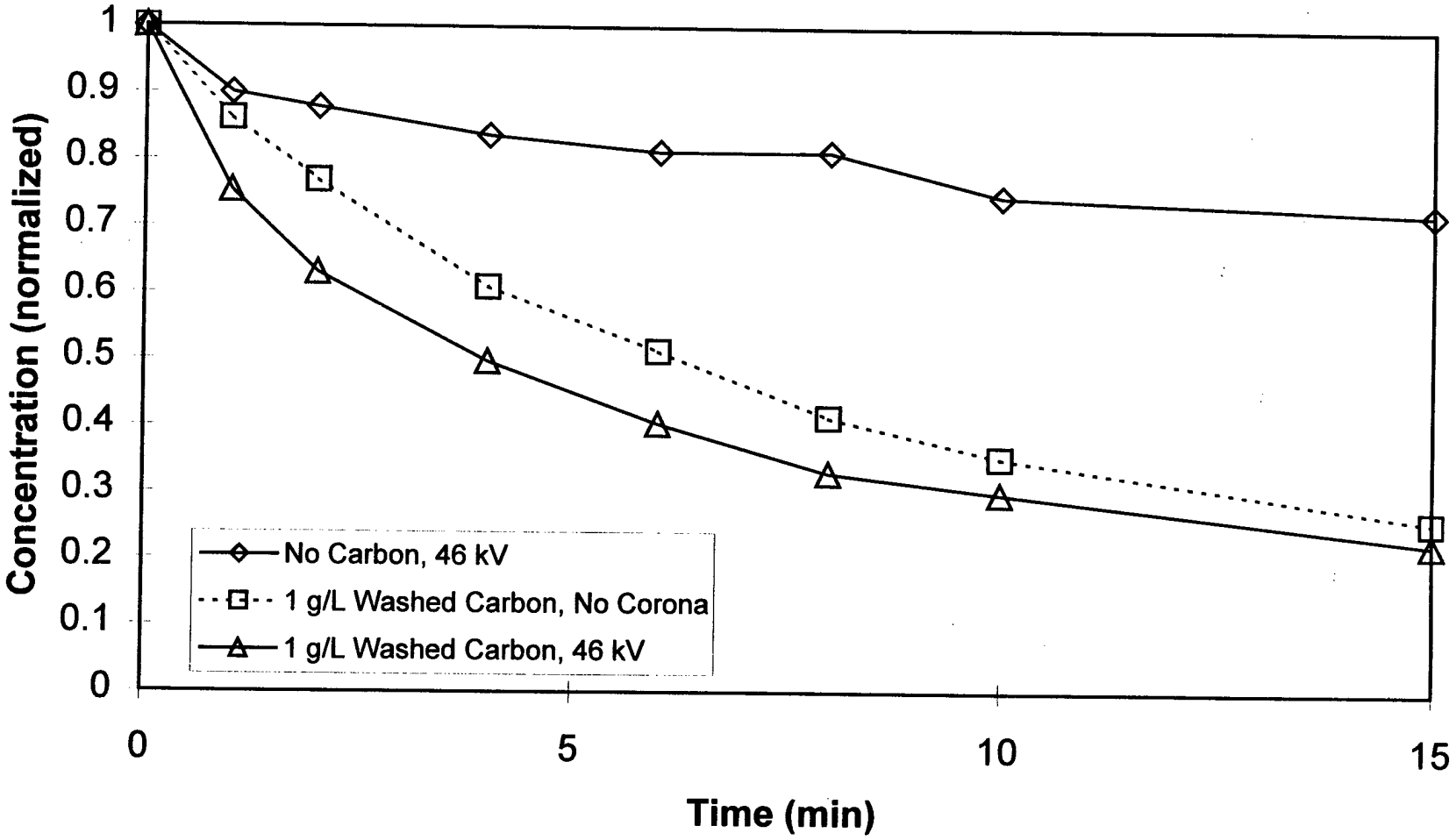


Figure 33. Phenol Removal at 46 kV with and without 1 g/L Washed Activated Carbon

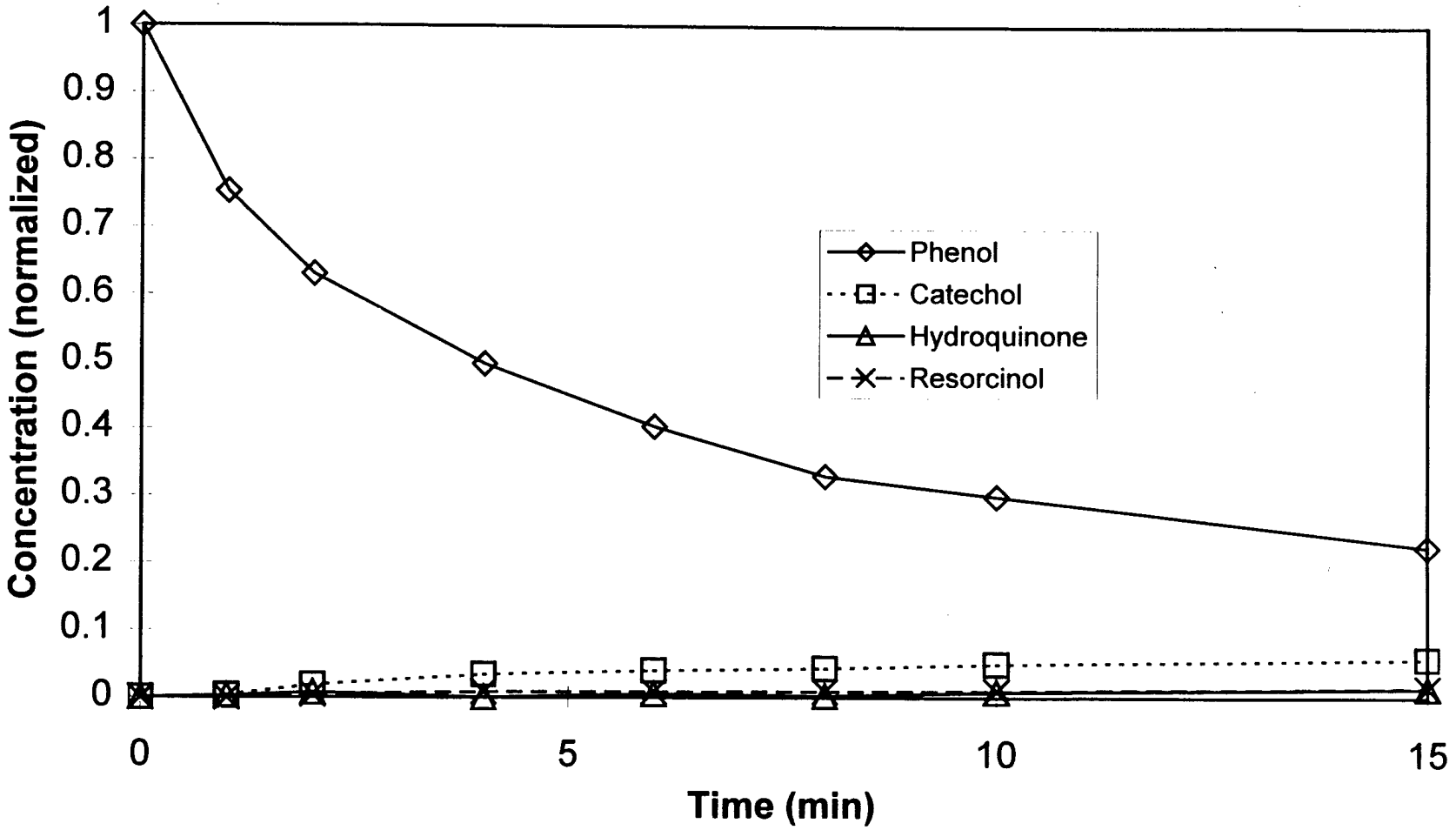


Figure 34. The Degradation of Phenol at 46 kV and 1 g/L Washed Activated Carbon

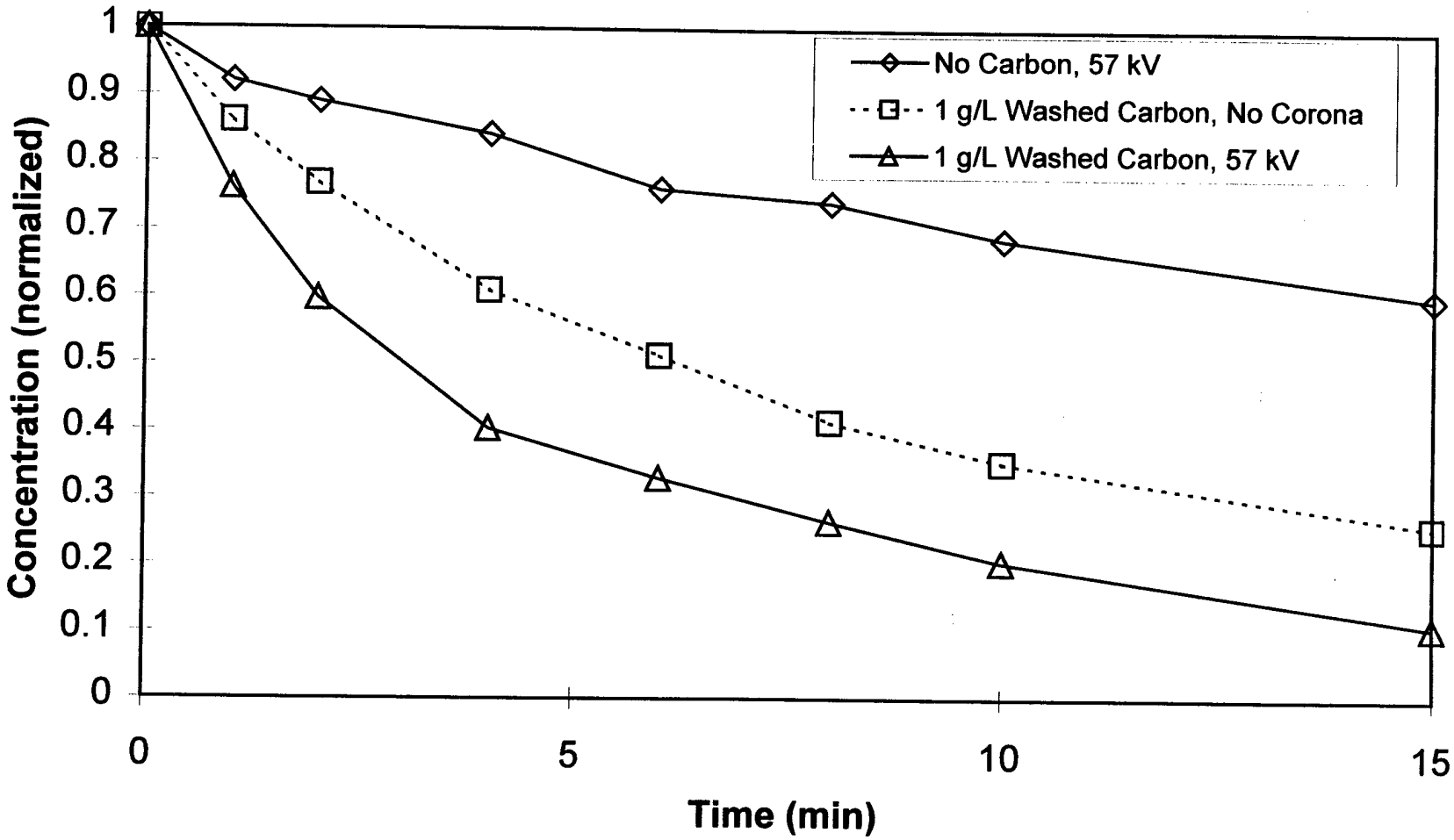


Figure 35. Phenol Removal at 57 kV with and without 1 g/L Washed Activated Carbon

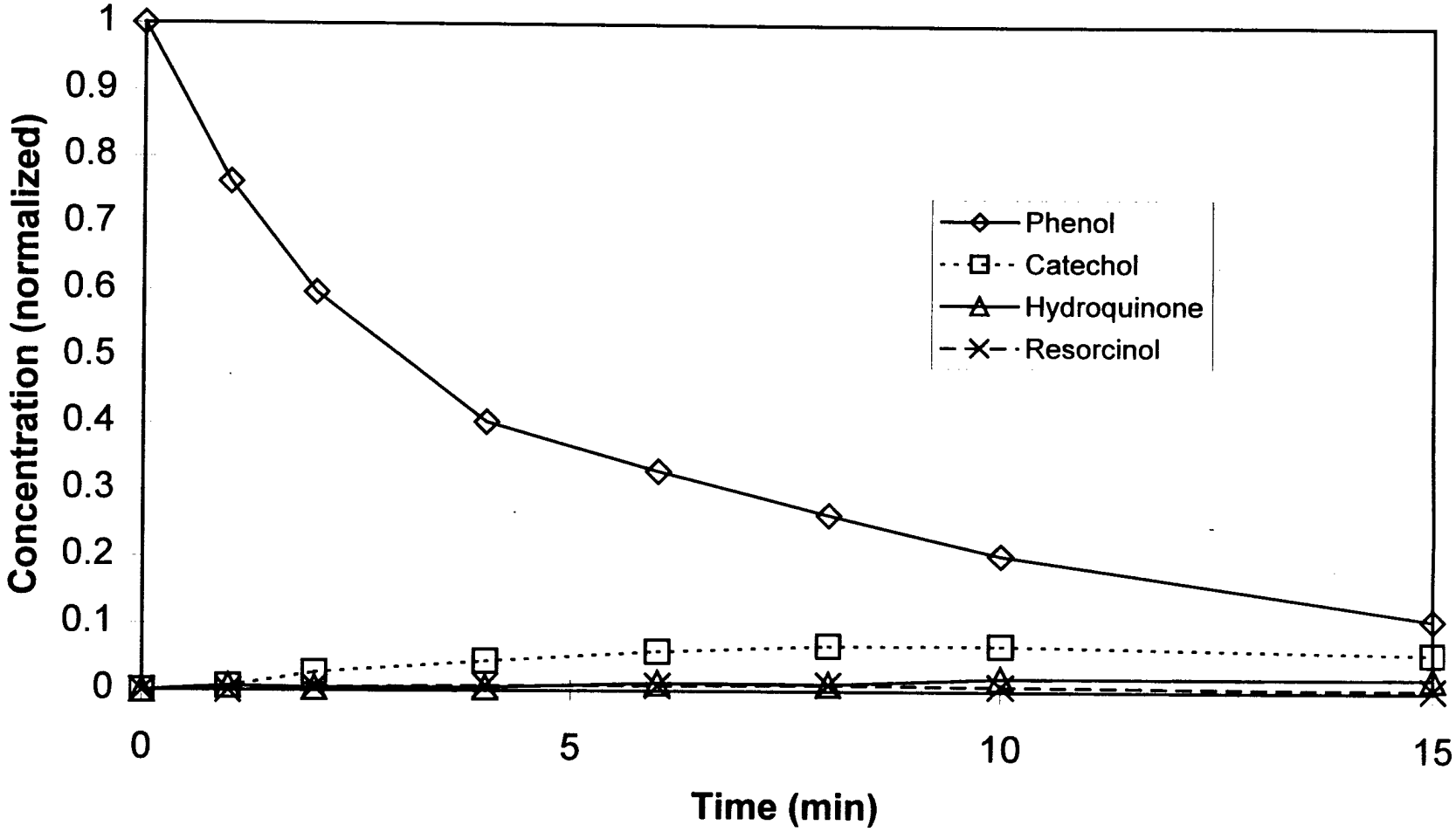


Figure 36. The Degradation of Phenol at 57 kV and 1 g/L Washed Activated Carbon

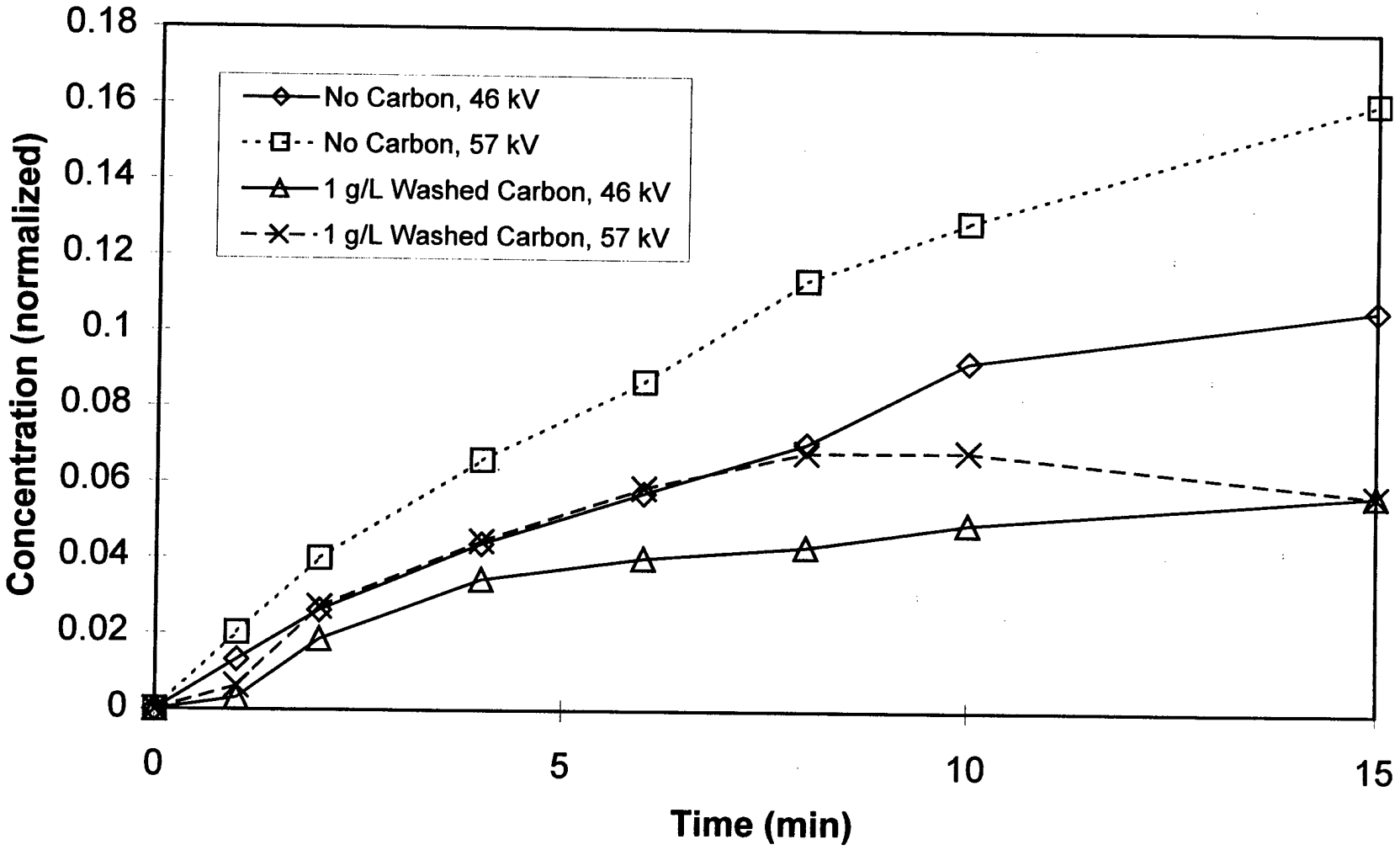


Figure 37. Catechol Formation at Various Conditions

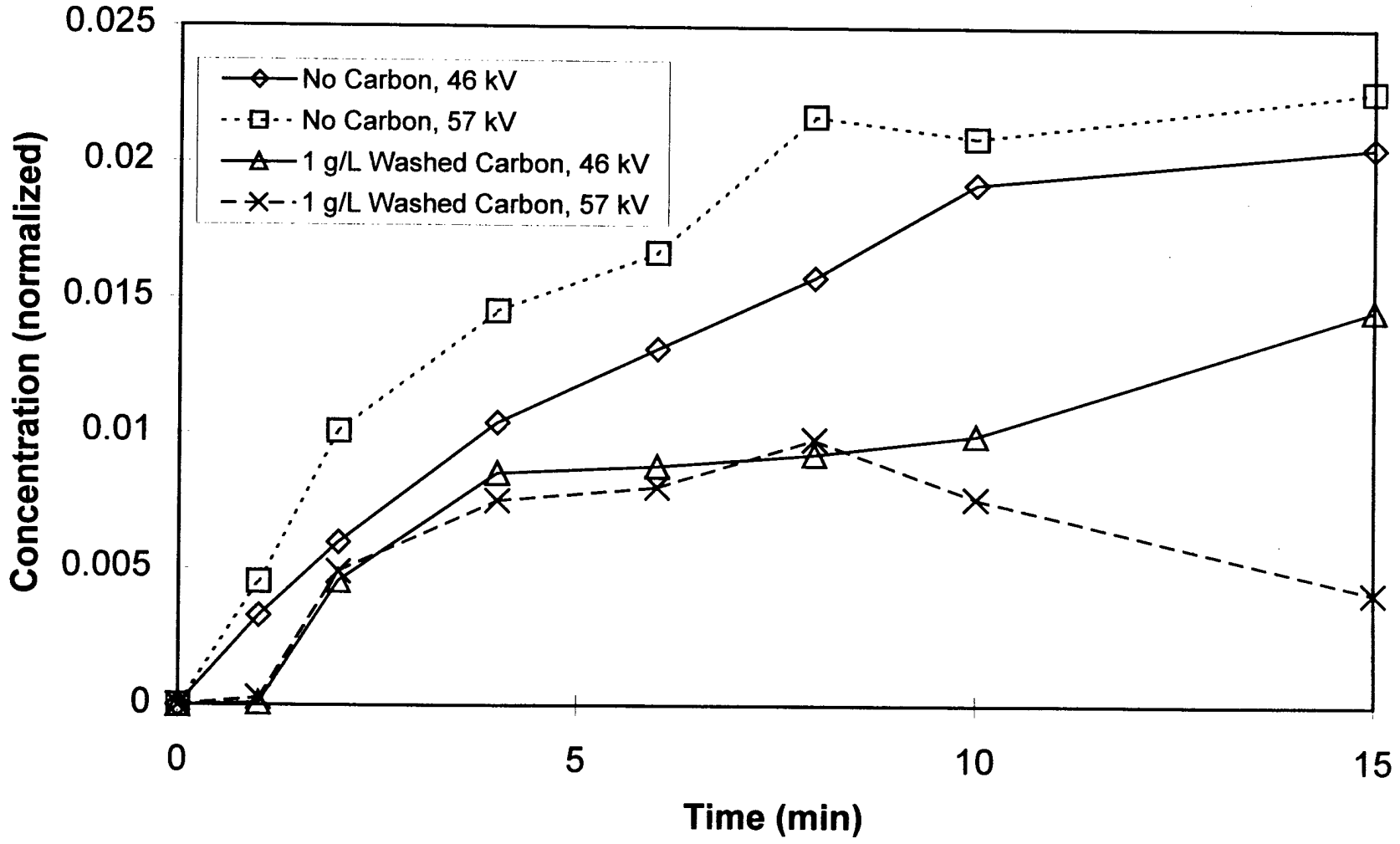


Figure 38. Resorcinol Formation at Various Conditions

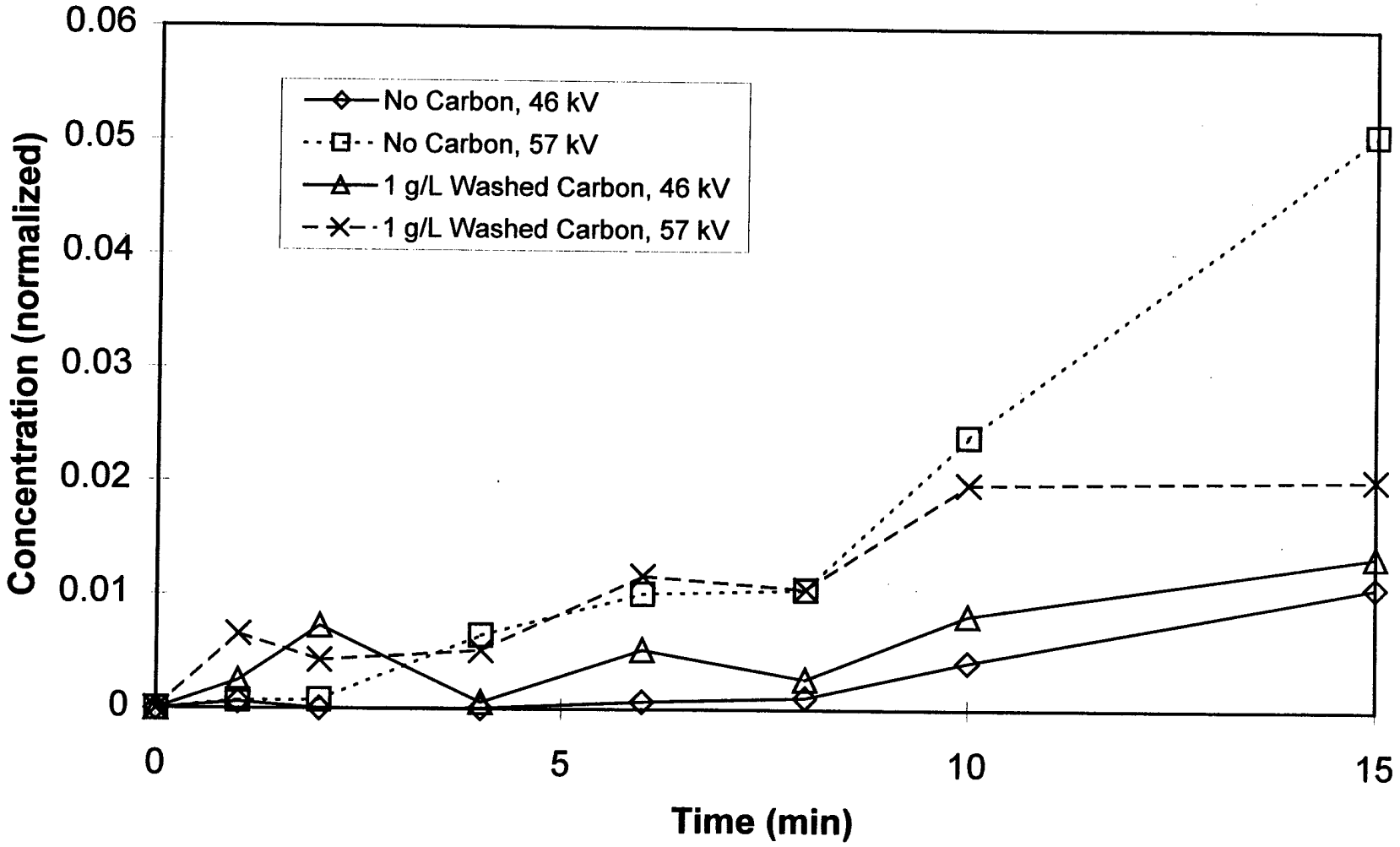


Figure 39. Hydroquinone Formation at Various Conditions

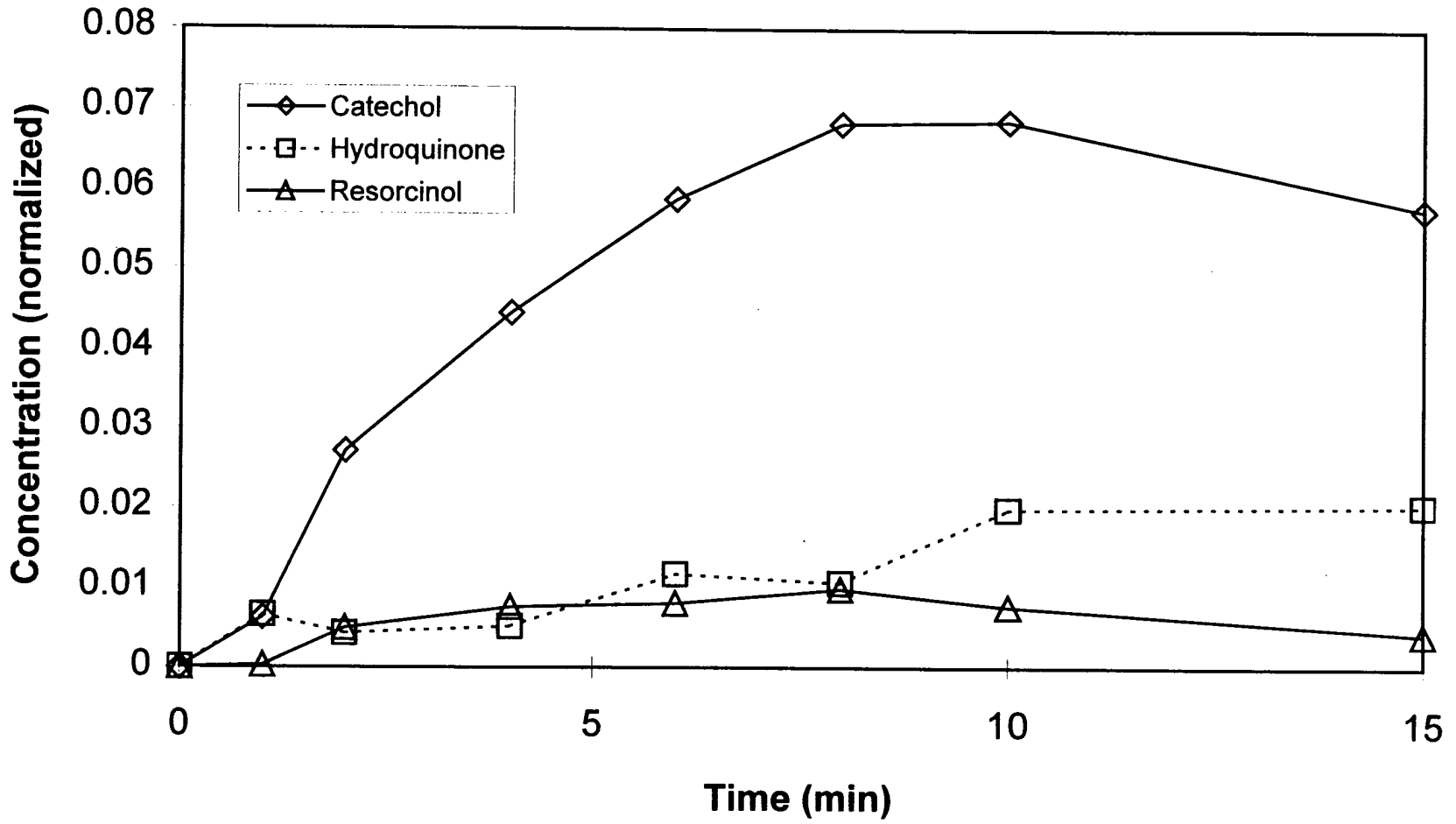


Figure 40. Byproduct Formation at 57 kV and 1 g/L Washed Activated Carbon

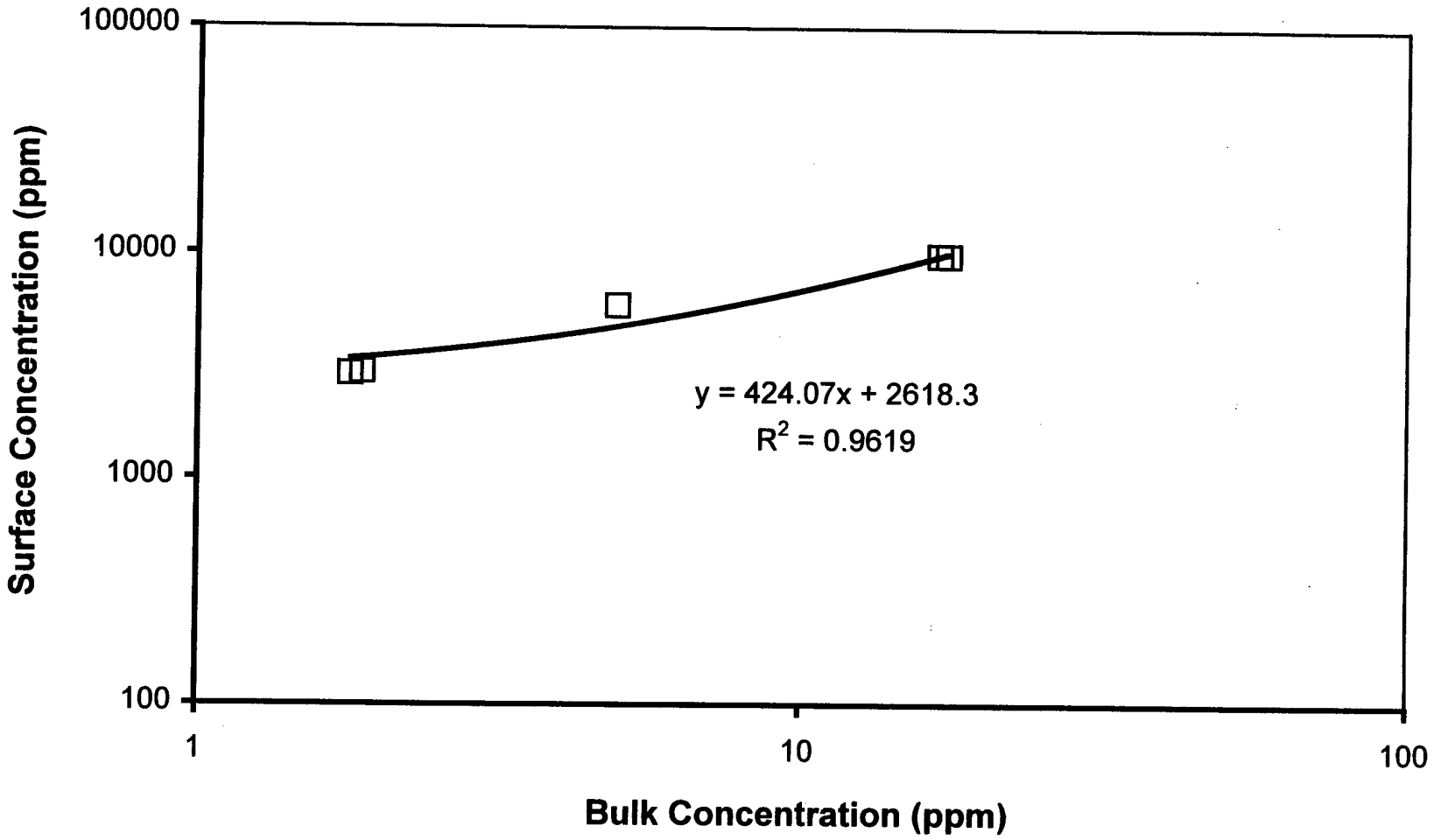


Figure 41. Phenol Adsorption Equilibrium onto 1 g/L Washed Activated Carbon

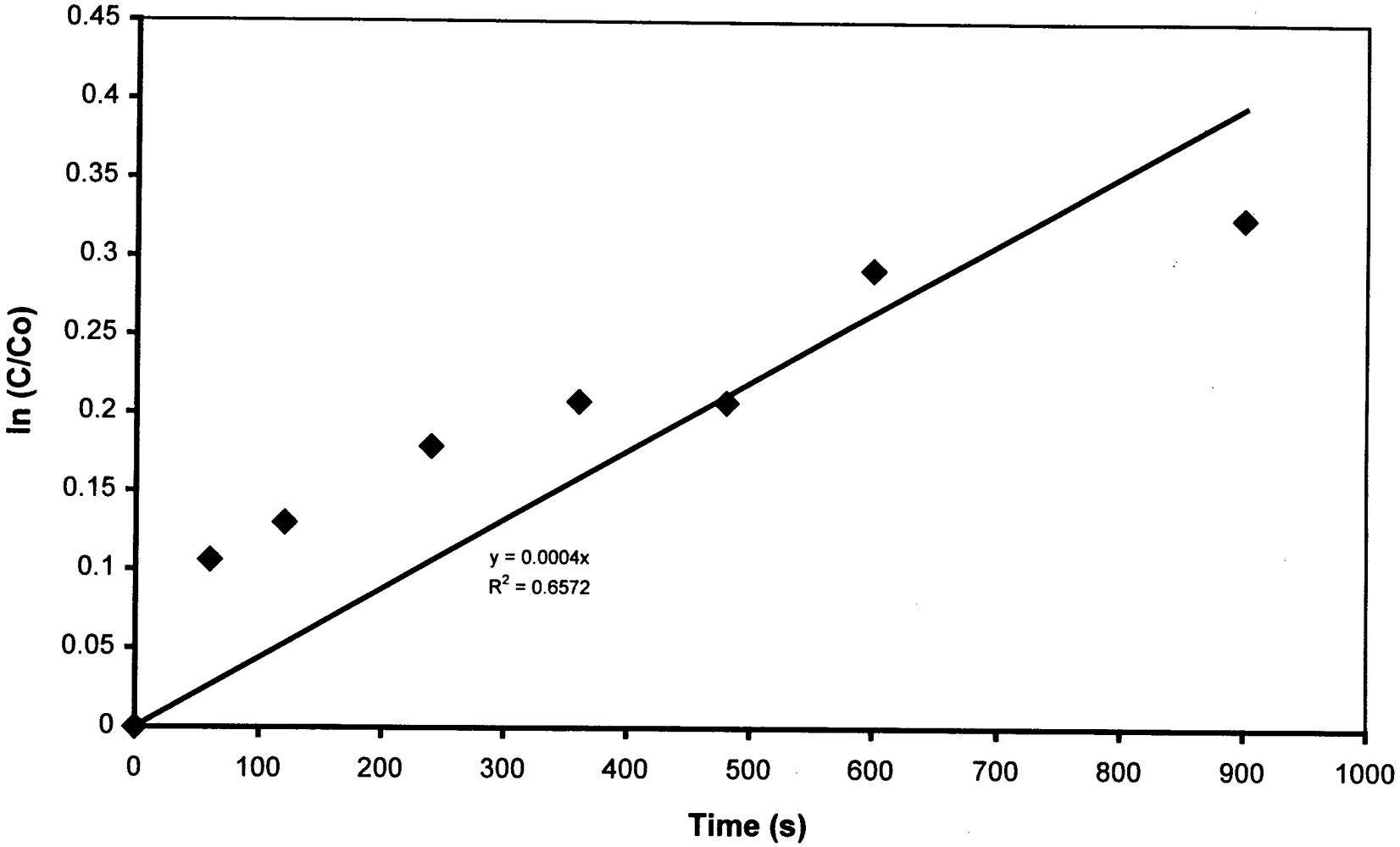


Figure 42. Rate Determination for Phenol Decomposition at 46 kV

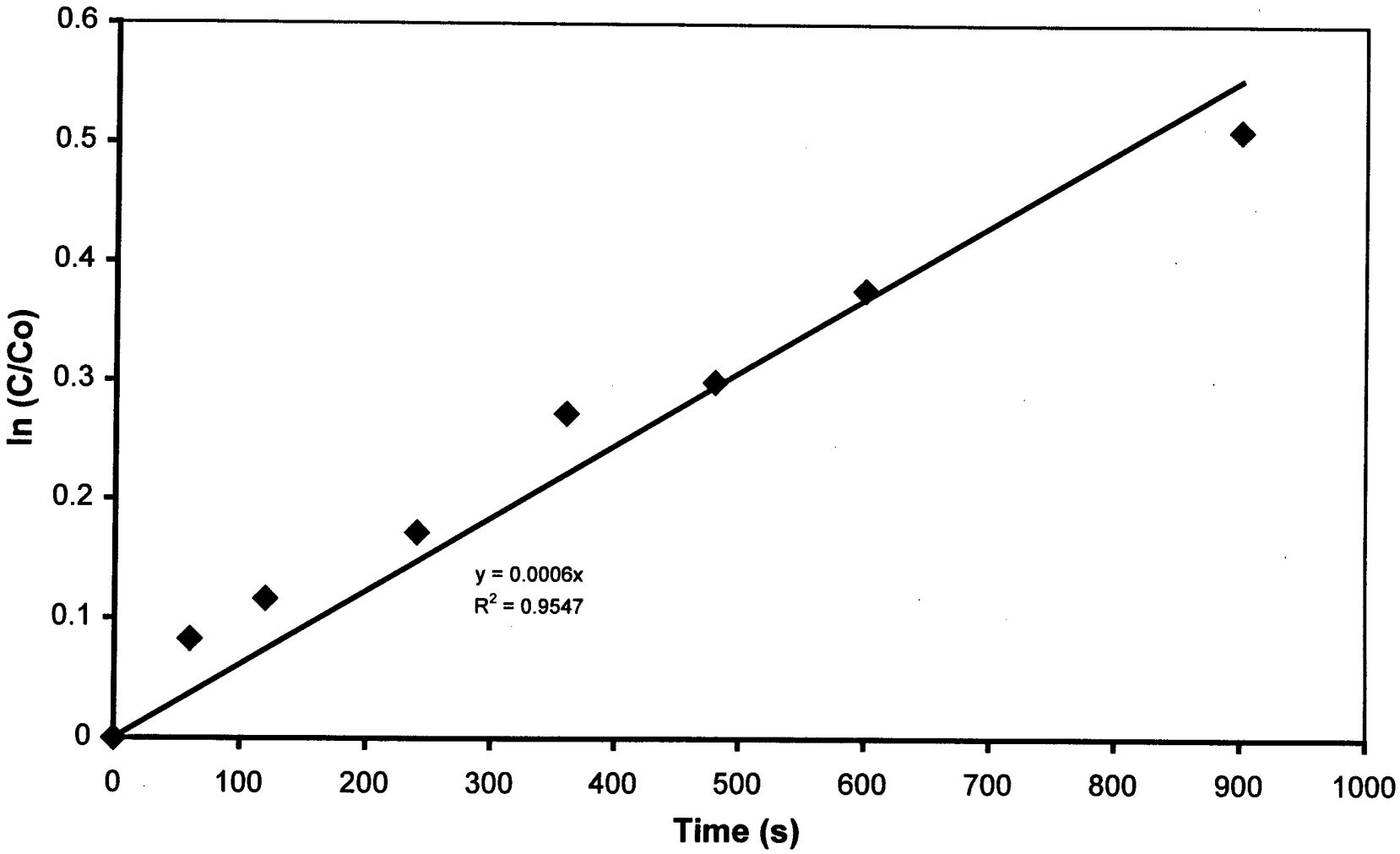


Figure 43. Rate Determination for Phenol Decomposition at 57 kV

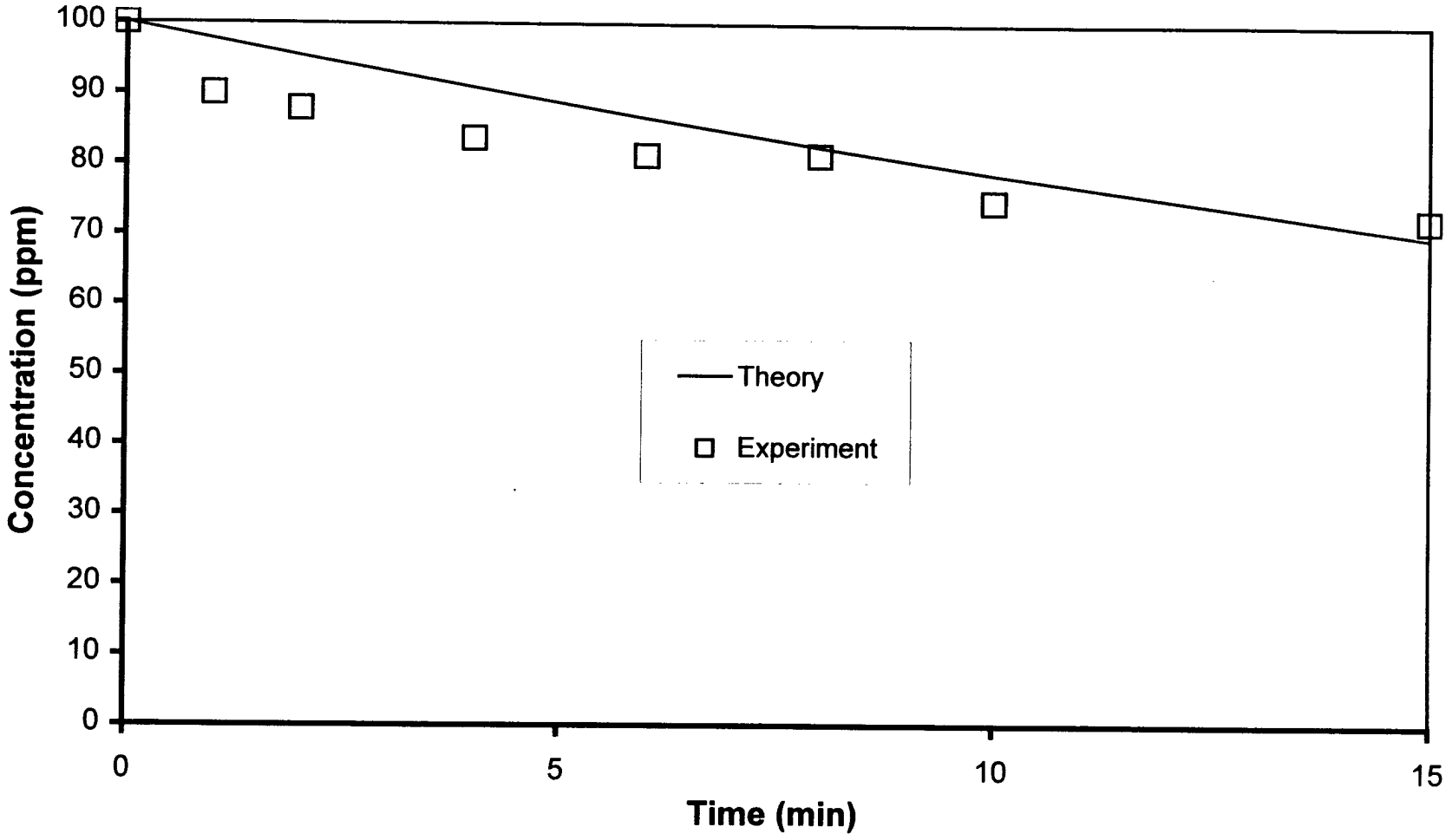


Figure 44. The Comparison of Experimental and Theoretical Results at 46 kV

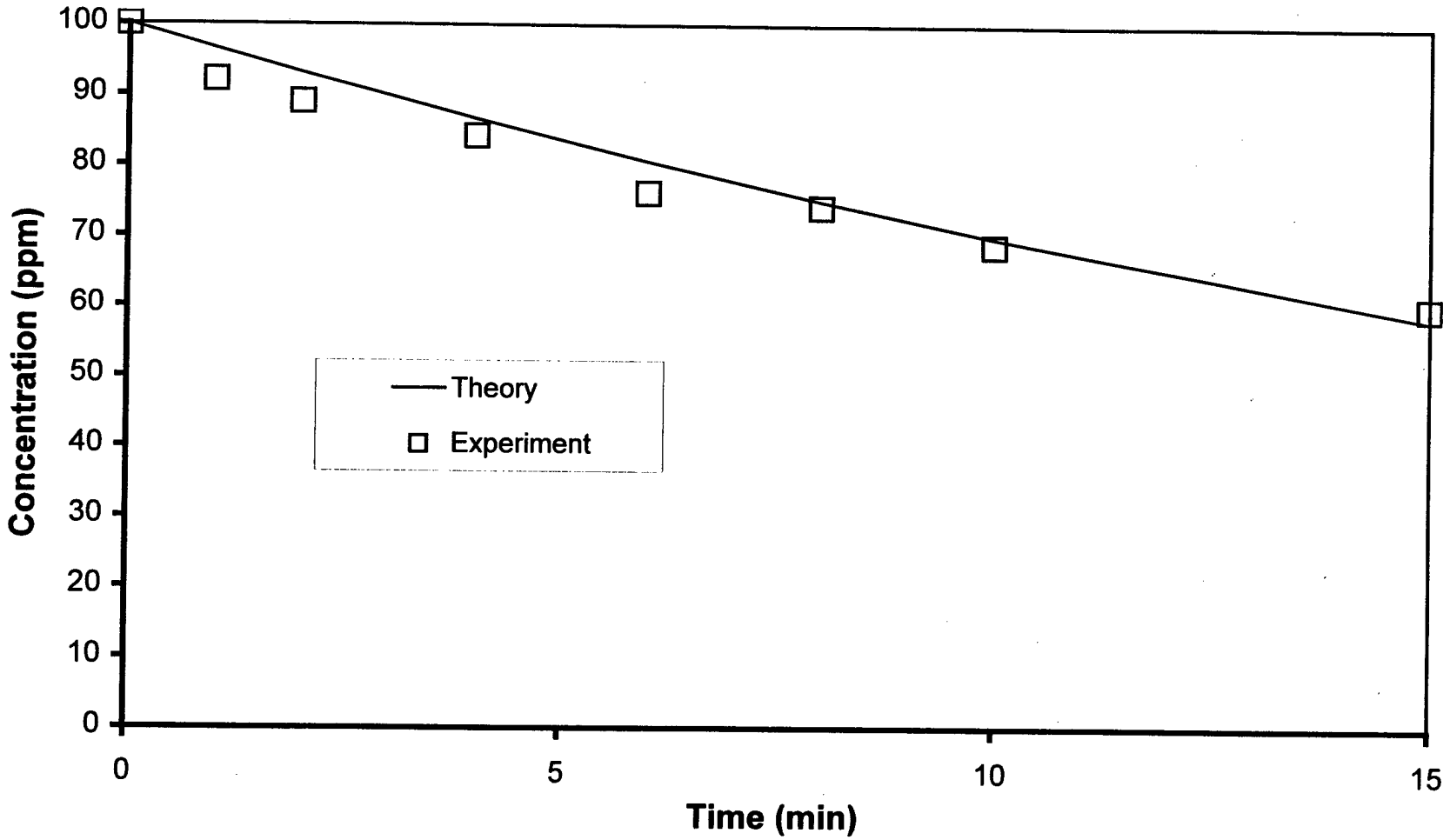


Figure 45. The Comparison of Experimental and Theoretical Results at 57 kV

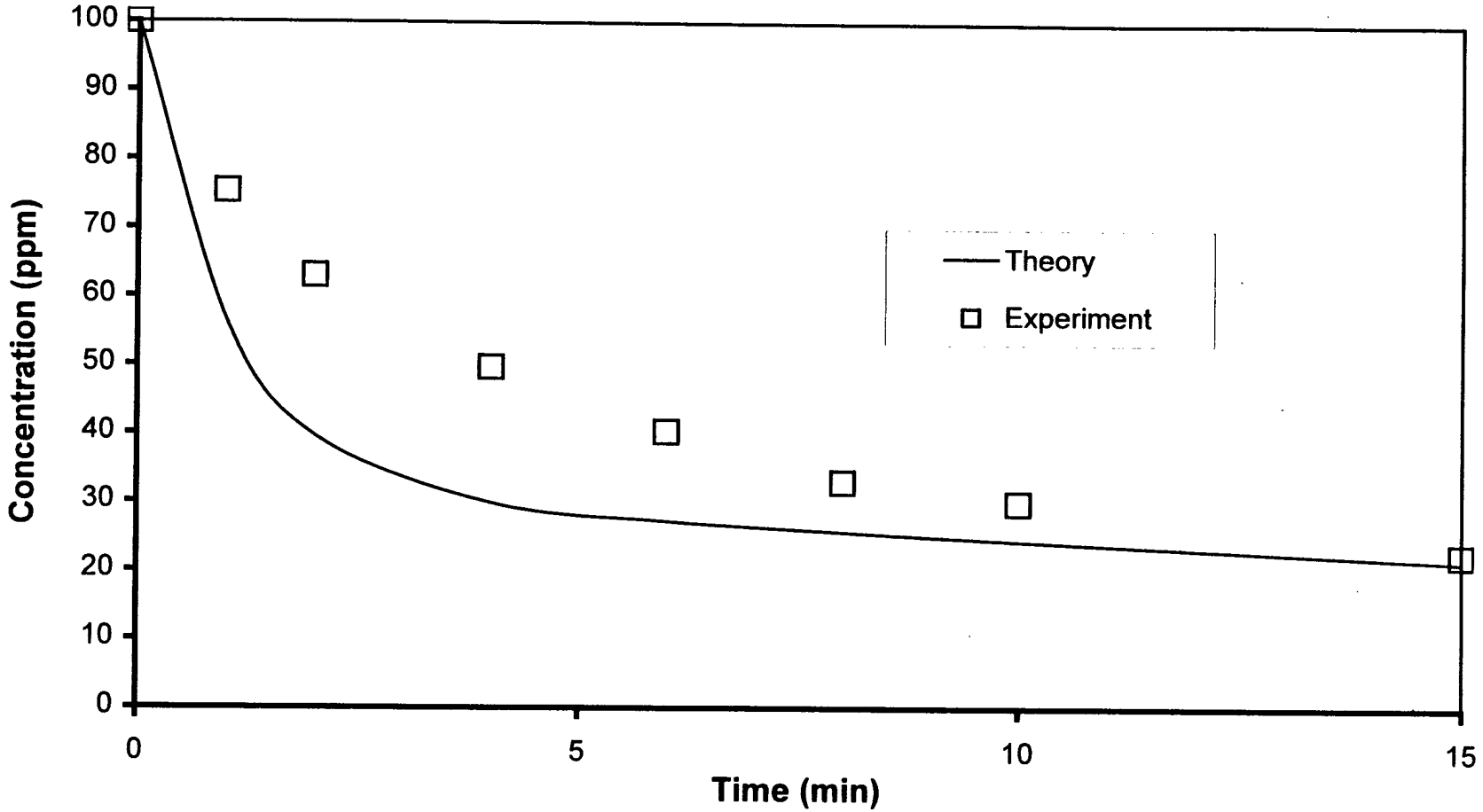


Figure 46. The Comparison of Experimental and Theoretical Results at 46 kV and 1 g/L Washed Activated Carbon ($k_p = 0.00045\ sec^{-1}$)

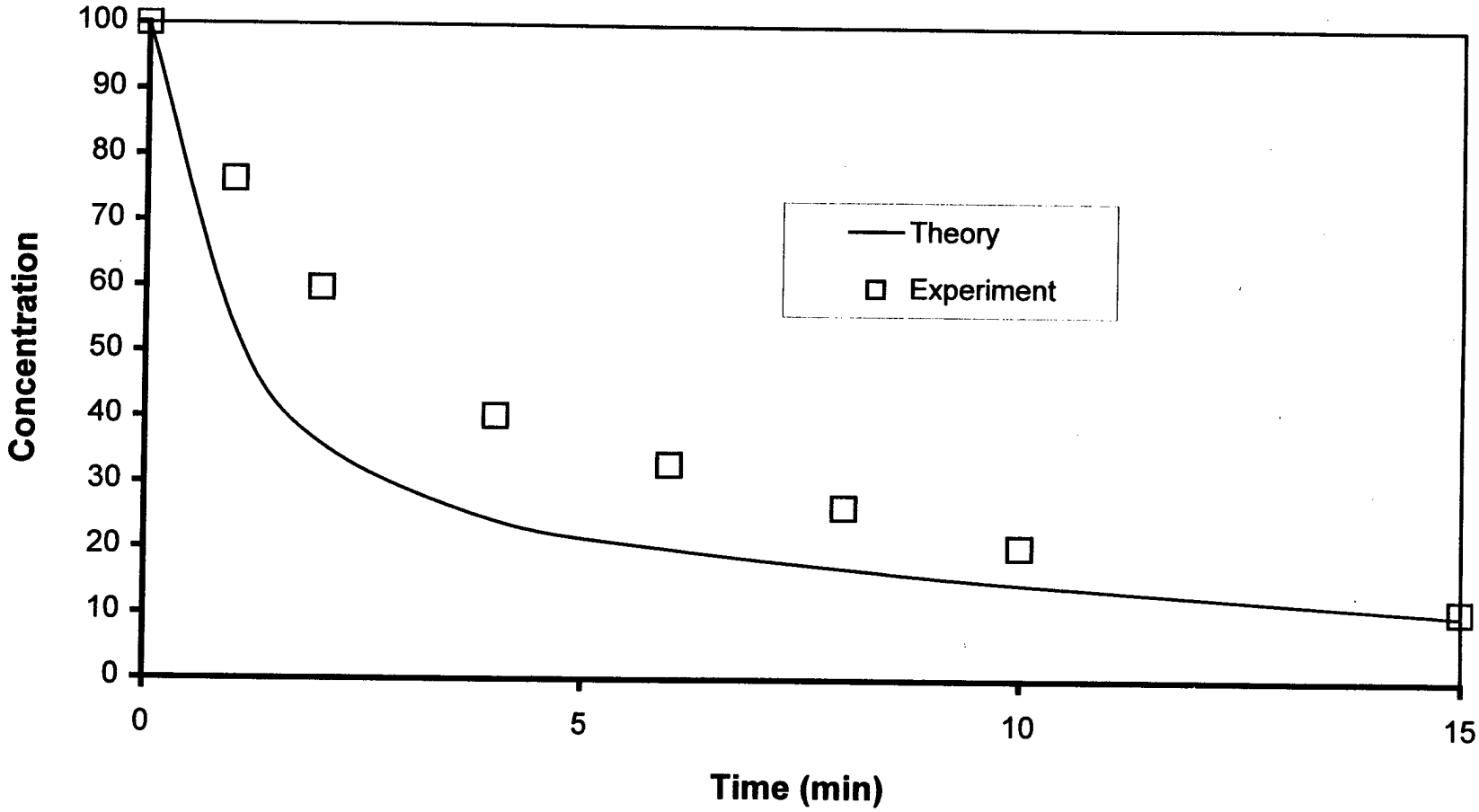


Figure 47. The Comparison of Experimental and Theoretical Results at 57 kV and 1 g/L Washed Activated Carbon ($k_p = 0.00175\ sec^{-1}$)

APPENDIX

Nomenclature (from Model Formulation):

A	total external area of all particles in suspension
c	particle phase concentration
c_b	bulk phase concentration
c_{b0}	initial bulk phase concentration
$< c >$	average particle concentration
$\tilde{c}$	particle phase spatial deviation variable
$< \tilde{c} >$	average of particle phase spatial deviation variable
D	effective particle diffusion constant
f(s)	f-field variable
$< f >$	average f-field
g(s)	g-field variable
$< g >$	average g-field
k_b	bulk phase reaction rate constant
k_p	effective particle phase reaction rate constant
K	adsorption constant
K_{mt}	mass transfer resistance coefficient
r	spatial variable, spherical coordinates
s	non-dimensional spatial variable
t	time
V	bulk phase volume
x	spatial variable, rectangular coordinates
ϕ_b	Thiele modulus, bulk phase
ϕ_p	Thiele modulus, particle phase
τ	non-dimensional time variable

Table A1.
Power Consumption for
1 g/L Unwashed Carbon in DI Water

Applied Voltage (kV)	Power (μVVs)	Power (μVVs)	Power (μVVs)	Power (μVVs)	Avg. Power (mJ/pulse)	95% Confidence
28	0	-	-	-	2	-
31	1	-	-	-	5	-
33	1	1	-	2	12	6
36	2	2	2	3	21	6
38	3	7	9	4	57	26
41	-	20	30	-	250	98
44	30	32	34	30	313	17
46	41	44	47	46	444	24
49	59	60	52	61	579	39
51	74	76	83	74	768	41
54	90	93	-	93	921	17
57	-	116	-	-	1160	-

Table A2.
Power Consumption for
2 g/L Unwashed Carbon in DI Water

Applied Voltage (kV)	Power (μVVs)	Power (μVVs)	Power (μVVs)	Avg. Power (mJ/pulse)	95% Confidence
31	-	1	2	14	3
33	-	2	2	23	3
36	-	11	9	102	17
38	24	22	22	220	14
41	36	38	33	355	25
44	48	52	48	498	28
46	61	69	63	661	47
49	80	86	81	836	37
51	94	99	96	973	25
54	111	118	111	1146	44
57	132	134	133	1333	13
59	148	150	148	1488	15
62	152	167	156	1616	91

Table A3.
Power Consumption for
No Particles and 140 μS/cm NaCl Solution

Applied Voltage (kV)	Power (μVVs)	Power (μVVs)	Avg. Power (mJ/pulse)	95% Confidence
31	18	17	174	4
33	22	26	238	43
36	28	28	278	4
38	38	37	376	16
41	48	48	480	8
44	59	60	594	12
46	75	76	754	4
49	91	92	914	12
51	109	119	1142	98
54	138	141	1394	35
57	163	165	1642	20
59	188	185	1864	24
62	212	207	2094	43

Table A4.
Power Consumption for
1 g/L Washed Carbon and 14 μS/cm NaCl Solution

Applied Voltage (kV)	Power (μVVs)	Power (μVVs)	Avg. Power (mJ/pulse)	95% Confidence
31	12	12	124	-
33	14	15	142	12
36	18	19	182	12
38	22	22	218	4
41	27	26	266	4
44	32	30	306	20
46	38	35	362	27
49	45	-	452	-

Table A5.
Power Consumption for
2 g/L Washed Carbon and 14 μS/cm NaCl Solution

Applied Voltage (kV)	Power (μVVs)	Power (μVVs)	Avg. Power (mJ/pulse)	95% Confidence
31	13	13	128	4
33	15	15	148	4
36	18	19	184	8
38	22	23	224	12
41	27	28	276	12
44	32	33	324	4
46	38	38	380	-

Table A6.
Power Consumption for
1 g/L Washed Carbon and 140 μS/cm NaCl Solution

Applied Voltage (kV)	Power (μVVs)	Power (μVVs)	Avg. Power (mJ/pulse)	95% Confidence
31	16	16	164	-
33	21	20	206	4
36	29	28	286	4
38	40	39	392	8
41	50	48	488	24
44	63	64	634	4
46	82	81	814	4
49	103	100	1016	24
51	121	122	1214	12
54	143	144	1434	12
57	165	163	1640	16
59	185	182	1834	27
62	202	202	2022	4

Table A7.
Power Consumption for
2 g/L Washed Carbon and 140 μS/cm NaCl Solution

Applied Voltage (kV)	Power (μVVs)	Power (μVVs)	Avg. Power (mJ/pulse)	95% Confidence
31	18	17	173	6
33	22	21	216	8
36	30	28	290	12
38	40	38	390	12
41	51	48	495	25
44	66	67	662	12
46	85	86	856	16
49	107	105	1062	20
51	126	123	1245	33
54	144	152	1480	78
57	168	171	1698	27
59	190	192	1908	24
62	209	215	2118	59

Table A8.
Power Consumption for
1 g/L Washed Glass Spheres and 14 μS/cm NaCl Solution

Applied Voltage (kV)	Power (μVVs)	Power (μVVs)	Avg. Power (mJ/pulse)	95% Confidence
31	15	15	150	4
33	17	17	172	-
36	21	22	214	4
38	26	26	258	4
41	30	31	308	8
44	35	35	348	-
46	41	40	408	8
49	46	-	456	-

Table A9.
Power Consumption for
1 g/L Washed Glass Spheres and 140 μS/cm NaCl Solution

Applied Voltage (kV)	Power (μVVs)	Power (μVVs)	Avg. Power (mJ/pulse)	95% Confidence
31	19	18	185	6
33	23	22	223	10
36	31	30	302	12
38	42	41	412	8
41	54	53	535	10
44	68	67	676	16
46	87	85	857	22
49	110	111	1101	10
51	128	130	1287	22
54	145	147	1461	18
57	169	168	1684	8
59	184	182	1828	16
62	200	202	2012	16

Table A10.
Power Consumption for
No Particles and 140 μS/cm $CaCl_2$ Solution

Applied Voltage (kV)	Power (μVVs)	Power (μVVs)	Avg. Power (mJ/pulse)	95% Confidence
31	11	12	115	10
33	25	24	247	6
36	43	41	421	18
38	54	56	550	20
41	65	66	657	14
44	81	80	807	6
46	97	94	957	25
49	105	110	1074	47
51	122	125	1236	31
54	147	146	1463	14
57	163	166	1645	29
59	189	190	1893	6
62	214	211	2126	27

Table A11.
Power Consumption for
1 g/L Washed Carbon and 14 μS/cm $CaCl_2$ Solution

Applied Voltage (kV)	Power (μVVs)	Power (μVVs)	Avg. Power (mJ/pulse)	95% Confidence
31	8	9	84	8
33	12	13	126	12
36	16	18	172	24
38	24	25	244	8
41	34	33	336	8
44	41	41	409	2
46	50	48	492	16
49	59	58	587	6

Table A12.
Power Consumption for
2 g/L Washed Carbon and 14 μS/cm $CaCl_2$ Solution

Applied Voltage (kV)	Power (μVVs)	Power (μVVs)	Avg. Power (mJ/pulse)	95% Confidence
31	9	10	94	4
33	12	13	125	2
36	17	16	165	2
38	22	21	214	12
41	25	27	259	18
44	33	34	337	14
46	40	42	408	16
49	48	50	492	24

Table A13.
Power Consumption for
1 g/L Washed Carbon and 140 μS/cm $CaCl_2$ Solution

Applied Voltage (kV)	Power (μVVs)	Power (μVVs)	Avg. Power (mJ/pulse)	95% Confidence
31	18	20	192	16
33	30	31	306	4
36	49	48	485	2
38	61	62	615	2
41	70	72	712	24
44	83	85	841	22
46	100	102	1012	24
49	115	120	1173	45
51	129	134	1313	45
54	146	151	1484	47
57	172	173	1726	12
59	197	194	1955	29
62	216	213	2146	27

Table A14.
Power Consumption for
2 g/L Washed Carbon and 140 μS/cm $CaCl_2$ Solution

Applied Voltage (kV)	Power (μVVs)	Power (μVVs)	Avg. Power (mJ/power)	95% Confidence
33	4	-	40	-
36	17	13	148	39
38	29	25	270	43
41	40	42	414	20
44	52	57	542	51
46	66	69	672	31
49	81	82	814	12
51	93	99	960	55
54	112	118	1148	63
57	130	132	1306	20
59	149	151	1498	20
62	168	170	1691	25

Table A15.
Power Consumption for
1 g/L Washed Glass Spheres and 14 μS/cm $CaCl_2$ Solution

Applied Voltage (kV)	Power (μVVs)	Power (μVVs)	Avg. Power (mJ/pulse)	95% Confidence
31	11	7	90	43
33	15	12	132	31
36	20	17	185	25
38	26	24	248	24
41	34	32	326	20
44	42	41	412	8
46	50	50	500	8
49	60	62	612	24

Table A16.
Power Consumption for
1 g/L Washed Glass Spheres and 140 μS/cm $CaCl_2$ Solution

Applied Voltage (kV)	Power (μVVs)	Power (μVVs)	Avg. Power (mJ/pulse)	95% Confidence
31	18	20	190	20
33	30	28	289	22
36	46	45	454	12
38	60	59	592	8
41	71	72	712	8
44	85	85	850	4
46	101	101	1010	4
49	116	117	1166	4
51	132	131	1316	8
54	151	152	1512	8
57	175	174	1746	12
59	196	195	1954	4
62	214	219	2164	47

Table A17.
Power Consumption for
No Particles and 140 μS/cm KCl Solution

Applied Voltage (kV)	Power (μVVs)	Power (μVVs)	Avg. Power (mJ/pulse)	95% Confidence
31	4	6	48	24
33	11	11	112	-
36	29	24	263	53
38	45	38	415	65
41	58	54	558	35
44	73	69	710	35
46	91	88	896	24
49	106	109	1072	31
51	122	124	1232	16
54	141	145	1429	41
57	164	167	1656	31
59	186	187	1866	12
62	206	204	2050	20

Table A18.
Power Consumption for
1 g/L Washed Carbon and 14 μS/cm KCl Solution

Applied Voltage (kV)	Power (μVVs)	Power (μVVs)	Avg. Power (mJ/pulse)	95% Confidence
31	-	2	24	-
33	-	2	24	-
36	-	4	44	-
38	5	5	50	4
41	5	5	52	-
44	6	7	68	8
46	8	10	94	20
49	13	14	132	8

Table A19.
Power Consumption for
2 g/L Washed Carbon and 14 μS/cm KCl Solution

Applied Voltage (kV)	Power (μVVs)	Power (μVVs)	Avg. Power (mJ/pulse)	95% Confidence
31	6	6	62	4
33	7	7	70	4
36	9	8	87	10
38	11	11	110	4
41	12	12	122	4
44	14	14	142	4
46	18	18	176	-
49	22	22	220	-

Table A20.
Power Consumption for
1 g/L Washed Carbon and 140 μS/cm KCl Solution

Applied Voltage (kV)	Power (μVVs)	Power (μVVs)	Avg. Power (mJ/pulse)	95% Confidence
31	2	4	28	24
33	5	7	60	24
36	10	14	124	39
38	18	22	200	31
41	25	27	260	24
44	30	32	308	24
46	36	41	384	47
49	43	47	452	39
51	52	55	536	31
54	62	63	628	8
57	71	72	716	8
59	83	82	824	16
62	93	91	920	16

Table A21.
Power Consumption for
2 g/L Washed Carbon and 140 μS/cm KCl Solution

Applied Voltage (kV)	Power (μVVs)	Power (μVVs)	Avg. Power (mJ/pulse)	95% Confidence
31	11	10	105	2
33	13	12	123	6
36	16	17	165	2
38	21	22	215	2
41	29	28	283	6
44	35	34	343	6
46	46	44	450	20
49	53	52	523	14
51	59	58	587	6
54	66	66	662	4
57	76	79	773	25
59	85	87	861	22
62	93	96	947	33

Table A22.
Power Consumption for
1 g/L Washed Glass Spheres and 14 μS/cm KCl Solution

Applied Voltage (kV)	Power (μVVs)	Power (μVVs)	Avg. Power (mJ/pulse)	95% Confidence
33	9	9	90	-
36	17	18	173	6
38	20	21	206	12
41	26	27	264	8
44	32	32	318	4
46	39	38	385	10

Table A23.
Power Consumption for
1 g/L Washed Glass Spheres and 140 μS/cm KCl Solution

Applied Voltage (kV)	Power (μVVs)	Power (μVVs)	Avg. Power (mJ/pulse)	95% Confidence
31	17	18	173	6
33	20	22	208	16
36	29	30	297	14
38	42	43	424	8
41	54	55	544	8
44	66	67	664	8
46	83	83	829	2
49	107	106	1064	12
51	122	120	1210	20
54	143	140	1415	29
57	168	165	1666	27
59	190	188	1890	20
62	204	203	2033	14

Table A24.
46 kV Corona Treatment with No Washed Carbon
Phenol Removal

Time (min)	ppm	ppm	ppm	Avg. (ppm)	95% Confidence	Avg. (µmoles)
0	100.0	100.0	100.0	100.0	-	1062.6
1	90.3	89.9	89.6	89.9	0.4	955.6
2	87.1	88.0	88.4	87.8	0.8	933.3
4	86.0	82.8	82.1	83.6	2.4	888.7
6	84.9	77.3	81.6	81.3	4.3	863.5
8	83.5	76.7	83.8	81.3	4.5	864.2
10	75.8	73.6	-	74.7	1.8	793.8
15	73.5	66.8	76.4	72.2	5.6	767.5

Table A25.
46 kV Corona Treatment with No Washed Carbon
Catechol Formation

Time (min)	ppm	ppm	ppm	Avg. (ppm)	95% Confidence	Avg. (µmoles)
0	0.000	0.000	0.000	0.000	-	0.000
1	1.232	1.315	1.408	1.318	0.100	11.973
2	2.630	2.724	2.493	2.616	0.131	23.755
4	4.556	4.315	4.255	4.375	0.180	39.736
6	5.640	6.069	5.455	5.721	0.356	51.960
8	7.389	6.897	6.848	7.045	0.339	63.978
10	9.328	9.131	-	9.230	0.158	83.821
15	11.161	10.329	10.474	10.655	0.503	96.764

Table A26.
46 kV Corona Treatment with No Washed Carbon
Hydroquinone Formation

Time (min)	ppm	ppm	ppm	Avg. (ppm)	95% Confidence	Avg. (μmoles)
0	0.000	0.000	0.000	0.000	-	0.000
1	0.064	0.075	0.061	0.067	0.008	0.605
2	0.004	0.003	0.002	0.003	0.001	0.027
4	0.006	0.009	0.005	0.007	0.002	0.061
6	0.052	0.065	0.068	0.062	0.010	0.560
8	0.093	0.117	0.099	0.103	0.014	0.935
10	0.379	0.453	-	0.416	0.059	3.778
15	0.991	1.246	1.000	1.079	0.164	9.799

Table A27.
46 kV Corona Treatment with No Washed Carbon
Resorcinol Formation

Time (min)	ppm	ppm	ppm	Avg. (ppm)	95% Confidence	Avg. (μmoles)
0	0.000	0.000	0.000	0.000	-	0.000
1	0.318	0.319	0.348	0.328	0.019	2.982
2	0.587	0.590	0.614	0.597	0.017	5.422
4	1.038	1.123	0.955	1.039	0.095	9.433
6	1.305	1.392	1.239	1.312	0.087	11.915
8	1.671	1.624	1.433	1.576	0.143	14.313
10	1.843	2.001	-	1.922	0.126	17.455
15	2.131	2.124	1.924	2.060	0.133	18.706

Table A28.
57 kV Corona Treatment with No Washed Carbon
Phenol Removal

Time (min)	ppm	ppm	ppm	Avg. (ppm)	95% Confidence	Avg. (μmoles)
0	100	100	100	100.0	-	1062.6
1	90.7	91.2	94.3	92.1	2.2	978.3
2	86.2	84.8	96	89.0	6.9	945.7
4	82.3	82.7	87.6	84.2	3.3	894.7
6	75.8	74.9	77.8	76.2	1.7	809.3
8	71.2	74.5	76.7	74.1	3.1	787.7
10	68.2	69.2	68.5	68.6	0.6	729.3
15	61.5	60.4	58	60.0	2.0	637.2

Table A29.
57 kV Corona Treatment with No Washed Carbon
Catechol Formation

Time (min)	ppm	ppm	ppm	Avg. (ppm)	95% Confidence	Avg. (μmoles)
0	0	0	0	0.000	-	0.000
1	2.185	2.156	1.728	2.023	0.290	18.373
2	3.899	3.83	4.23	3.986	0.242	36.203
4	6.651	6.69	6.416	6.586	0.168	59.810
6	8.834	8.545	8.634	8.671	0.167	78.749
8	10.995	11.239	11.89	11.375	0.524	103.303
10	12.969	12.74	13.065	12.925	0.189	117.380
15	17.119	15.53	15.767	16.139	0.970	146.569

Table A30.
57 kV Corona Treatment with No Washed Carbon
Hydroquinone Formation

Time (min)	ppm	ppm	ppm	Avg. (ppm)	95% Confidence	Avg. (μmoles)
0	0	0	0	0	-	0
1	0.062	0.075	0.08	0.072	0.011	0.657
2	0.078	0.068	0.078	0.075	0.007	0.678
4	0.629	0.631	0.673	0.644	0.028	5.852
6	0.961	1.01	1.064	1.012	0.058	9.188
8	1.086	1.024	1.101	1.070	0.046	9.721
10	2.361	2.306	2.53	2.399	0.132	21.787
15	5.019	4.77	5.436	5.075	0.381	46.090

Table A31.
57 kV Corona Treatment with No Washed Carbon
Resorcinol Formation

Time (min)	ppm	ppm	ppm	Avg. (ppm)	95% Confidence	Avg. (μmoles)
0	0	0	0	0	-	0
1	0.475	0.461	0.419	0.452	0.033	4.102
2	1.054	1.043	0.921	1.006	0.084	9.136
4	1.48	1.488	1.382	1.450	0.067	13.169
6	1.779	1.673	1.549	1.667	0.130	15.139
8	2.135	2.247	2.152	2.178	0.068	19.780
10	2.093	2.14	2.042	2.092	0.055	18.996
15	2.417	2.493	2.191	2.367	0.178	21.497

Table A32.
46 kV Corona Treatment and 1 g/L Washed Activated Carbon
Phenol Removal

Time (min)	ppm	ppm	ppm	Avg. (ppm)	95% Confidence	Avg. (μmoles)
0	100	100	100	100.0	-	1062.6
1	70.3	76.9	78.8	75.3	5.0	800.5
2	57.5	66.2	65.4	63.0	5.4	669.8
4	48.4	50	50.6	49.7	1.3	527.8
6	37.6	42.3	41.1	40.3	2.8	428.6
8	33.4	33.8	31.7	33.0	1.3	350.3
10	29.6	29.3	30.7	29.9	0.8	317.4
15	21.9	21.4	23.7	22.3	1.4	237.3

Table A33.
46 kV Corona Treatment and 1 g/L Washed Activated Carbon
Catechol Formation

Time (min)	ppm	ppm	ppm	Avg. (ppm)	95% Confidence	Avg. (μmoles)
0	0	0	0	0	-	0
1	0.301	0.334	0.297	0.311	0.023	2.821
2	1.853	1.94	1.764	1.852	0.100	16.823
4	3.246	3.602	3.444	3.431	0.202	31.157
6	3.831	4.157	4.032	4.007	0.186	36.388
8	4.061	4.43	4.475	4.322	0.257	39.252
10	4.491	5.312	5.017	4.940	0.471	44.864
15	5.578	5.404	6.298	5.760	0.536	52.311

Table A34.
46 kV Corona Treatment and 1 g/L Washed Activated Carbon
Hydroquinone Formation

Time (min)	ppm	ppm	ppm	Avg. (ppm)	95% Confidence	Avg. (μmoles)
0	0	0	0	0.000	-	0.000
1	0.213	0.24	0.284	0.246	0.041	2.231
2	0.732	0.612	0.729	0.691	0.077	6.276
4	0.072	0.058	0.04912	0.060	0.013	0.542
6	0.63	0.437	0.487	0.518	0.113	4.704
8	0.245	0.242	0.307	0.265	0.042	2.404
10	0.985	0.696	0.787	0.823	0.167	7.471
15	1.088	1.622	1.344	1.351	0.302	12.273

Table A35.
46 kV Corona Treatment and 1 g/L Washed Activated Carbon
Resorcinol Formation

Time (min)	ppm	ppm	ppm	Avg. (ppm)	95% Confidence	Avg. (μmoles)
0	0	0	0	0		0
1	0.009	0.007	0.005	0.007	0.002	0.064
2	0.477	0.471	0.418	0.455	0.037	4.135
4	0.8	0.867	0.887	0.851	0.052	7.732
6	0.816	0.915	0.905	0.879	0.062	7.980
8	0.878	0.928	0.963	0.923	0.048	8.383
10	0.93	1.035	1.062	1.009	0.079	9.164
15	1.3614	1.611	1.406	1.459	0.151	13.255

Table A36.
57 kV Corona Treatment and 1 g/L Washed Activated Carbon
Phenol Removal

Time (min)	ppm	ppm	Avg. (ppm)	95% Confidence	Avg. (μmoles)
0	100.0	100.0	100.0	-	1062.6
1	74.4	78.8	76.6	4.3	813.9
2	58.0	61.3	59.7	3.2	633.8
4	39.0	41.3	40.2	2.3	426.6
6	32.7	33.1	32.9	0.4	349.6
8	25.7	27.0	26.4	1.3	280.0
10	19.9	20.9	20.4	1.0	216.8
15	10.6	11.1	10.9	0.5	115.3

Table A37.
57 kV Corona Treatment and 1 g/L Washed Activated Carbon
Catechol Formation

Time (min)	ppm	ppm	Avg. (ppm)	95% Confidence	Avg. (μmoles)
0	0	0	0	-	0
1	0.607	0.641	0.624	0.033	5.667
2	2.627	2.783	2.705	0.153	24.566
4	4.297	4.587	4.442	0.284	40.341
6	5.733	6.004	5.869	0.266	53.297
8	6.617	7.019	6.818	0.394	61.920
10	6.444	7.253	6.849	0.793	62.197
15	5.639	5.848	5.744	0.205	52.161

Table A38.
57 kV Corona Treatment and 1 g/L Washed Activated Carbon
Hydroquinone Formation

Time (min)	ppm	ppm	Avg. (ppm)	95% Confidence	Avg. (μmoles)
0	0	0	0	-	0
1	0.675	0.632	0.654	0.042	5.935
2	0.447	0.402	0.425	0.044	3.855
4	0.493	0.531	0.512	0.037	4.650
6	1.242	1.092	1.167	0.147	10.598
8	1.121	0.989	1.055	0.129	9.581
10	2.062	1.897	1.980	0.162	17.977
15	2.115	1.941	2.028	0.171	18.418

Table A39.
57 kV Corona Treatment and 1 g/L Washed Activated Carbon
Resorcinol Formation

Time (min)	ppm	ppm	Avg. (ppm)	95% Confidence	Avg. (μmoles)
0	0	0	0	-	0
1	0.027	0.028	0.027	0.001	0.250
2	0.464	0.515	0.490	0.050	4.446
4	0.726	0.777	0.752	0.050	6.825
6	0.785	0.817	0.801	0.031	7.275
8	0.939	1.019	0.979	0.078	8.891
10	0.743	0.777	0.760	0.033	6.902
15	0.382	0.445	0.414	0.062	3.755

Calculations

For Power Consumption:

46 kV, No Carbon (800 mJ/pulse, 28 mg phenol removed in 15 minutes)

$$2.3\frac{g}{kWhr} = \frac{0.028g}{\left(800\frac{mJ}{pulse}\right)\left(\frac{1J}{1000mJ}\right)(15\min)\left(60\frac{s}{\min}\right)\left(60\frac{pulses}{s}\right)\left(\frac{1kWhr}{3.6\times10^6 J}\right)}$$

For Error Analysis:

$$Standard\ Deviation = \frac{n\sum x^2 - \left(\sum x\right)^2}{n(n-1)}$$

$$Confidence = \bar{x} \pm \alpha\left(\frac{\sigma}{\sqrt{n}}\right)$$

where n is the number of samples, x is one sample, $\bar{x}$ is the average of all the samples, α is the factor related to the confidence interval of interest (1.96 for 95% confidence interval) and σ is the standard deviation.

For Power per Pulse:

(1 V/1000 V Voltage Probe, 1 V/10 A Current Probe)

$$10\frac{\mu VVs}{pulse} = 10(1000\mu V)(10A)\frac{s}{pulse} = 100\frac{mJ}{pulse}$$

Bulk Diffusion Constant (Sitaraman, et al., 1963):

$$D_{AB} = 16.79 \times 10^{14} \left(\frac{M_B^{1/2} \Delta H_B^{1/3} T}{\mu_B V_A^{1/2} \Delta H_A^{0.3}} \right)^{0.93} = 3.68 \times 10^{-10} m^2 / s$$

M_B = molecular weight of solvent = 18 kg/kgmole

ΔH_A = latent heat of vaporization of solute = 4.97 x 10^7 J/kg

ΔH_B = latent heat of vaporization of solvent = 2.25 x 10^6 J/kg

T = Temperature = 293 K

μ_B = solvent viscosity (dilute solution) = 1.05 cP

V_A = molar volume of solute = 0.121 m^3/kgmol

Mass Transfer Coefficient (Frössling, 1938):

$$K_{mt} = \frac{D_{AB}}{d_p} \left(2 + 0.6 \left(\frac{d_p U}{\upsilon} \right)^{1/2} \left(\frac{\upsilon}{D_{AB}} \right)^{1/3} \right)$$

This equation is valid for a convective flow around a sphere at low Reynolds numbers. In the suspension of the activated carbon particles, the velocity of the particles is very close to that of the bulk fluid velocity. At the limit where both velocities become equal (U=0), the above equation reduces to

$$K_{mt} = \frac{2 D_{AB}}{d_p} = 3.68 \times 10^{-6} m / s$$

d_p = particle diameter = 200 x 10^{-6} m

Effective Diffusion in Particle (Satterfield, 1970)

$$D_{eff} = 194 \frac{\varepsilon^2}{\tau S \rho_B} \left(\frac{T}{M_A} \right)^{1/2} = 3.3 \times 10^{-8} m^2 / s$$

ε = particle porosity = 0.5

τ = particle tortuosity = 2

S = particle surface area = 1100 x 10^3 m^2/kg

ρ_B = particle density = 1.2 x 10^3 kg/m^3

T = temperature = 293 K

M_A = molecular weight of phenol = 94 g/mole

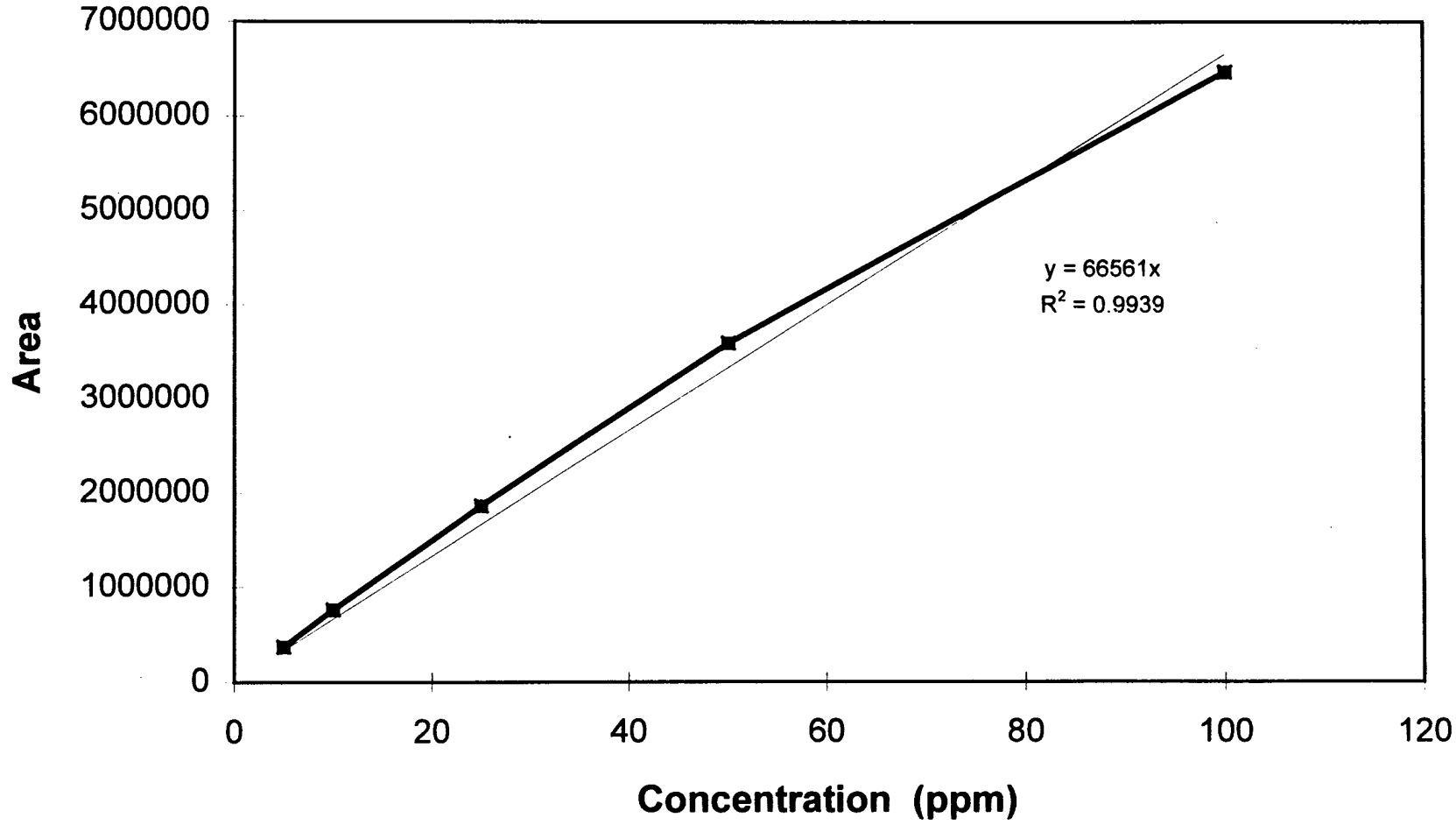


Figure A1. HPLC Calibration for Phenol

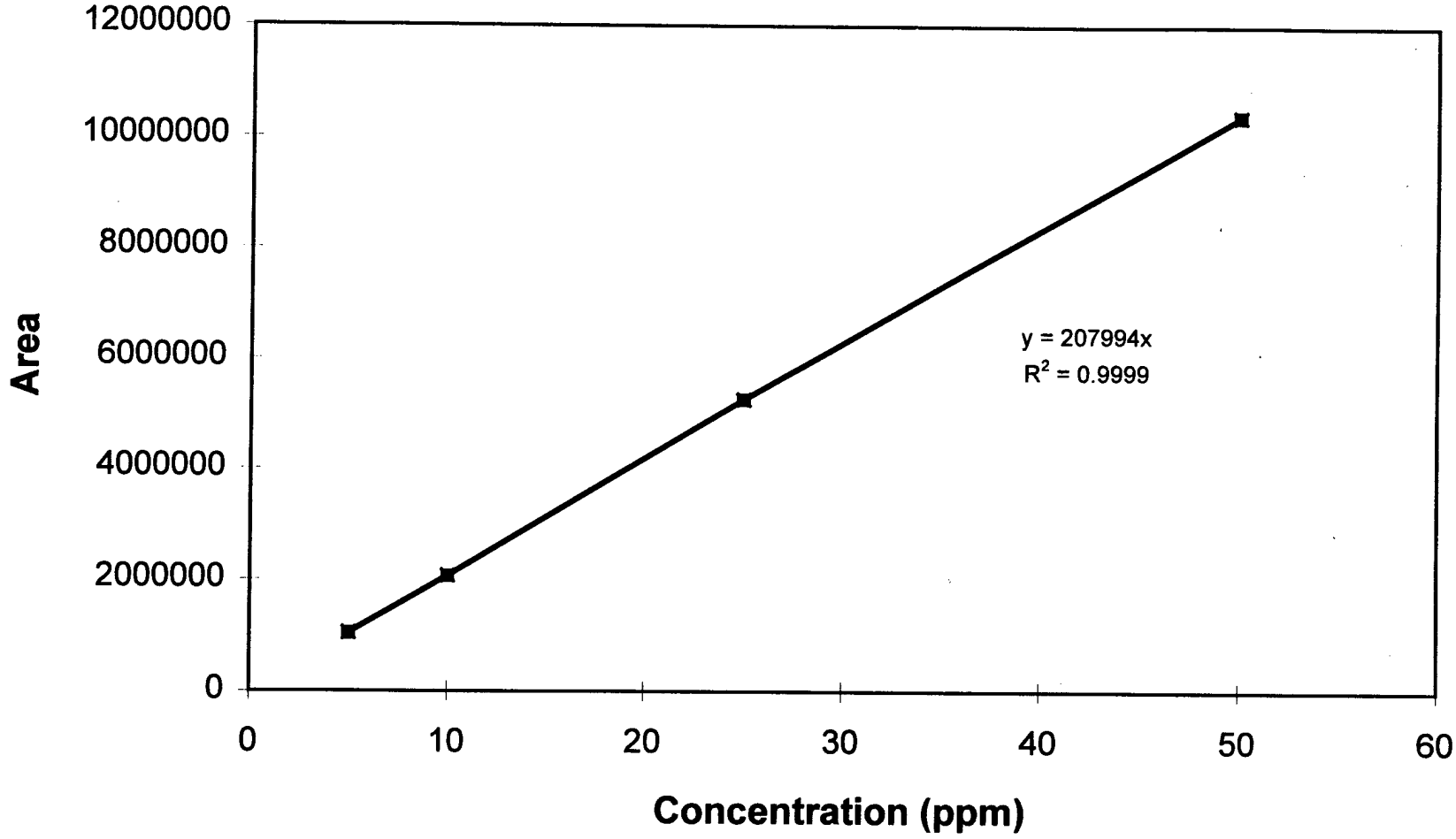


Figure A2. HPLC Calibration for Catechol

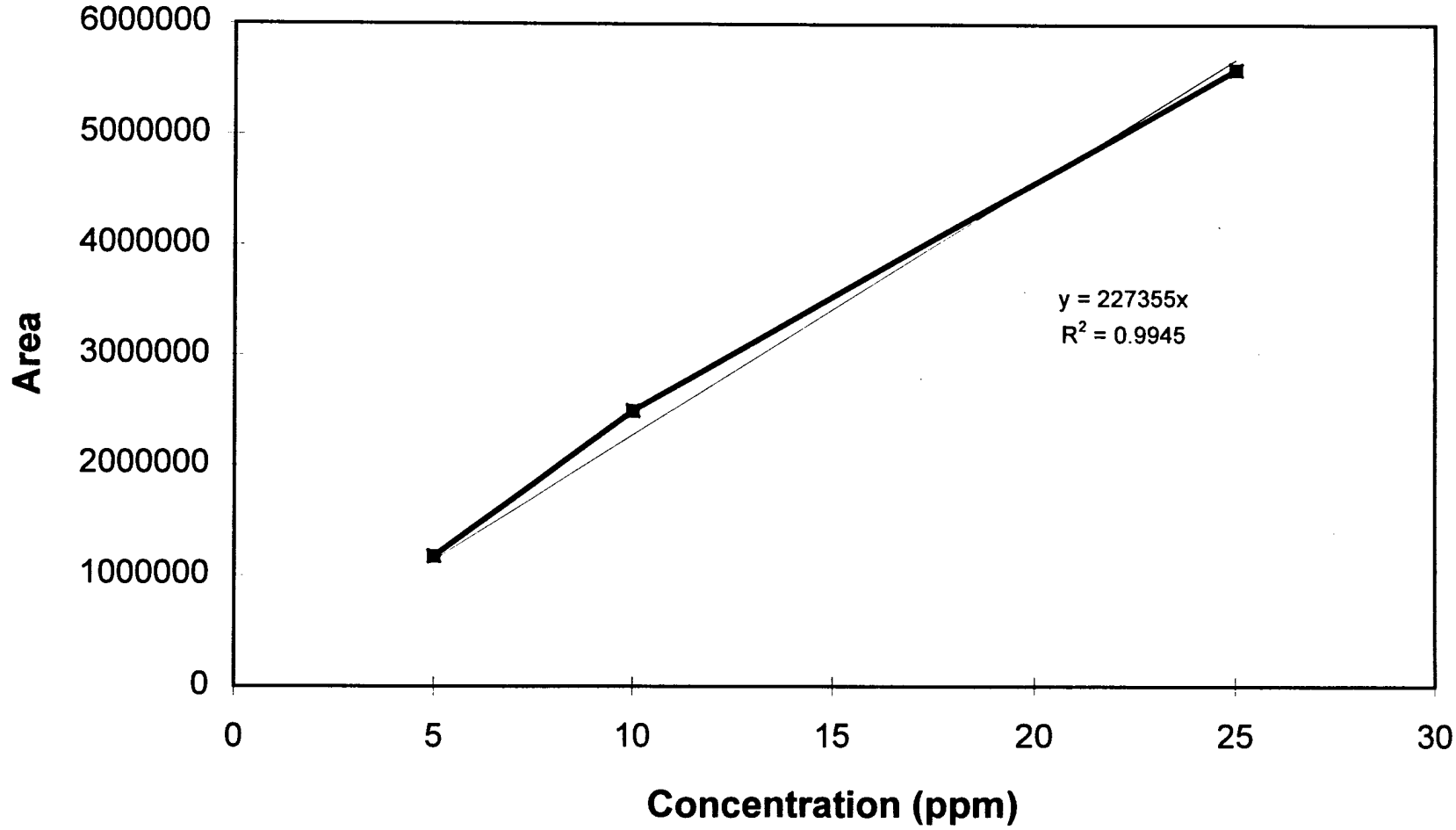


Figure A3. HPLC Calibration for Hydroquinone

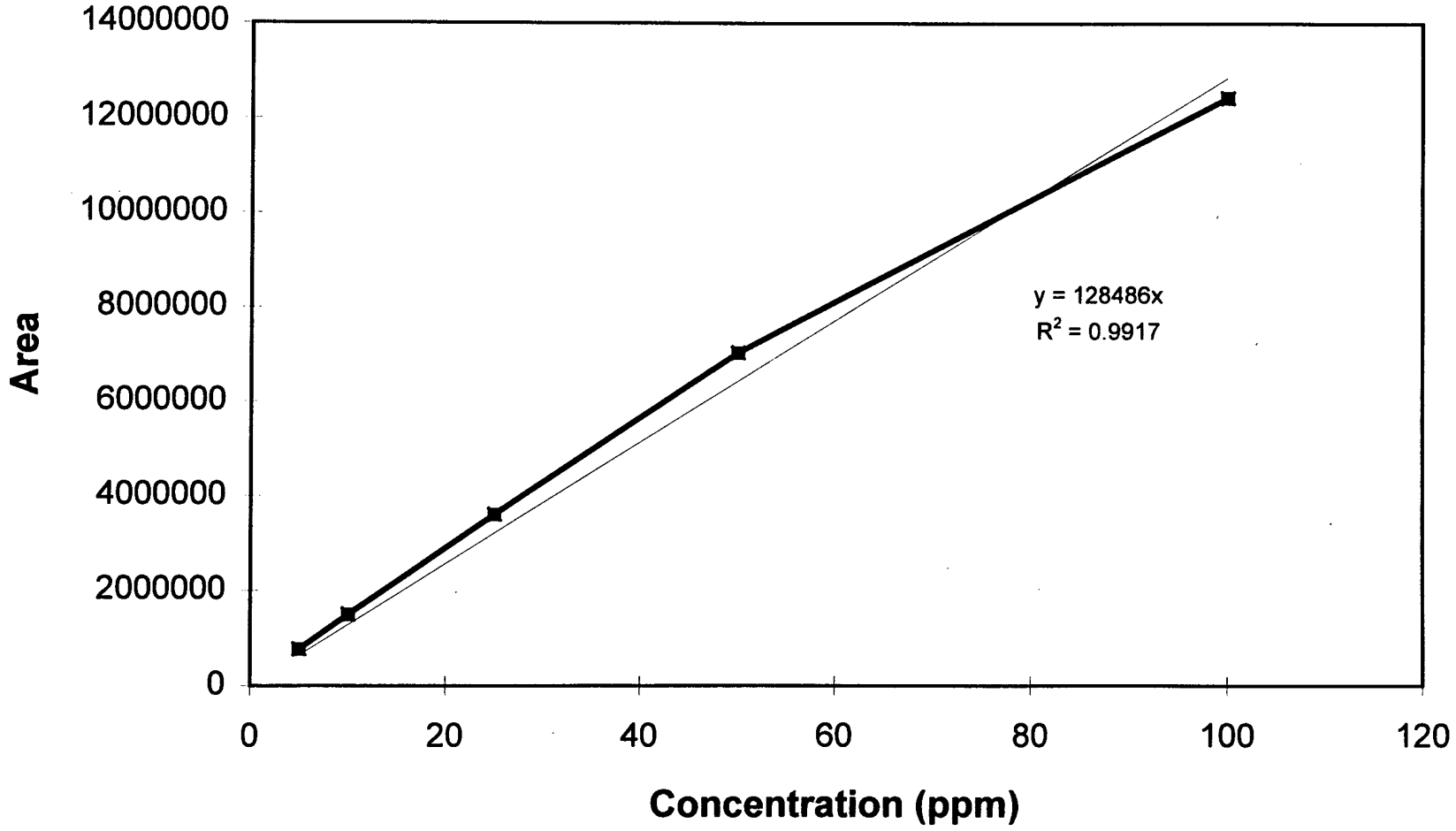


Figure A4. HPLC Calibration for Resorcinol

REFERENCES

Bansal, R.C., Donnet, J.B., and Stoeckli, F., 1988; Active Carbon, Marcel Dekker, Inc., New York.

Brandt, N.B., Chudinov, S.M., and Ponomarev, Y.G., 1988; Semimetals 1. Graphite and its Compounds, North-Holland, Amsterdam.

Chang, J.S., Lawless, P.A., and Yamamoto, J., 1991, Corona Discharge Processes, *IEEE Trans. Plasma Sci.*, **19**, p. 140.

Clements, J.S., Sato, M., and Davis, R.H., 1985: Preliminary Investigation of Prebreakdown Phenomena and Chemical Reactions Using a Pulsed High Voltage Discharge in Water. *IEEE Trans. Ind Appl.* **IA-23**, p. 1372.

Clements, J.S., Mizuno, A., Finney, W. C., and Davis, R. H., 1989: Combined Removal pf SO_2, NO_x, and Fly Ash from Simulated Flue Gas Using Pulsed Streamer Corona, *IEEE Trans. On Ind. Appl*, **25** (1), p. 62.

Creyghton, Y.M.L., 1994: Pulsed Positive Corona Discharges, Fundaental Study and Applications to Flue Gas Treatment, CIP-DATA Kononkijke Biblitheck, Den Haag, The Netherlands.

Creyghton, Y.M.L., 1997a: Direct Plasma Treatment of Polluted Water, *Abstracts from The Fourth International Conference on Advanced Oxidation Technologies for Water and Air Remediation*, p. 58.

Creyghton, Y.M.L., 1997b: Personal Correspondence.

Devins, J.C., Rzad, S.J.,and Schwabe, R.J., 1981:Breakdown and Prebreakdown Phenomena in Liquids, *J. Appl. Phys.*, **52** (7), p.4531.

Eisenhauer, H.R., 1968: The Ozonation of Phenolic Wastes., *Journal WPCF*, **40**(11), p.1887.

Fogler, H.S., 1992: Elements of Chemical Reaction Engineering, Pretince Hall, Englewood Cliffs, New Jersey.

Frössling, N., 1938, *Beitr. Geophys.*, **52**, p. 170.

Gohenn, S. C., Durham, D. E., McCulloch, M., and Heath, W. O., 1992: The Degradation of Organic Dyes by Corona Discharge, *Proceedings of the Second International Symposium Chemical Oxidation: Technology for the Nineties*, p. 356.

Gray, W.G., 1975: A Derivation of the Equations for Multicomponent Transport, *Chem. Eng. Sci.*, **30**, p. 229.

Hoeben, W.F.L.M., Van Veldhuizen, E.M., Claessens, H.A., Rutgers, W.R., 1997: The degradation pf Phenol and Atrazine in Water by Pulsed Corona Discharges, *Proceedings of the 13th ISCP*, Beijing, p. 1843.

Jankowska, H., Swiatkowski, A., Choma, J., 1991:Active Carbon, Ellis Horwood, New York, 1991.

Jones, H. M., and Kundhardt, E. E., 1995, Development of Pulsed Dielectric Breakdown in Liquids. *Journal of Physics D: Applied Physics,* **28** , p.178-188.

Jones, H.M., and Kunhardt, E.E., 1995: Pulsed Dielectric Breakdown of Pressurized Water and Salt Solutions, *J. Appl. Phys.*, **77** (2), p.795.

Joshi, A.A., 1994: Formation of Hydroxyl Radicals, Hydrogen Peroxide, and Aqueous Electrons by Pulsed Streamer Corona Discharge in Aqueous Solutions, M.S. Thesis, Florida State University, Tallahassee, FL.

Joshi, A.A., Locke, B.R., Arce, P., and Finney, W.C., 1995: Formation of Hydroxyl Radicals, Hydrogen Peroxide and Aqueous Electron by Pulsed Streamer Corona Discharge in Aqueous Solution, *J. Hazardous Materials*, **41**(1) 3 (1995).

Kalyana, S., 1996: The Removal of NO_x Using a Pulsed Streamer Corona Discharge in the Presence of Ethylene. M.S. Thesis, Florida State University, Tallahassee, FL.

Kinoshita, K., 1988: Carbon, Electrical and Physicochemical Properties, John Wiley And Sons, United States.

Klimkin, V. F., and Ponomarenko, A. G., 1979: Interferometric Study of Pulsed Breakdown in a Liquid. *Sov. Psys. Tech. Phys.* **24**(9), p.1067.

Klimkin, V. F. , 1990: Mechanisms of Electric Breakdown of Water from Pointed Anode in the Nanosecond Range. *Sov. Psys. Tech. Phys.* **16**(2), 14 p.6.

Klimkin, V. F., 1991: A Multiframe Ultrafast Laser Schlieren System for the Observation of Pre-breakdown Phenomena in Liquids in the Nanosecond Range. *Sov. Psys. Tech. Phys.* **36**(9), p.375.

Klimkin, V.F., 1992: A Multifram Ultrafast Laser Schlieren system for the Observation of Pre-breakdown Pheomena in Liquids in the Nanosecond Time Range, *Sov. Phys. Tech. Phys.* **36**(9) p.975.

Kok, J.A., 1961, Electrical Breakdown of Insulating Liquids, Phillips Tech. Lib., Cleaver-Hum, London.

Krajnc, M., and Levec, J., 1996: On the Kinetics of Phenol Oxidation in Supercritical Water. *AIChE Journal*, **42**(7), p.1977.

Kuskova, N. I., 1983: Mechanism of Leader Propagation in Water. *Sov. Psys. Tech. Phys.* **28**(5), p.591.

Logemann, F.P., and Annee, J.H.J., 1997: Water Treatment with a Fixed Bed Catalytic Ozonation Process, *Wat. Sci. Tech.*, **35** (4), p.353.

Lubicki, P., Cross, J. D., Jayaram, S., Staron, J., and Mazurek, B., 1996: Effect of Water Conductivity on its Pulse Electric Strength, Conference Record of the *1996 IEEE International Symposium on Electrical Insulation, Montreal, Quebec.*

Lubicki, P., Jayaram, S., Cross, J.D., and Al-Arainy, A.A., 1996: Pulsed Corona Discharge for Advanced Oxidation in Water Purification Technology. *1996 IEEE Annual Report – Conference on Electrical Insulation and Dielectric Phenomena*, San Fransico, CA.

Mizuno, A., Inoue, T., Yamaguchi, S., Sakamoto, K., Saeki, T., Matsumoto, Y.,and Minamiyama, K., 1990: Inactivation of Viruses using Pulsed High Electric Field, *Conference Record of IEEE/IAS Annual Meeting*, pp 713-719.

Mikula, M., Panak, P., and Dvonka, V., 1997: The Destruction Effect of Pulse Discharge in Water Suspensions. *Plasma Sources Science Technology*, **6**, p.179.

Neigowski, S.J, 1953: Destruction of Phenols by Oxidation with Ozone. *Industrial and Engineering Chemistry*, **45**(3), p.632.

Ochoa, J.A., Stroeve, P., and Whitaker, S., 1986: Diffusion and Reaction in Cellular Media. *Chemical Engineering Science*, **41**(12), p. 2999.

Pétrier, C., Lamy, M., Francony, A., Benahcene, A., David., B., Renaudin, V., and Gondrexon, N., 1994: Sonochemical Degradation of Phenol in Dilute Aqueous Solutions: Comparison of the Reaction Rates at 20 and 487 kHz. *Journal of Physical Chemistry*, **98**, p. 10514.

Ryan, D., Carbonell, R.G., and Whitaker, S., 1981: A Theory of Diffusion and Reaction in Porous Media. *AIChE Symposium Series*, **77**(202) p. 46.

Sato, M., Ohgiyama, T., and Clements, J.S., 1996: Formation of Chemical Species and their Effects on Microorganisms using a Pulsed High Voltage Discharge in Water. *IEEE Transactions on Industry Applications*, **32**, p.106.

Satterfield, C.N., 1970, Mass Transfer in Heterogeneous Catalysis, MIT Press, Cambridge, Mass.

Sharbaugh, A.H., Deinvs, J.C.,and Rzad, S.J., 1978: Progress in the Field of Electric Breakdown in Dielectric Liquids, *IEEE Trans. Electr. Insul.*, **EI-13**(4) 249.

Sharma, A. K., 1993: High Voltage Pulsed Streamer Corona Discharges for the Removal of Organic Contaminants From Aqueous Solutions, M.S.. Thesis, Florida State University, Tallahassee, FL.

Sharma, A. K., Locke, B. R., Arce, P., Finney, W. C., 1993, A Preliminary Study of Pulsed Streamer Corona Discharge for the Degradation of Phenol in Aqueous Solutions. *Hazardous Waste & Hazardous Materials*, **10** (2), p. 209.

Sharma, A.K., Camaioni, D.M., Josephson, G.B., Goheen, S.C., and Mong, G.M., 1997: Formation and Measurement of Ozone and Nitric Acid in a High Voltage DC Negative Metallic Point-to-Aqueous-Plane Continuous Corona Reactor, *J. Adv. Oxid. Technol.*, **2** (1), p. 239.

Sitaraman, R., Ibrahim, S.H., and Kuloor, N.R., 1963. *J. Chem. Eng. Data*, **8**, p. 198.

Sun, Y., Pignatello, J.J., 1993: Photochemical Reactions Involved in the Total Mineralization of 2,4-D by $Fe^{3+}/H_2O_2/UV$. *Environmental Science and Technology*, **27**(2), p.304.

Thornton, T.D., and Savage, P.E., 1992: Kinetics of Phenol Oxidation in Supercritical Water. *AIChE Journal*, **38**(3), p.321.

Thornton, T.D., LaDue, D.E., and Savage, P.E., 1991: Phenol Oxidation in Supercritical Water: Formation of Dibenzofuran, Dibenzo-p-dioxin, and Related Compounds. *Environmental Science and Technology*, **25**, p.1507.

Vidic, R. D., Suldan, M. T., and Brenner, R. T., 1993 : Oxidative Coupling of Phenols on Activated Carbon : Impact on Adsorption Equilibrium. *Environ. Sci. Technol.* **27**, p. 2085.

Whitaker, S., 1967:Diffusion and Dispersion in Porous Media. *J. A.I.Ch.E.*, **13**, p. 420.

Whitaker, S., 1987: Mass Transport and Reaction in Catalyst Pellets. *Transport in Porous Media*, **2**, p.269.

Whitaker, S., 1991: The Method of Volume Averaging: An Application to Diffusion and Reaction in Porous Catalysts. *Proceedings of the National Science Council, Part A: Physical Science and Engineering*, Taipei, Taiwan.

Wong, P., and Forster, E. O., 1977: High-Speed scliieren studies of Electrical Breakdown in Liquid Hydrocarbons, *Can. J. Chem.*, **55**, p.1890.

Zepp, R.G., Faust, B.C., Hoingé, J., 1992: Hydroxyl Radical Formation in Aqueous Reactions (pH 3-8) of Iron (II) with Hydrogen Peroxide: The Photo-Fenton Reaction. *Environmental Science and Technology*, **26**(2), p.313.

Zhekul, V.G.,and Rakovskii, G.B., 1983: Theory of Electrical Discharge Formation in a Conducting Liquid, *Sov. Phys. Tech. Phys.*, **28**(1), p.4.

BIOGRAPHICAL SKETCH

David Grymonpré was born in Denver, Colorado on May 29, 1972. He grew up travelling around the United States and Canada. He graduated from Pike High School in Indianapolis, Indiana during 1990. In the fall of 1990, he started a long, productive career at Florida State University. He graduated in 1995 with a Bachelor of Science degree in Chemical Engineering. While he was an undergraduate student, he began working for Dr. Bruce Locke on pulsed corona treatment of airborne and aqueous wastes. Also during his undergraduate years, David was involved in music, playing the bassoon in several orchestras in Georgia and Florida, as well as performing several solo and chamber recitals.

Continuing on at Florida State University, he is currently finishing the degree of Master of Science in Chemical Engineering. After finishing this degree, David plans to pursue his doctorate in Chemical Engineering, again attending Florida State University. His hobbies include fishing, golf, and beer brewing. He plans to attend several more football seasons at Florida State University in hopes of one more National Championship.